UDMA PHOTO-CURED ADHESIVE SYSTEMS WITH ENHANCED MECHANICAL PROPERTIES FOR TREATING DENTAL CARIES

by

ZINAH N. ALABDALI

A dissertation submitted to the

School of Graduate Studies

Rutgers, The State University of New Jersey

In partial fulfillment of the requirements

For the degree of

Doctor of Philosophy

Graduate Program in Materials Science and Engineering

written under the direction of

Adrian B. Mann

And approved by

_____

_____

_____

_____

_____

New Brunswick, New Jersey

October, 2020

ABSTRACT OF THE DISSERTATION

UDMA photo-cured adhesive systems with enhanced mechanical properties for treating dental caries

By ZINAH N. ALABDALI

Dissertation Advisors:

Adrian B. Mann

Dental caries are a global oral health disease caused by acidogenic bacterial on teeth whereby acid causes demineralization, loss of ions, from the tooth into the saliva. The resulting cavities can be filled with light-cured, composite, resin restorations which are less toxic than amalgam, less expensive than gold and the resin can match the natural tooth color. However, composite resins tend to suffer from polymerization shrinkage after exposure to light, this can result in a gap forming between the adhesive layer at the base of the composite restoration and the tooth surface. The gap occurs due to the combination of polymer shrinkage and weak bonding between the adhesive layer and dental tissue, this then permits microleakage and eventually secondary caries to develop.

A Dental adhesive system acts as the key intermediate layer between a composite resin restoration and the tooth tissues (enamel and dentin). Ideally, the adhesive is able to penetrate into a roughened, porous enamel surface and into open tubules in dentin, hence forming a strong interlocking bond call a hybrid layer. The properties of the hybrid layer depend on the chemical composition of the adhesive system, including the monomers, photointiators, and additives, as well as its mechanical and rheological properties.

The aim of this thesis was to develop a new photo-cured dental adhesive with improved rheological and mechanical properties to enable a good interlocking hybrid layer and reduce gap formation. Firstly, commercially available products, including self-etch and three-step adhesive systems, were investigated, applied to cow teeth, and evaluated. Graphene and hydroxyapatite were blended with the three-step adhesive as an additive in an attempt to improve performance of the hybrid layer. Secondly, a new adhesive system was developed composed of high and low molecular weight monomers, diurethane dimethacrylate (UDMA) and methyl methacrylate (MMA), respectively. Thirdly, graphene and hydroxyapatite were added in different weight percentages to UDMA-MMA blends to optimize the mechanical properties of the photo-cured adhesive system. The viscosity, mechanical properties (using nanoindentation and tensile test), and degree of conversion (using FTIR and micro-Raman) were characterized for the UDMA-MMA blends with and without additives. Samples were imaged using optical microscopy, helium ion microscopy, and scanning electron microscopy, and surface topography was viewed using AFM. Thermography was used to monitor curing rate and temperature during curing.

For the commercial adhesive systems, results indicate that gap formation occurs between the adhesive and tooth tissues, which is related to the weak adhesive and hybrid layers. For the UDMA-MMA blends, results indicate that the viscosity and mechanical properties may be tuned and optimized to improve adhesion. For example, low weight % UDMA in MMA provides low viscosity, which allows penetration into tubules in the dentin and enamel forming a good hybrid layer while still providing good mechanical properties. For UDMA-MMA blends addition of even a small weight % of graphene or hydroxyapatite gave results indicating that mechanical properties are significantly

increased while viscosity can be tailored for the application. The enhanced mechanics are due to changes in bonding when the additives are present. Graphene provided a more significant increase in mechanical properties than hydroxyapatite as the additive. It is concluded that UDMA-MMA blends or UDMA-MMA blends with suitable additives are potentially a new and improved option for photo-cured dental adhesive system with the potential to avoid gap formation and microleakage.

ACKNOWLEDGEMENTS

I would like to express my deepest appreciation to my professors and colleagues in the Materials Engineering Department in University of Technology for giving me a chance to complete my PhD in USA.

Thank you to my supervisor professor Adrian B. Mann, who suggested this research topic, encouraged my development as an independent researcher, made himself readily available to discuss solutions, and helped me publish throughout my journey as PhD student.

I want to express my gratitude to professor Jennifer K. Lynch-Branzoi for guiding me in each step and helping me with writing, overcoming obstacles, and suggesting new ideas when I was stuck.

Thank you to professor Goel and his group for allowing me to use their lab. I would like to acknowledge the MSE administrative assistants, Nahed Assal and Sheela Sekhar, for helping me with any document details.

I would like to appreciate my second mother in Rutgers, Alex Bachmann- senior administrator for student service in graduate school, who always offered me guidance.

I am grateful to all my new friends here in the United States who have supported me along the way- Shawn Ward, Fred Foster, Marry Reiter, Ahmed Al-abdel Abass, Berra Beyoglu, Elaheh Taghaddos, Paul Kim, Hao Wang, Jessica Johnson, Michael Grzenda, Justin Hendrix, Arya Tewatia, Yoliem Miranda.

A special thank you to all my friends in Iraq, who supported me during my long journey across the seas, especially, Farah Flayyeh.

Finally, thank you to my family for encouraging me to finish my study in the U.S. I hardly have the words to express how important the support of my family has been. Thank you to

my niece and nephew (Shams and Ali) for always asking how my studies are developing and reminding me how much they miss me.

Mom, you are no longer with us but your spirit continued to strengthen me in my journey to complete my PhD. Thank you for your 30 years of love, care, and dedication that will last me a lifetime.

Dad, you are no longer with me but I remembered how you are thinking about me every day, how you are encouraging me. I'm pretty sure you are proud of me with getting my degree. Thank you for 38 years of support and love.

CONFERENCE PRESENTATIONS AND PUBLICATIONS

A portion of this thesis has been presented as a poster and presentation in conference proceedings.

Poster presentation

1. Zinah N. Alabdali, Jennifer K. Lynch-Bronzio, Adrian B. Mann "Improved adhesive materials for dental composite restorative," Biomedical Engineering Department- Rutgers University, December 13, 2018.

2. Emanuel Irizarry, Zinah N. Alabdali, Jennifer K. Lynch-Bronzio "Enhancement of dental adhesives with graphene and hydroxyapatite," Research Intensive Summer Experience, Rutgers University, July 31, 2019.

3. Emma Nichols, Zinah N. Alabdali, Jennifer K. Lynch-Bronzio, "New dental adhesive enhanced with graphene," May, 2020.

Conference presentation

Zinah N. Alabdali, Jennifer K. Lynch-Branzoi, Adrian B. Mann, "Effect of composition on nanomechanics of dental adhesive," 45th Annual Northeast Bioengineering Conference, Rutgers University, March 21, 2019.

Publications

1. Zinah N. Alabdali, Mary P. Reiter, Jennifer K. Lynch-Branzoi, Adrian B. Mann, "Compositional Effects on Mechanical Properties and Viscosity in MMA-UDMA Blends", International Journal of Adhesion Science and Technology

2. Zinah N. Alabdali, Emanuel Irizarry, Mary P. Reiter, Ali Ashraf, Jennifer K. Lynch-Branzoi, Adrian B. Mann, "Low weight fractions of graphene and hydroxyapatite enhance mechanics in photo-cured methacrylate adhesives", Journal of Applies polymer science

TABLE OF CONTENTS

LIST OF FIGURES

LIST OF TABLES

1 CHAPTER 1. INTRODUCTION

1.1 Background

Dental caries are the most common oral diseases, affecting a high percentage of the US population, and equally prevalent in all ages. Caries arise from destruction of dental tissues by acid produced by bacteria, and manifest as pain in the mouth, infection, and discoloration of teeth.

Materials such as amalgam and gold have traditionally been used to treat cavities. Amalgam, a mixture of mercury, silver, and copper, is considered an undesirable material because it has a high percentage of mercury, which is a toxic metal. Additionally, many patients do not appreciate its dark color and, for cosmetic reasons, would prefer a filling that matches the tooth's color. Gold is can be used and has good mechanical properties, but it is prohibitively expensive, and also introduces undesirable color.

Recently, light-cured composite resins have gained preference for filling cavities. These materials have better aesthetic properties than gold and amalgam, are easy to handle, and require minimum invasion of healthy dental tissues. A composite resin consists of two important parts: the matrix and additives (fillers). The matrix contains two or more monomers, which polymerize upon exposure to light. Additives in the composite resin are used to improve the mechanical properties of the matrix. However, composite resins suffer from gap formation (microleakage) at the interface between the composite and the tooth surface after curing and polymerization. This is as a result of polymerization shrinkage during conversion of monomer to polymer or from weak bond formation between the adhesive system, especially the composite resin, and dental tissues. This gap formation means it is then susceptible to bacteria and saliva penetration, causing secondary cavities

under the filler as shown in Figure 1.1. Research is underway to identify materials and methods to solve the shrinkage problem by improving the properties of the composite resin and the adhesive system, but the gap formation problem still exists in clinical application.

Figure 1.1. Longitudinal section of human tooth illustrating the gap and secondary cavity between the composite and human teeth [1].

1.1.1 Human Teeth

Human teeth are categorized into four types, these are incisors, canines, premolars, and molars. Each type of tooth has four layers, including enamel, dentin, pulp, and cement, as shown in Figure 1.2. Enamel is the outer hardest layer and is the most highly mineralized tissue in the human body. It contains about 90-92 % by volume inorganic materials, such as hydroxyapatite (HA), carbonate, potassium, and fluoride, as well as 1-2 % vol. organics and 4-6 % vol. water. Dentin is the second layer located under the enamel. This porous layer contains 50 % vol. of carbonated HA mineral, 30 % vol. of collagens and non-collagenous proteins, and water. The pulp layer occupies the pulp cavity in the tooth and is a unique, specialized organ of the human body made up of living connective tissue and cells called odontoblasts. Cement is a light-yellow, thin layer of the hard dental tissue covering the roots of the teeth [2].

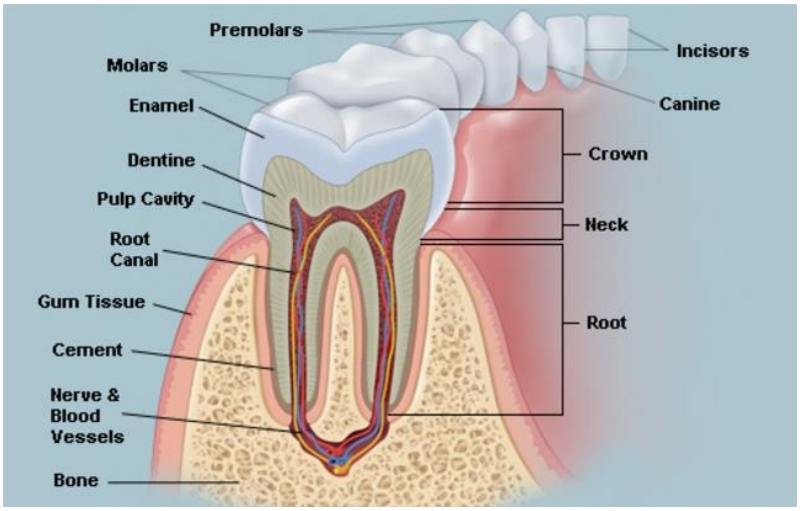

Figure 1.2. Longitudinal section of human teeth illustrating different types and layers [3].

The Dentin-Enamel junction (DEJ) is the interface between enamel and dentin [4] . It has a scalloping, or wave like, structure, which increases the surface area and permits a good bond between the outer layer (enamel) and inner layer (dentin). It is bridged by collagen fiber type I, which decreases the stress concentration during mastication [5].

1.1.2 Dental Caries

Dental caries is one of the most common diseases that occurs in teeth; it is a result of acid produced by bacteria, which leads to an imbalance between tooth mineral and saliva. This demineralization occurs in the tooth tissues with some ions like calcium, phosphate, and carbonate diffusing out of the tooth into the saliva. The demineralization process, that becomes dental caries, begins on the enamel and progresses through each tooth layer until it reaches the root [6], as shown in Figure 1.3. Caries can be detectable by feeling pain in the mouth, discoloration of the tooth enamel, and missing or damaged teeth [7]. Caries are classified into groups depending on their rate of progression (acute or chronic); tooth layer affected (enamel, dentin, cement); and their location (tooth type and position on cusp)[8].

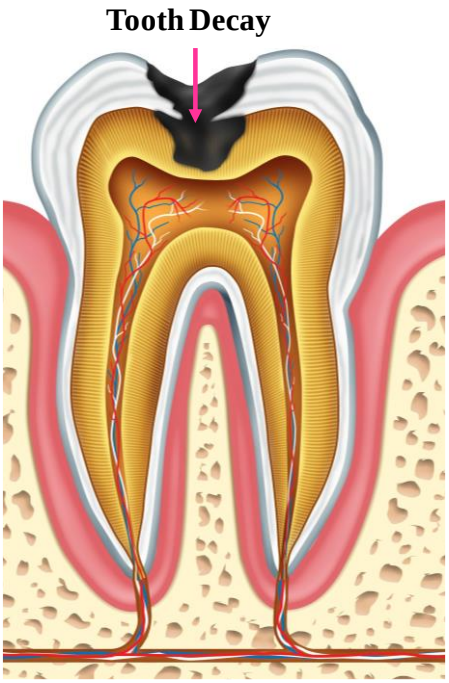

Figure 1.3. Schematic of dental caries (tooth decay) [9].

1.1.3 Clinical Procedure to Repair Dental Caries

The clinical procedure for filling cavities includes three steps: cavity preparation, application of adhesive system and restorative composite, followed by light curing [10], as shown in Figure 1.4. During cavity preparation, a rotary drill or hand tool is used to remove the damaged carious tissue which results in debris formation of crushed hydroxyapatites and fragmented collagen, known as the smear layer. The morphology and thickness of this smear layer depends on the size and location of the cavity. Once cleaned and prepared, an adhesive layer is applied followed by the restorative composite resin to fill the cavity. The adhesive layer is applied in an attempt to form a good bond between the tooth surface and the restorative composite, and hence it is vital in determining the future efficacy of the restoration.

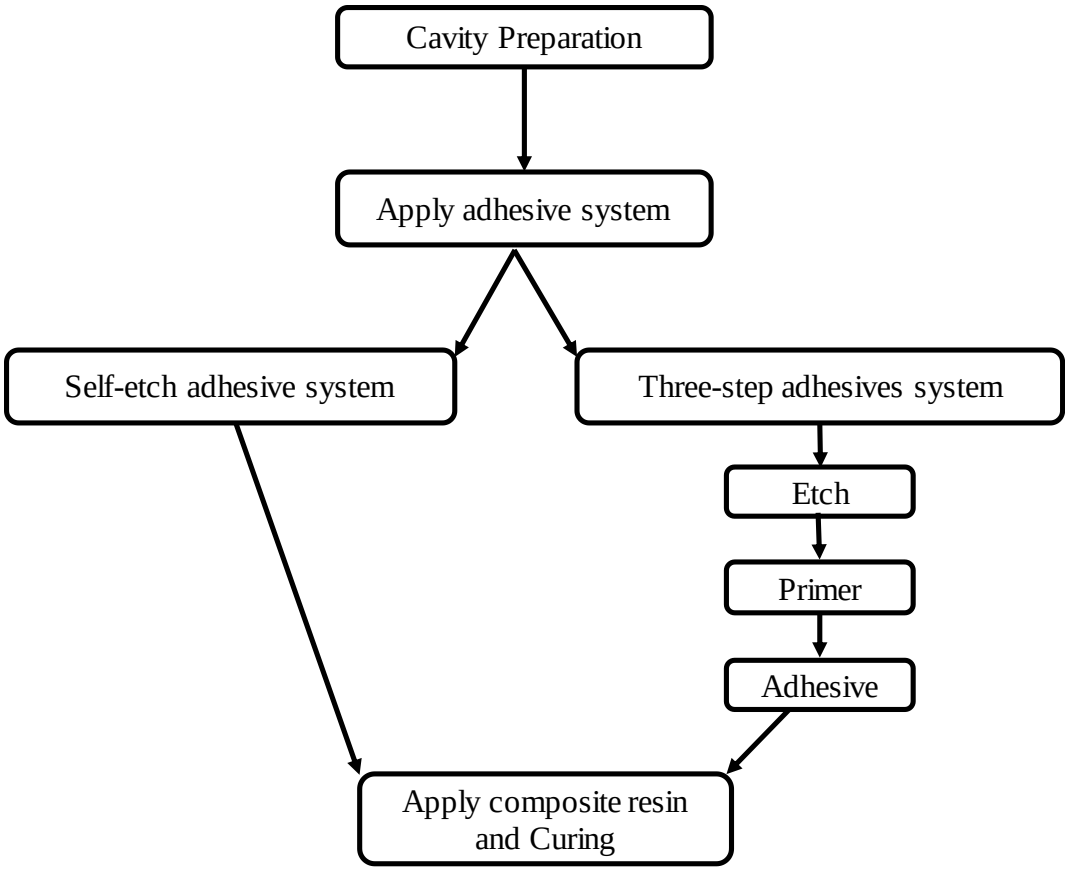

Figure 1.4. Schematic showing clinical procedure to repair dental caries

1.1.4 Adhesive Systems

The adhesive system, or bonding layer, is used to connect two substances. In dental applications, a good adhesive creates a strong bond to the surface of the tooth on one side and the composite on the other side, stabilizing it against mechanical force and preventing gap formation between the composite and tooth. Typically, the adhesive system is a low viscosity monomer, which penetrates into the dental tissues and forms a hybrid layer and resin tag that penetrates into the healthy dental tissues, as shown in Figure 1.5. The hybrid layer is the interface between adhesive and dental tissue (enamel, dentin) that forms as a result of chemical and mechanical bonding in this area. Resin tag formation occurs when the adhesive penetrates into the dentin tubules. Micromechanical and ionic bonding occur

as a result. The etching step of Figure 1.5 causes demineralization, which permits a pathway for the adhesive monomer to flow into the porous parts of the dental tissue, thus forming an interlock with the dental tissue, and creating a micromechanical bond. Further, ionic bonding should occur between the acid monomer and calcium in HA. Therefore, it is very important to use adhesive monomers with an affinity for HA to form a good hybrid layer and strong bond. If a good bond is not formed between the tooth surface and adhesive layer, the adhesive layer is more prone to shrinkage upon light curing which results in a gap forming between the tooth and adhesive [11].

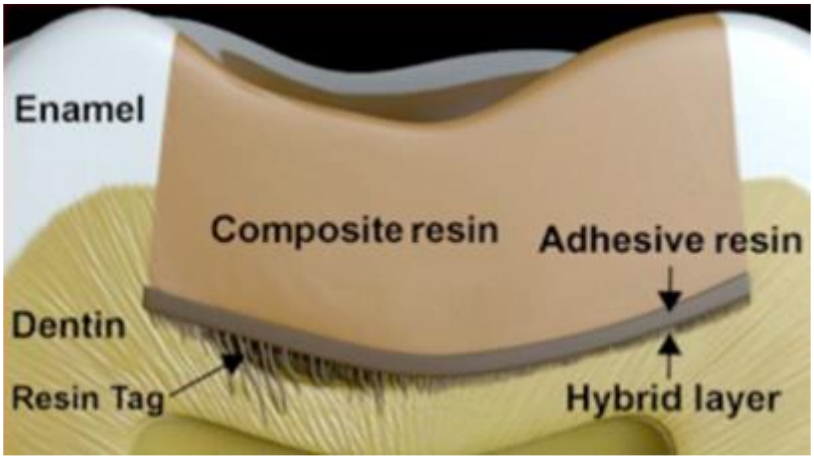

Figure 1.5. Composite resin–tooth interface, showing adhesive layer, resin tag, and hybrid layer between adhesive resin and dentin [12]

Different types of adhesive systems have been developed in an attempt to create the best bond and have been classified by the number of steps required for application, including one step, two-step, and three-step adhesive systems [13].

I. One-step adhesive system: The one-step system, or self-etch adhesive (as will be labeled going forward), is an “all in one “solution containing acid functional monomer with pH higher than phosphoric acid. Di- or multi-functional group monomers help to increase the strength of the matrix after polymerization and 2-

hydroxyethyl methacrylate (HEMA) monomers increase the wettability of the surface. In these products the etchant, primer, and adhesive are combined in the same solution; therefore, most dentists prefer this kind of adhesive because the application is simple, takes less time, and is less sensitive to handling [14].

II. Two-step adhesive system: two-step adhesive system has simplified the clinical procedure in to two steps. It can be etching in one step and primer with adhesive in another step or it can be etchant with primers in one step and adhesive in another step.

III. Three-step adhesive system: A Three step adhesive system consists of three different solutions namely etchant, primer, and bonding solutions.

- Etching is the first step, which contains phosphoric acid and acts to remove the smear layer and decalcify the area around the tubules structure in the enamel layer. The efficiency of this system depends on pH, viscosity, concentration, and time of application. The etching acid gives the best result with 30-40 % phosphoric acid; below these values gives less roughness.
- Primer resin is the second step, which is applied to increase the surface energy and wettability of the surface. It contains two functional groups, one hydrophilic and one hydrophobic. Hydrophilic functional groups have an affinity with the surface of teeth and hydrophobic functional groups with the composite resin.
- Finally, the bonding agent contains two or more monomers and initiator [15].

1.1.5 Composite Resin

Composite resins have been used to treat cavities and consist of two important parts: matrix (organic) and fillers (inorganic);

I. Matrix contains two or more monomers, initiator system, and stabilizer materials for storage. Biphenyl A glycol dimethacrylate (Bis-GMA) is a difunctional monomer typically used in the matrix. Bis-GMA is a large molecule with low volatility, low polymerization shrinkage, and a high molecular weight (512.599 g/mol.) leading to high viscosity. The viscosity of Bis-GMA is 1,000,000 mPa. /s at (23 °C) whereas the viscosity of water is ~ 1 mPa. /s at (23 °C). Consequently, many diluents are used to decrease the viscosity, like ethylene glycol dimethacrylate (EGDMA) and triethyleneglycol dimethacrylate (TEGDMA), as shown in Figure 1.6 [16].

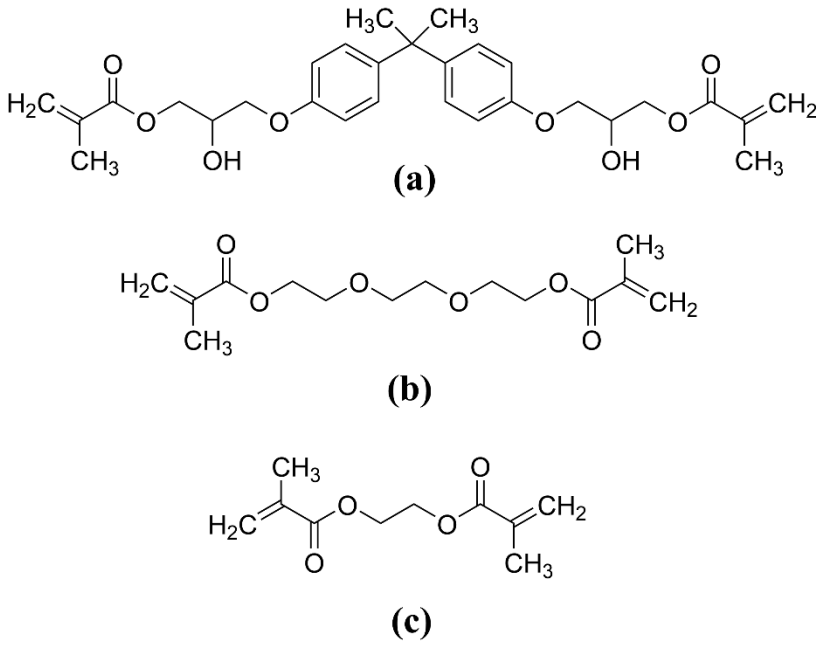

Figure 1.6. Chemical structures of cross-linking monomers used in dental application: (a) Bis-GMA; (b) EGDMA; (c) TEGDMA

II. Fillers are the hard material dispersed in the matrix for reinforcement. Quartz particles were the first types of filler used, followed by glass and ceramic materials. In general, the fillers improve mechanical properties of the matrix, but this depends

on the amount, shape, and size of the filler. A high percentage of fillers gives good mechanical properties, but there are limits to that because an increase in the percentage of filler leads to a decrease in wettability of monomers. Shape and size of filler also affect the properties of the matrix. For example, a higher surface area of fillers gives good mechanical retention within the matrix [17].

After application of the composite resin, light curing is used to polymerize the monomers. Polymerization is the process by which the monomers convert to a polymer. The monomer matrix contains carbon-carbon double bonds, which are unstable when exposed to light and convert to carbon-carbon single bonds, allowing crosslinking or covalent bonding to occur between monomer molecules to form a network of long polymer chains. The amount of conversion from double to single carbon-carbon bonds is quantified as degree of conversion (DC). Upon crosslinking, the distance decreases between covalent bonds that leads to an overall shrinkage of the polymerized composite resin, which may result in a gap formation between the composite and tooth [18]. This gap formation often leads to secondary cavities later, requiring another dental caries remedial procedure.

1.2 Current Research to Solve the Gap Formation Issue

1.2.1 Composite Resins

Numerous studies focus on solving the gap formation problem due to shrinkage of the composite resin post curing, including changing the matrix phase in different ways, using different monomers, and using different size and shape additives.

Bis-GMA is the most common monomer used in dental applications. This monomer has the best mechanical properties and less shrinkage than other monomers, but has high viscosity, which makes it difficult to handle. The high viscosity is related to the presence

of hydroxyl groups and aromatic rings in the chemical structure which increase intra-and inter-molecular bonding. Many studies focus on methods to decrease the viscosity of Bis-GMA.

The blending of Bis-GMA with a diluent like TEGDMA has been studied [19]. Different types, percentages, and molecular weights of diluents were mixed with Bis-GMA to investigate the effect of these variables on the viscosity. Although increased percentage of diluents led to a decrease in viscosity, while water sorption and volumetric shrinkage increased. Therefore, further research is needed to develop materials that meet these requirements [20].

The effect of chemical structure, or chain length, of the monomer on viscosity, polymerization shrinkage, and degree of conversion was investigated [21]. Ethoxylation and acetylation are the ways to increase the chain length. An increased chain length decreased the concentration of double bonds and reduced the polymerization shrinkage, but still the viscosity was very high compared with the base monomer(Bis-GMA)[22,23] .

In an attempt to solve viscosity and shrinkage issues, other dimethacrylate monomers were synthesized and studied as a substitute for (Bis-GMA). Results showed higher double bond conversion (higher degree of conversion) and lower polymerization shrinkage than the commercial products already described, but suffer from increased water uptake [24].

Moreover, B. Kusai and M. Rasha studied lowering monomer viscosity by changing the chemical structure. They used hydroxyl free (Bis-GMA) instead of TEGDMA as a diluent, which helped with the problem of viscosity, but increased water sorption [25].

Fluorinated dimethacrylate monomer (FUDMA), instead of Bis-GMA, has been blended with diluents in some studies. The results show FUDMA has better double bond conversion, less volumetric shrinkage, and less water sorption, but it still needs more studies to check biocompatibility [26,27].

Expanding monomers exhibit high volume expansion due to ring opening in their structure during polymerization [28]. The addition of these types of monomers with methacrylate monomers reduces the polymerization shrinkage and concentration stress, but biocombatibility still needs further study [29-31]. Expanding monomers were blended with epoxy and acrylate monomers, decreasing the shrinkage, but also decreasing degree of conversion [32]. Liquid crystalline epoxy resin expands during photopolymerization and was used as an organic matrix to lower shrinkage, with results showing better physical and chemical properties than commercial products [33].

Many researchers focus on the effect of particles, or fillers, in the matrix to mitigate shrinkage upon photopolymerization. In general, high filler concentration is associated with lower polymerization [34] because monomer concentration decreases [35]. Filler size and shape also affects shrinkage of the matrix. Spherical particles cause less shrinkage than irregular-shaped particles, which may be related to the difference in the degree of conversion between the particles [36]. The degree of conversion is correlated with shrinkage, which is affected by particle size, increasing spherical of particle size decrease shrinkage [37,38]. As well as the degree of conversion affected by the amount of additives, increase the percentage of additives decrease the degree of conversion as well as the polymerization shrinkage [39]. The fillers also influence the light transmission during the

curing process, with small particles causing a significant reduction in light transmission [40].

1.2.2 Photoinitiators

The influence of different types of photoinitiator on the degree of conversion and microleakage has been studied [41]. Increasing photoinitiator concentration causes increased rate of polymerization, resulting an increased degree of conversion and hardness. Increasing photoinitiator concentration dose give a high degree of conversion, however, in some cases, yellowing, shrinkage stress, and microleakage increased [42].

1.2.3 Adhesive System

The adhesive layer is used to bond the composite resin with the enamel and dentin, and to resist the stresses generated as a result of polymerization shrinkage of the composite. Several authors have focused on the properties of self-etch adhesives. One of these studies concentrated on how the tensile bond strength changed with single or multiple consecutive applications. The highest tensile bond strength was obtained with two alternate applications of the adhesive [43]. Adding filler to the self-etch adhesive system had no influence on the microleakage because the unfilled system infiltrated into the dental tissues better than the filled adhesive [44]. Moreover, phosphoric acidic ester monomers with different chain lengths were studied in the self-etch adhesive system. Long chain length had the best chemical interaction with dental tissues, giving a thicker hybrid layer, and better bond between adhesive and tooth [45]. More hydrophilic functional monomers in self-etch adhesives give higher wettability, but more water uptake, which also gives lower bonding durability [46].

1.3 Objectives of this Research

The main motivation of this study is to develop materials and methods that achieve better bonding between the composite and the surface of the tooth (enamel and dentin) by improvement in the chemical and mechanical properties of the adhesive layer. This will subsequently minimize gap formation and avoid the gap issue, as shown in Figure 1.7.

In this study, Diurethane dimethacrylate (UDMA) monomer was used as a high molecular weight monomer. A low molecular weight monomer, namely Methyl methacrylate (MMA) was used as diluent. Graphene and Hydroxyapatite were used as additives with several different concentrations used.

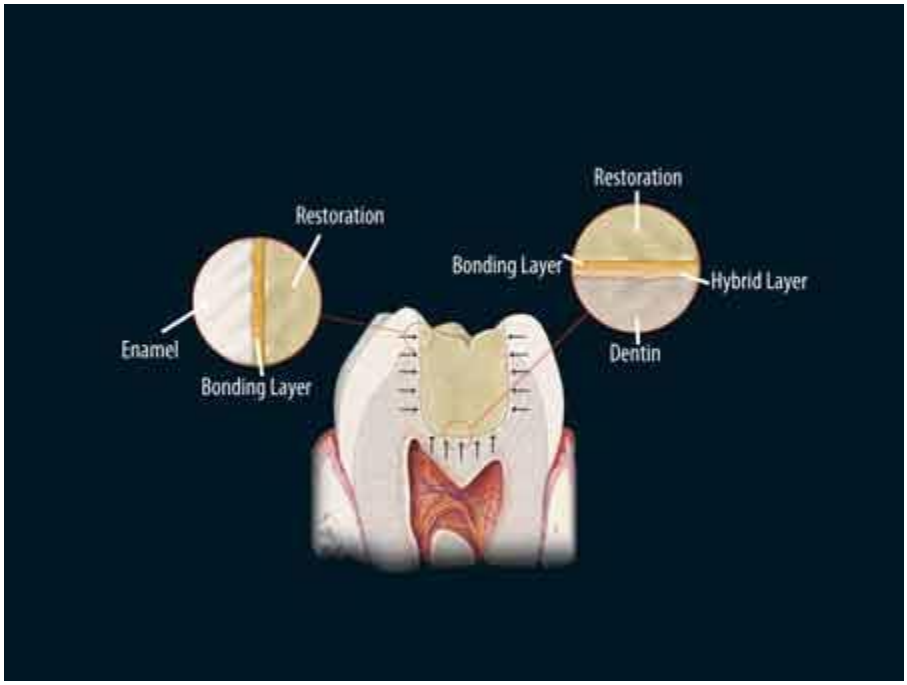

Figure 1.7. Image shows the bonding layer between restorative and dentin and the bonding layer between enamel and restorative [47]

2 CHAPTER 2: PRELIMINARY INVESTIGATION OF COMMERCIAL ADHESIVE SYSTEMS

2.1 Background

Photo-cured commercial adhesive systems were investigated, a self-etch adhesive system and a three-step adhesive system, with each being applied to cow teeth, and characterized. The self-etch adhesive system shows a gap between the adhesive and enamel layers, and between the adhesive and dentin layers. The three-step adhesive system show a weak bond between adhesive layer and the tooth with low mechanical properties. In this study these issues were addressed using two different additives, including graphene and hydroxyapatite, to optimize mechanical properties of the three-step adhesive system. The commercial adhesive systems when applied on cow teeth were characterized by helium ion microscopy (HIM), atomic force microscopy (AFM), scanning electron microscopy (SEM), and nanoindentation.

Cow teeth were used instead of human teeth in this research because; (1) it is easy to get a sufficient number of cow teeth from the same animal; (2) a cow tooth has a large flat surface, which makes characterization methods easy; (3) cow teeth have more uniform composition than human teeth; (4) the micromorphology of cow and human teeth are similar in that each have a similar number of tubules in the structure (although the diameter of enamel crystallites in cow teeth is larger than in human teeth); (5) cow and human teeth have a comparable ratio of calcium/phosphate at 37.9 % and 36.8 %, respectively [48].

2.2 Selected Adhesive Systems

2.2.1 Self-Etch Adhesive System

A self-etch adhesive system was purchased from 3M ESPE dental products, in a 5 mL bottle size and used directly without any additives.

2.2.2 Three-Step Adhesive System

Three-step adhesive system was purchased from 3M ESPE-Scotchbond Multipurpose, including a primer (#7542, 8ml) and an adhesive (#7543, 8ml). The primer contains water, 2-hydroxylethyl methacrylate, copolymer of itaconic-acrylic acid. The adhesive contains Bis-GMA, 2-hydroxylethyl methacrylate, Triphenylantimony. The three-step adhesive system was applied to cow teeth without any additives, as well as with two types of additives, Graphene (G) and Hydroxyapatite (HA) to optimize mechanical properties.

Graphene (G) is a honeycomb lattice composed of a single layer of carbon arranged in a hexagonal shape. The carbon atoms are covalently bonded to one another. Graphene has large surface area, strong van der Waal forces, carbon bonds, and chemical stability, and the aromatic nature of the bond makes it a good reinforcement agent in a polymer matrix. Graphene has unique mechanical, optical, thermal, and electrical properties, and for these reasons graphene is being studied for use in many applications [49].

Graphite was purchased from Asbury Carbons (Asbury, NJ, USA) and converted to graphene by thermal expansion using a microwave treatment (1100w, 1 min), followed by ultrasonication for one hour, and then drying at 80 ◦C overnight. The dry material was ball milled for 96 hours with a zirconia medium, then washed with a solution of 1:1 ratio deionized water: methanol, before drying again at 80◦C overnight, and finally sieving with

different meshes down to 320 mesh (63 micron). The graphene flakes were characterized using SEM.

HA is used as a filler for reinforcement in medical applications because it is the form of calcium and phosphate found in mineralized human tissues. HA is used in dentistry because it is biocompatible, can chemically bond with HA already present in cow teeth, and has the ability to bond strongly with proteins. HA comes in different shapes, including spherical, whiskers, and fibers [50,51]. For this work, HA was purchased from Sigma Aldrich (St. Louis, MO USA) as a nanopowder (< 200 nm particle size, 502.31 g/mol Mw.) and used without any purification.

2.3 Sample Preparation

2.3.1 Cow Teeth Substrate Preparation

Cow teeth were extracted from bovine skulls using pliers and a hammer, washed with tap water to remove blood, and then brushed to take off all the tissue cells remaining on the surface of the teeth. The teeth were cut to suitable sizes with an electrical saw (Dremel 200- Two Speed Rotary Tool) and then washed again to remove the debris after cutting. The surface of the tooth was ground with 400, 600, 800, and 1200 grit silicon carbide papers and then polished with diamond paste of particle size 10, 7, 5, 3.5, 2.5, 1, and 0.5 microns with a speed of 300 RPM. The teeth were kept in Hank's balanced salt solution (HBSS) purchased from Sigma Aldrich.

2.3.2 Cow Teeth Preparation with Self-Etch Adhesive System

The self-etch adhesive system was applied directly on the cow teeth. It was applied on the top surface of the teeth and spread with brush for 5 sec until the film no longer moved and then cured for 20 sec by light with a wavelength of 420-480 nm (hereafter

called light cure). The composite resin Z100 was applied on top of the adhesive layer with 2 mm thickness and polymerized by light cure for 30 sec. The composite resin Z100 was purchased from 3M ESPE dental products and contains Bis-GMA and TEGDMA with 66 % vol. zirconia/silica as the filler with particle size range from 3.5 to 0.01 μm and shade A1. Cold mounting was used to mount the samples by mixing 1 part by volume of fast cure acrylic powder with ½ acrylic liquid and mixing it together until the powder dissolved (Buehler sample-kwick- powder and liquid). The plastic mold was cleaned and lubricated in order to take out the samples easily. The samples were put in the mold and the acrylic mixture was poured above the samples and left for one day to fully cure. The samples were extracted from the molds and polished with 400, 600, 800, 1200 Grit Silicon Carbide Paper then with 10, 7, 5, 3.5, 2.5, 1, 0.5-micron diamond paste and kept in Hank's balanced salt solution (HBSS). The self-etch adhesive system was applied to cow teeth with different thicknesses in the same procedure as above to study the relationship between thickness of adhesive layer and mechanical properties of the adhesive.

2.3.3 Cow Teeth Preparation with Three-Step Adhesive System

First, the three-step adhesive system was applied to cow teeth. Sample preparation included:

1) etchant step, an acid etchant (Gel- 37% phosphoric acid) was applied to the cow tooth surface for 25 sec and washed with water,
2) a layer of primer was applied on the cow tooth and left for 5 sec to dry
3) a brush was used to apply the adhesive system on top of the primer layer and exposed to light cure for 10 sec

4) composite restorative Z100 was applied on top of the adhesive and polymerized with light cure for 30 sec
5) all the samples were stored in Hank's solution until the test.

Secondly, the three-step adhesive system with additives, hydroxyapatite (HA) and graphene (G) was applied to cow teeth. Five different weight percentages of HA were added to 2000 mg of primer and 2000 mg of adhesive separately as shown in Table 2.1. Samples were mixed using a shaking table in a dark room overnight with speed 250 rpm to get good dispersion. Five different weight percentages of graphene were added to 2000 mg of primer and 2000 mg of adhesive separately as shown in Table 2.2 and mixed using the method shown in Figure 2.1 for 1 min in a dark room. Lower weight percentage of graphene was used compared with weight percentage of hydroxyapatite because of difficult to mix. The components were submerged in a water bath to maintain low temperatures. Then, the same application procedure in steps 1-5 above were followed.

Table 2.1 Different weight percentage of HA to the primer and adhesive.

Sample No.	**Amount of HA in Primer mg (wt. %)**	**Amount of HA in adhesive mg (wt. %)**
1	5.3 (0.25)	5.3 (0.25)
2	10 (0.50)	10 (0.50)
3	15 (0.75)	15 (0.75)
4	20 (1.00)	20 (1.00)
5	25 (1.25)	25 (1.25)

Table 2.2 The weight percentage of graphene to the primer and adhesive

Sample No.	Amount of G in Primer mg (wt. %)	Amount of G in adhesive mg (wt. %)
1	1 (0.05)	1 (0.05)
2	2 (0.10)	2 (0.10)
3	3 (0.15)	3 (0.15)
4	4 (0.20)	4 (0.20)
5	5 (0.25)	5 (0.25)

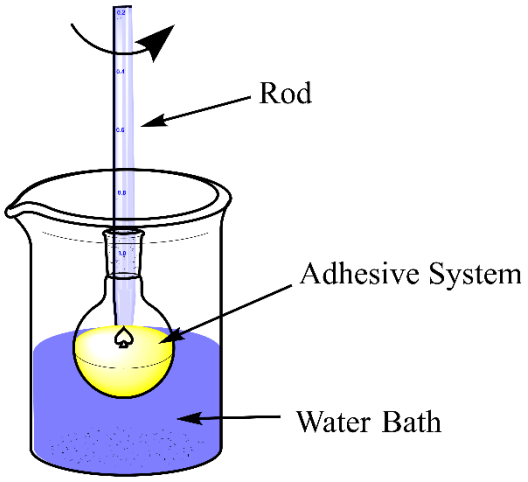

Figure 2.1. Mixing process to disperse graphene in adhesive system

2.4 Characterization Methods

2.4.1 Nanoindentation

A Hysitron TriboIndenter ™ (USA) was used to measure the mechanical properties, including hardness (H in GPa) and indentation modulus (Er in GPa, also called reduced modulus) for the prepared adhesive systems. A Berkovich diamond tip was used with a three pyramidal shape and average radius of curvature approximately 20 nm. The

maximum load in this machine is 30,000 µN and the maximum displacement is 5µm. The load-displacement curve, Figure 2.2 shows the loading and unloading on fused silica; the loading curve represents the tip penetrating into the sample surface. Unloading curves represents the tip being retracted. Stiffness is the slope of the unloading curve as shown in Figure 2.2[52]. Nanoindentation was used to measure the hardness and indentation modulus in the composite-adhesive-enamel junction and composite-adhesive-dentin junction using 3,000 µN peak load with a 5x5 nanoindent pattern and 10 µm distance between each indent to avoid residual stress from the previous nanoindent. Furthermore, nanoindentation was used to measure the mechanical properties of the cow teeth at different positions using 3,000 µN peak load with a 7x8 nanoindent pattern and 10 µm distance between each indent.

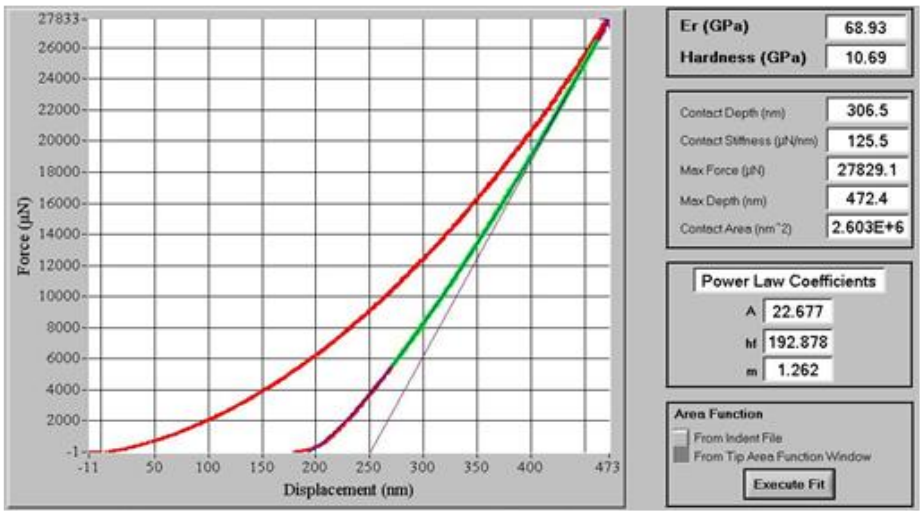

Figure 2.2. An example Load – displacement curve of fused quartz

2.4.2 Scanning Electron Microscopy (SEM) with Energy Dispersion Spectroscopy (EDS)

A Zeiss sigma field emission SEM with EDS was used to view the morphology of the cow teeth layers and measure the graphene flakes, which are used as additives for the

three-step adhesive system. SEM with EDS were used to determine the chemical composition of the dentin and enamel layers of cow teeth, in order to determine if the chemical composition affects the bond with the adhesive. Cow teeth samples were coated with the self-etch adhesive followed by the dental composite (as described in section 2.3.2), mounted on aluminum studs, and gold coated with a 10 nm thick gold coating (since the samples are not conductive), and stored in a vacuum desiccator overnight to remove the moisture. Prepared graphene flakes were fixed on an SEM pin mount without gold coating, since graphene is conductive.

2.4.3 Atomic Force Microscopy (AFM)

An NX-Hivac atomic force microscope (AFM) by Park (Santa Clara, CA 95054) was used to investigate the morphology of the cow teeth. The cow tooth was prepared using the same procedure described in section 2.3.2 and used directly without adhesive layer. The AFM images were taken over an area of 30 x 30 μm at a resolution of 256 pixels for all the area.

2.4.4 Helium Ion Microscopy (HIM)

HIM was carried out using a Carl Zeiss Orion plus helium ion microscope (Carl Zeiss Gmbh, Germany) operating at 30 keV acceleration voltage with a beam current of approximately 0.5 pA. HIM is a new technique similar, but with higher spatial resolution than other techniques like SEM. Ion beam microscopy supports research in different fields because of its high resolution imaging, small area of focus, high depth penetration into the sample, high brightness [53] and no need to coat the sample with gold as in SEM. The cow teeth were prepared in the same way as described in section 2.3.2 and stored overnight in a vacuum desiccator to ensure moisture removal. The cow teeth with the self-etch adhesive

system were using microscopy with a focus on the areas between adhesive-enamel and adhesive-dentin.

2.5 Results and Discussion

2.5.1 Cow Teeth Results

2.5.1.1 SEM

EDS was used to determine elemental composition of the dentin and enamel layers in cow teeth, as shown in Figure 2.3. Each peak represents a specific element, and the intensity of the peak is related to the quantity of this element. EDS results indicate that the enamel layer has a higher percentage of inorganic material, like calcium, when compared with dentin. Higher concentration of inorganic material increases the hardness, which means enamel has a higher hardness than dentin, and it is potentially possible to form a stronger bond with enamel than dentin. Figure 2.4 show the SEM image of graphene flakes. The diameter of the graphene flakes ranges from approximately 5-50 µm based on SEM.

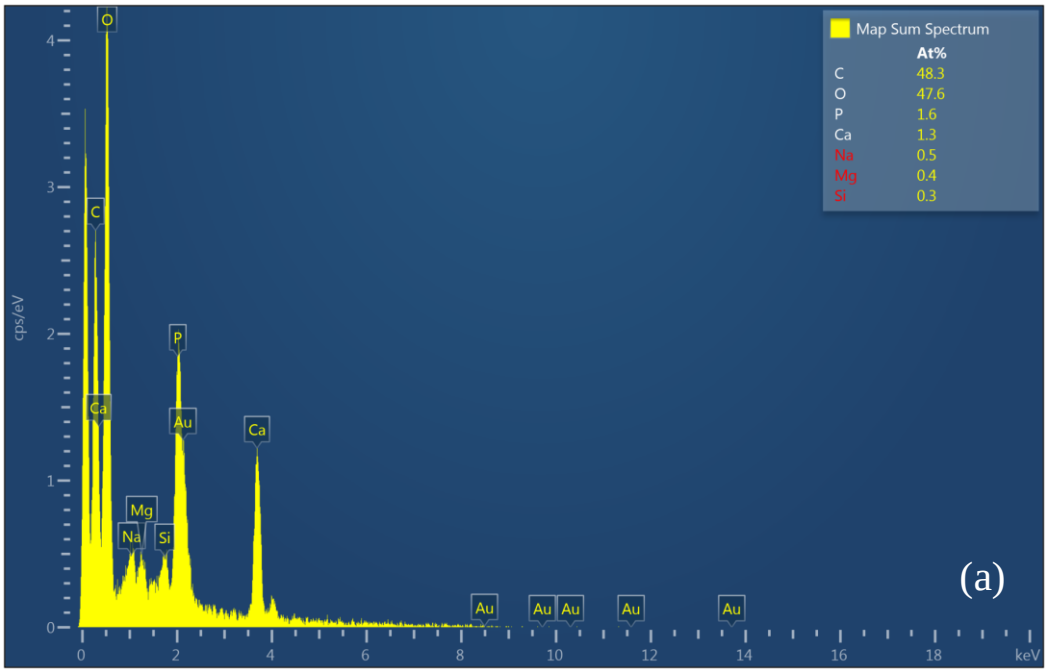

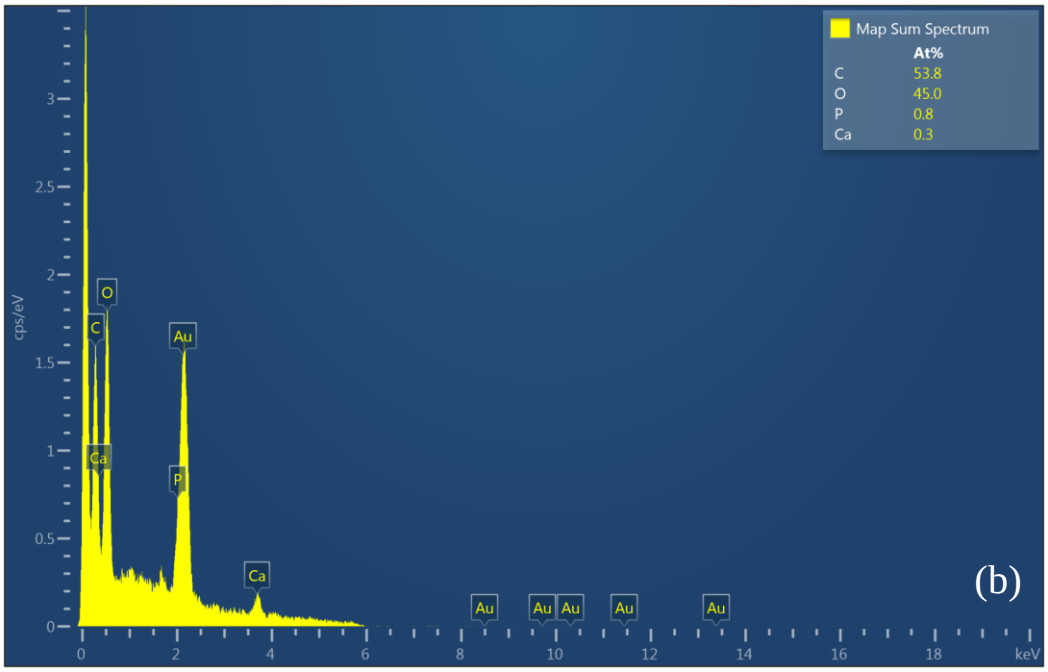

Figure 2.3. EDS results of cow teeth layers (a) enamel layer and (b) dentin layer

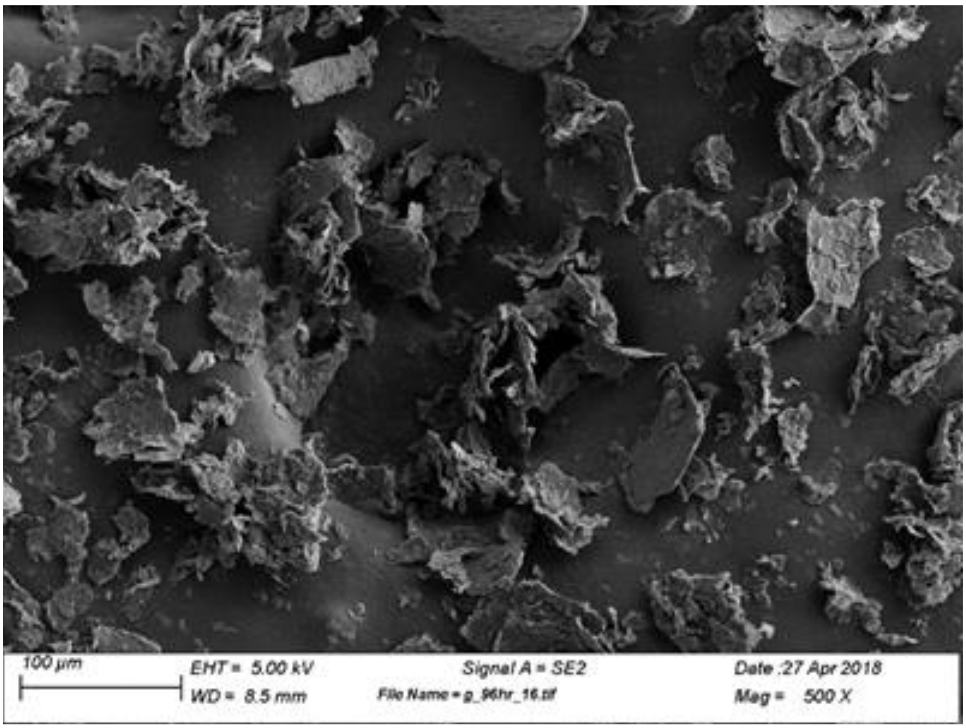

Figure 2.4. SEM image illustrate the graphene flakes

2.5.1.2 AFM

AFM results for cow teeth are shown in Figure 2.5, these show the topography differences for enamel and dentin layers. The results show the expected porosity in dentin and, hence, a higher percentage of inorganic material in the enamel than dentin, matching the previously shown EDS results. The dentin layer contains a relatively larger quantity of protein so it has a high percentage of organic material, as well as porous (tubules), and is in general more porous than the enamel layer. Thus, it should be easier to form a uniformly strong adhesive bond to enamel, but the resin tags described in chapter 1 are more likely for the dentin-adhesive layer.

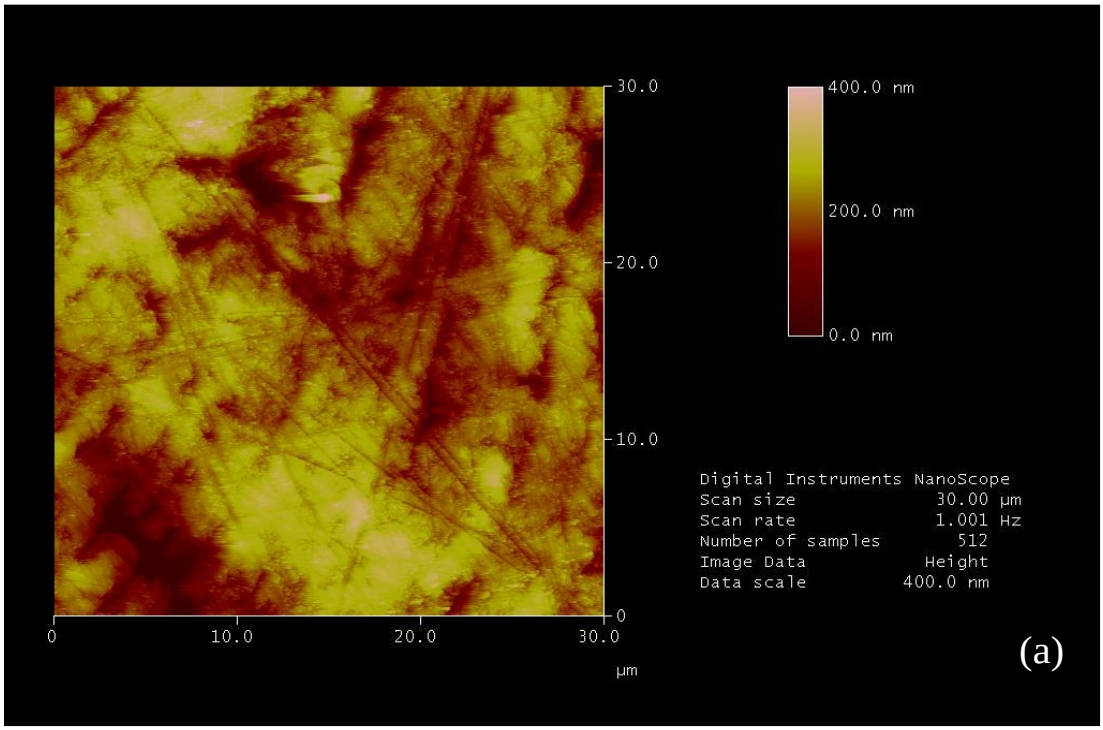

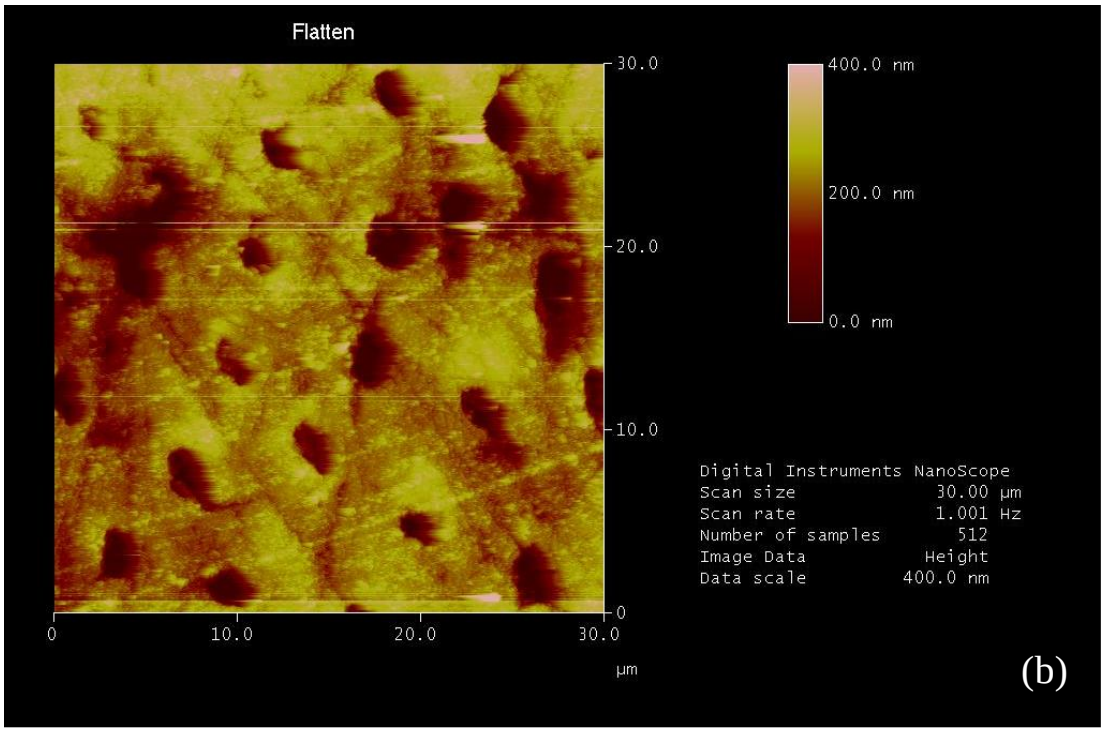

Figure 2.5. AFM results of cow teeth; (a) enamel layer, (b) dentin layer

2.5.1.3 Nanoindentation

The nanoindentation test was used to characterize the mechanical properties of the cow teeth's different layers (enamel and dentin). The nanoindentation results for cow teeth show that the mechanical properties of the enamel layer are higher than dentin layer, which is attributed to the difference in porosity and chemical composition between the enamel and dentin layers as illustrated in ESD results. Moreover, the mechanical properties within the same layer vary, as shown in Table 2.3 and Figure 2.6, which is similar to the mechanical property results of human teeth found in the literature [54]. The mechanical properties values, which are includes hardness and indentation modulus within enamel layer is 3.13 GPa and 20.54 GPa respectively. While, the mechanical properties within the same dentin layer differ with the minimum mechanical properties occurring toward the junction area.

Table 2.3. The nanoindentation results of three different position on the dentin layer

Position	H (GPa)	Standard error	Er (GPa)	Standard error	Depth (nm)
1	0.68	0.05	8.19	0.33	1057.90
3	0.98	0.01	10.38	0.12	851.59
2	1.05	0.02	10.9	0.09	766.13

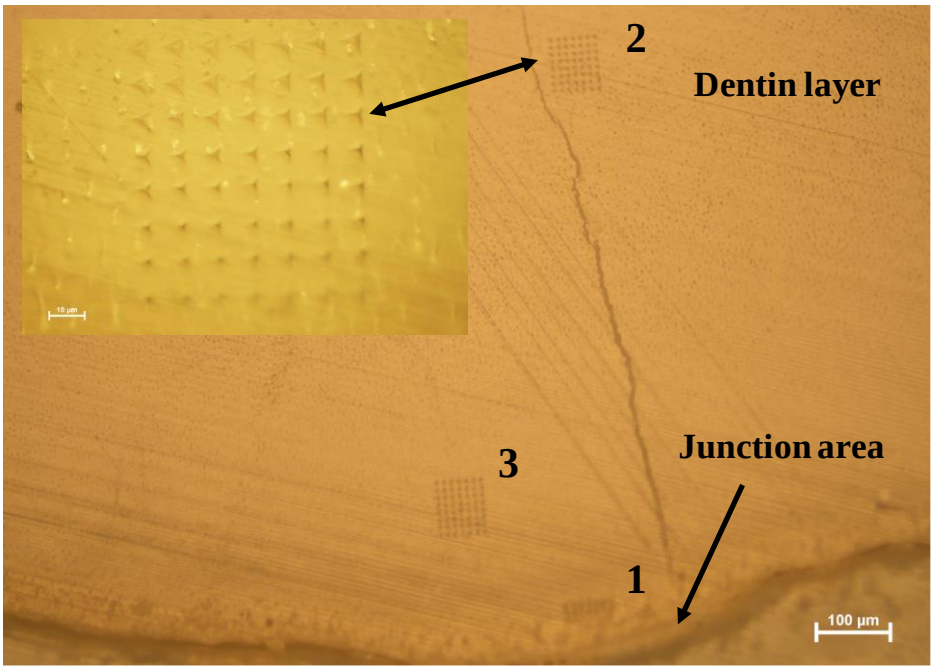

Figure 2.6. Nanoindents of three different locations in dentin layer

2.5.2 Commercial Adhesive System Applied on Cow Teeth

2.5.2.1 HIM

HIM images of the self-etch adhesive system applied on cow teeth are shown in Figure 2.7 for the composite-adhesive junction area (a, b), adhesive-dentin junction area (c), and adhesive-enamel junction area (d). These illustrate that there is no gap between the composite-adhesive junction indicating a strong bond, as shown Figure 2.7 (a, b). However,

a gap did form at the dentin-adhesive and enamel-adhesive junctions, with the largest gap occurring at the dentin-adhesive junction area, as shown in Figure 2.7 (c, d). As previously mentioned in the EDS and AFM results, the dentin layer has a higher percentage of organic materials than the enamel and the dentin layer is more porous than the enamel, because of this the dentin is relatively weak and the bond strength at the adhesive-dentin junction is low. In this case, the gap arises due to the weak adhesive bond on the tooth surface combined with the polymerization shrinkage of the restorative Z100 composite resin Figure 2.8, illustrate the gap formation that occurred with the three-step adhesive at the dentin junction. This is seen even without application of the composite resin which can create stresses due to shrinkage. However, all polymers can shrink as they cure and the adhesive layer may also shrink and pull-away from the dentin. This gives rise to a damaged dentin-adhesive junction layer with gaps and voids in it, as seen in Figure 2.8.

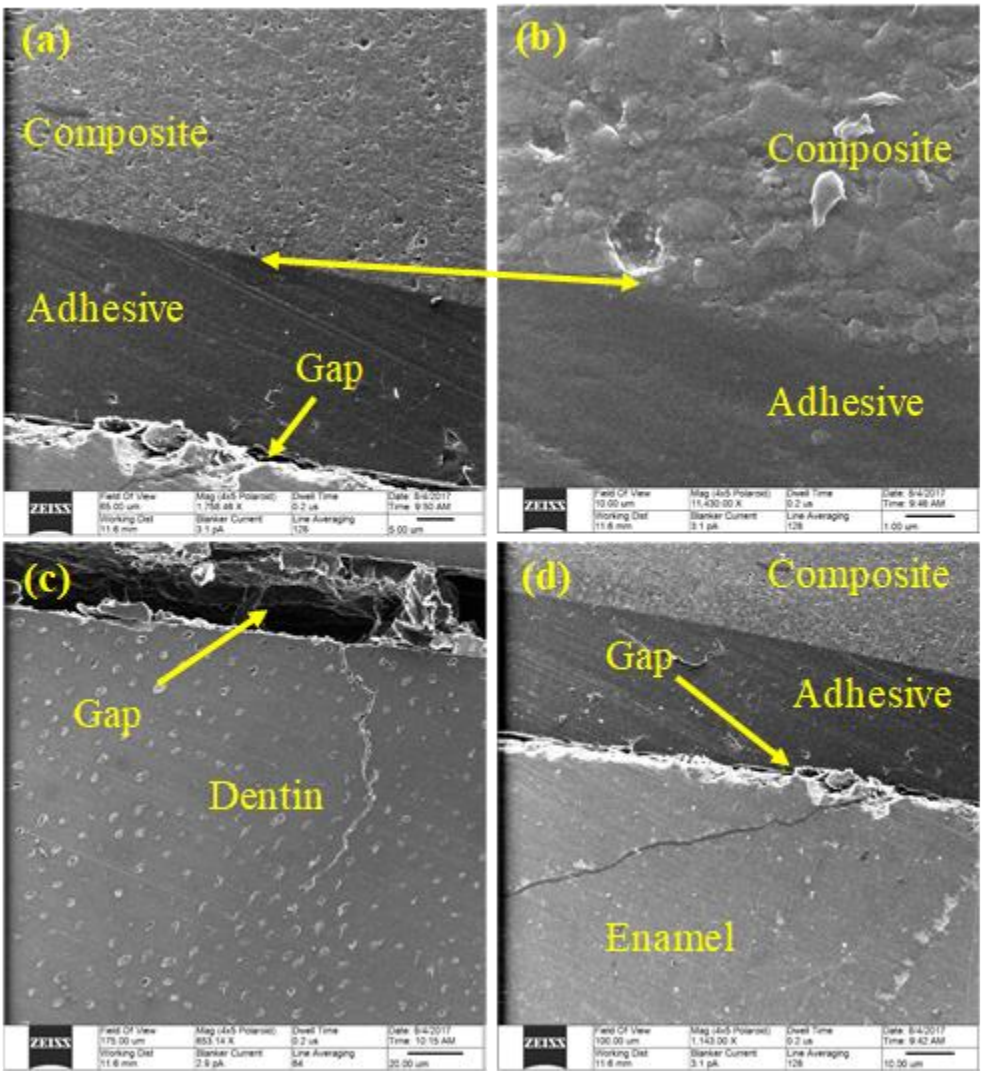

Figure 2.7. HIM images of cow teeth with self-etch adhesive system: (a) composite-adhesive junction area; (b) high magnification of the composite-adhesive junction area; (c) adhesive-dentin junction area; (d) adhesive-enamel junction area

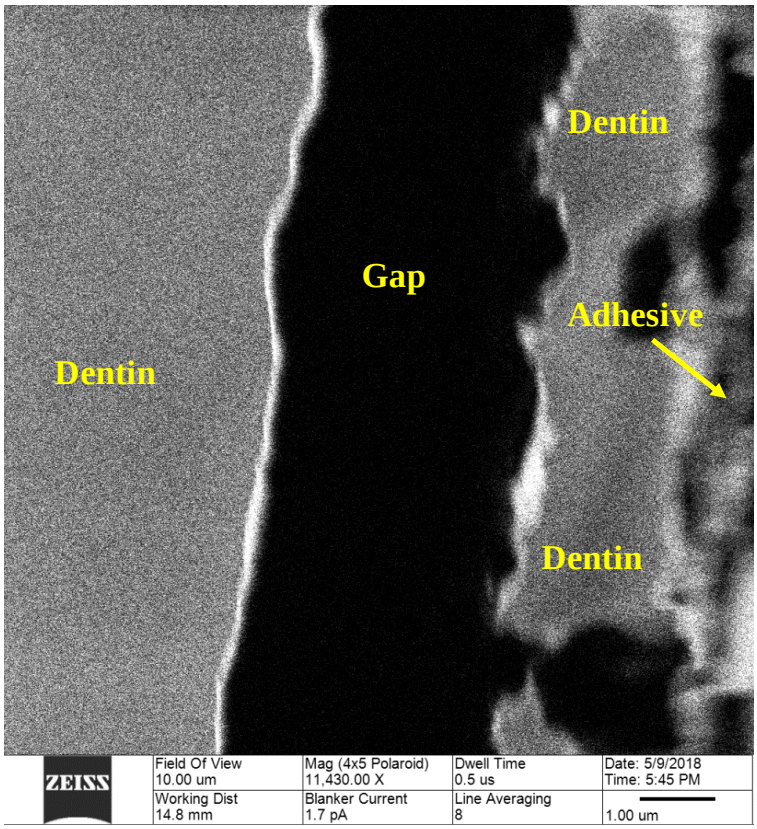

Figure 2.8. HIM images of three-step adhesive system on cow teeth without composite

2.5.2.2 Nanoindentation

Nanoindentation results for the self-etch adhesive system on the cow teeth are shown in Figure 2.9 (Hardness) and Figure 2.10 (Indentation Modulus) for the different layers, including composite (C), enamel (E), dentin (D), enamel-composite junction area (E-C), and dentin-composite junction area (D-C). The hardness and indentation modulus appear to follow similar trends that depend on layer tested. Results show that hardness is highest for the enamel, as expected based on the chemical composition and structure results determined from EDS and AFM for dentin and enamel.

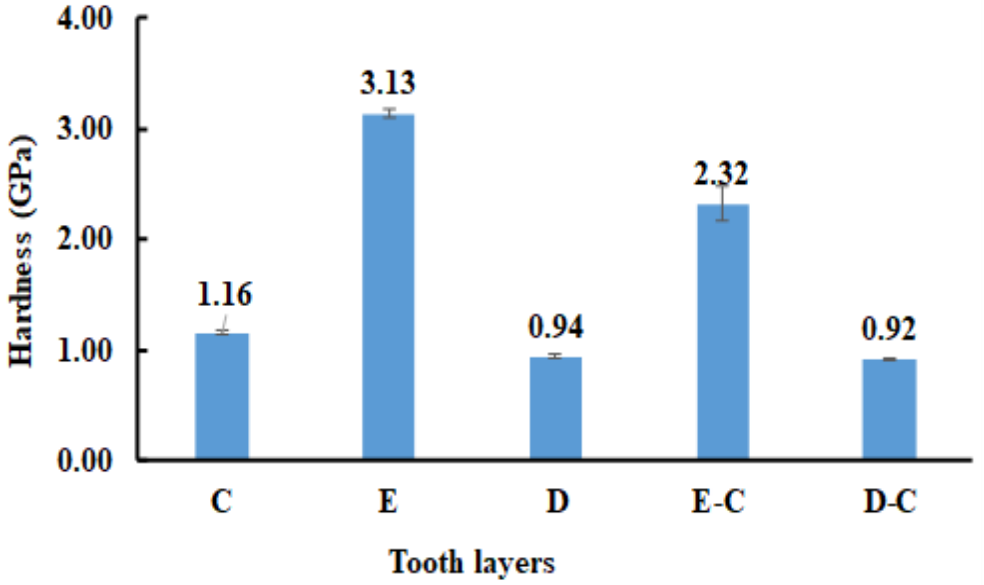

Figure 2.9. Hardness results of self-etch adhesive system on cow teeth in different regions and layers

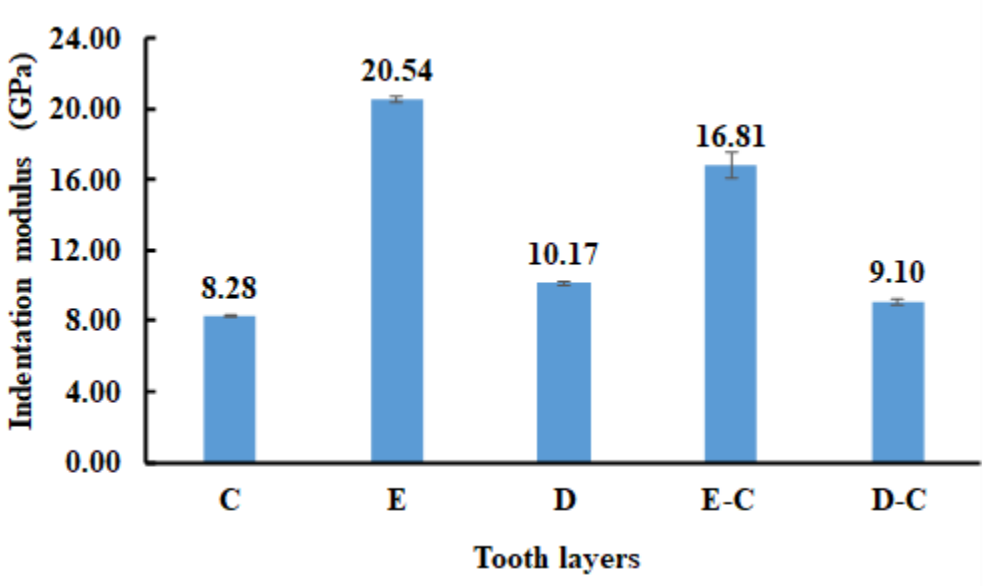

Figure 2.10. The indentation modulus results of self-etch adhesive system on the cow teeth in different regions and layers

Nanoindentation results for the self-etch adhesive system applied with different thicknesses as shown in Figure 2.11. Increasing the thickness (for instance increasing the number of adhesive layers applied) decreases hardness and indentation modulus. This suggests that it is not useful to apply more than two layers of adhesive. However, applying one layer is insufficient to cover the whole surface, but applying three layers, the stress created as it contracts during curing is greater the thicker adhesive layers. The same result was found in the literature for a self-etch adhesive system applied in consecutive applications [55].

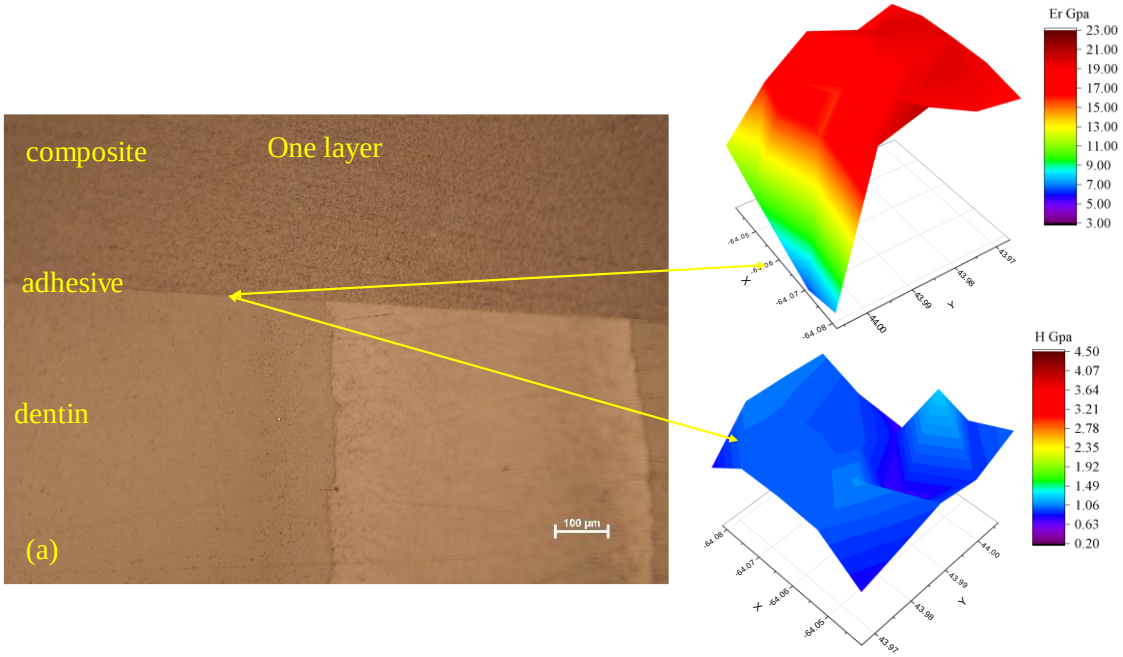

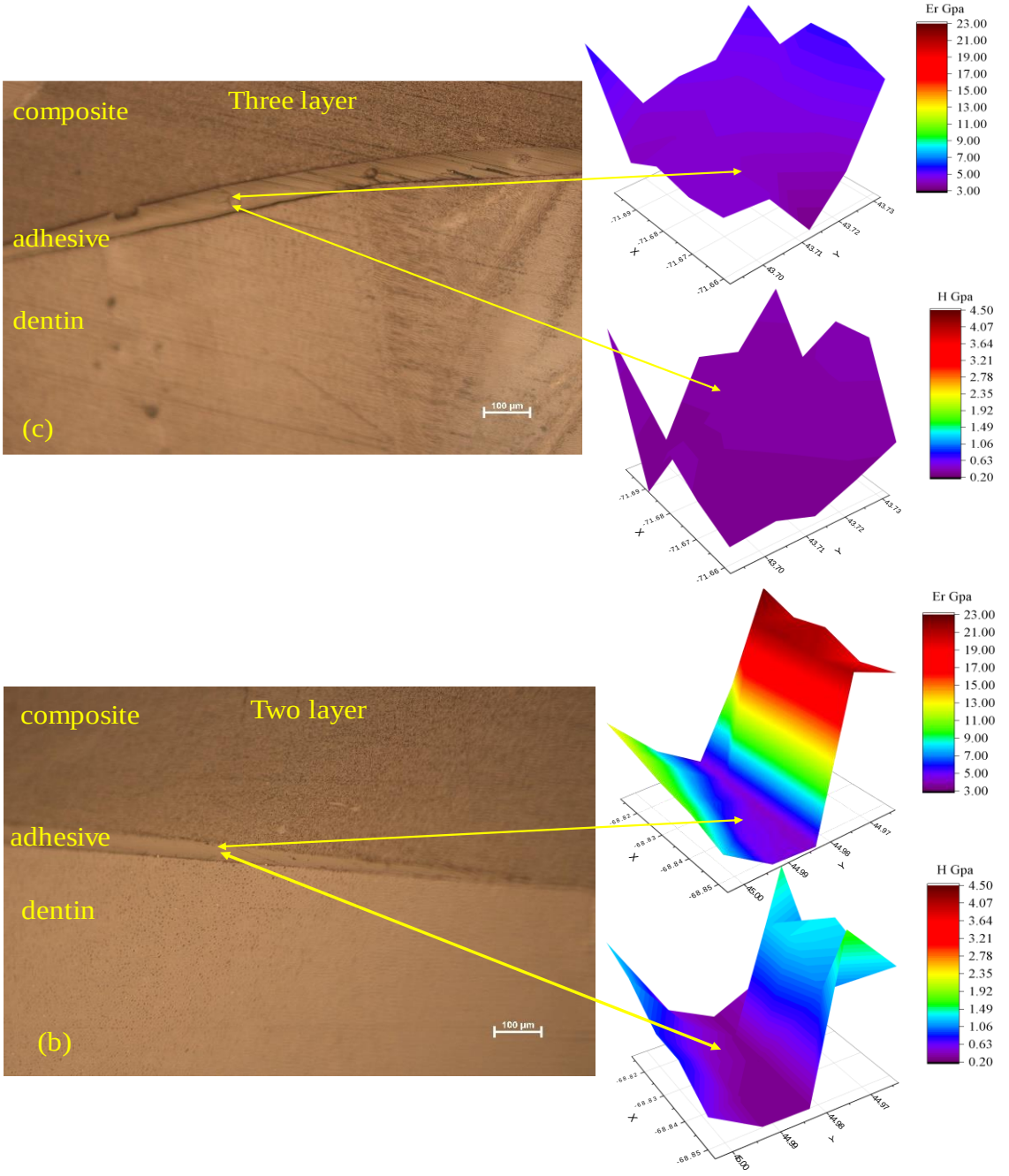

Figure 2.11. Nanoindentation results (Hardness, H, and Indentation modulus, Er) of self-etch adhesive system with different thicknesses (a) one layer, (b) two layers, and (c) three layers

Nanoindentation results for the three-step adhesive system applied on cow teeth and the three step adhesive system reinforced with either graphene or HA applied on cow teeth are shown in Figure 2.12 and Figure 2.13. Results show very low hardness and indentation modulus in the junction area with enamel and dentin for the unreinforced three-step adhesive. The addition of HA to the three-step adhesive system increases the mechanical properties of the junction area due to the relatively high hardness value of HA. The demineralization process decrease after applying the HA reinforced adhesive layer to the surface of tooth that creates an enhanced bond process. A similar result was also found in the literature after addition of 45S5 glass to the adhesive, this also increased hardness [56]. The effect of HA on the three-step adhesive system is more pronounced in the enamel junction area in term of both hardness and indentation modulus.

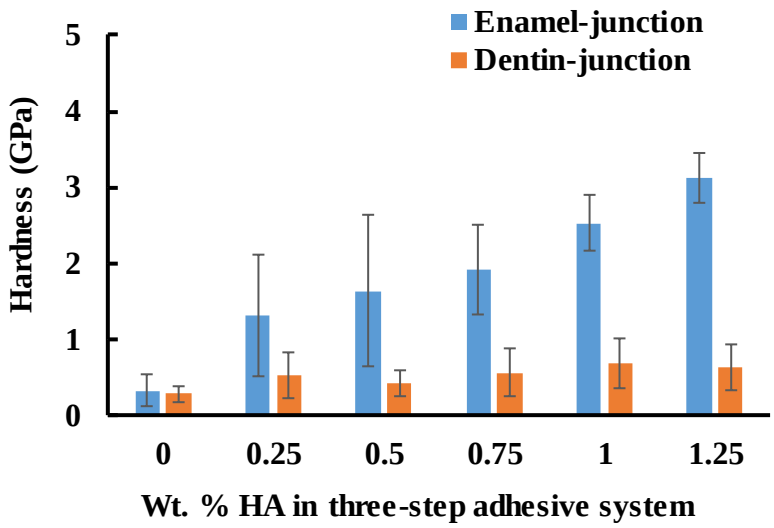

Figure 2.12. Hardness of three-step adhesive systems with increasing concentration of HA tested close to the enamel and dentin junctions, bars represent as a standard error

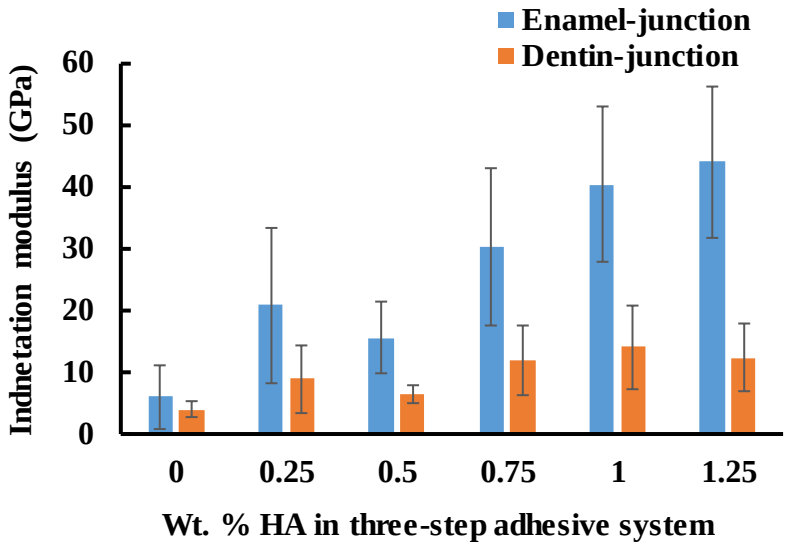

Figure 2.13. Indentation modulus of three-step adhesive systems with increasing concentration of HA tested close to the enamel and dentin junctions, bars represent as a standard error

Nanoindentation results for the three-step adhesive system reinforced with graphene on the cow teeth are shown in Figure 2.14 and Figure 2.15. The addition of graphene to the three-step adhesive system also increases the mechanical properties of the junction area, this is related to the higher mechanical properties of the graphene when compared to the polymers. Graphene reinforcement of the three-step adhesive system has a more pronounced effect at the enamel-adhesive junction than the dentin-adhesive junction, which is similar to HA reinforcement.

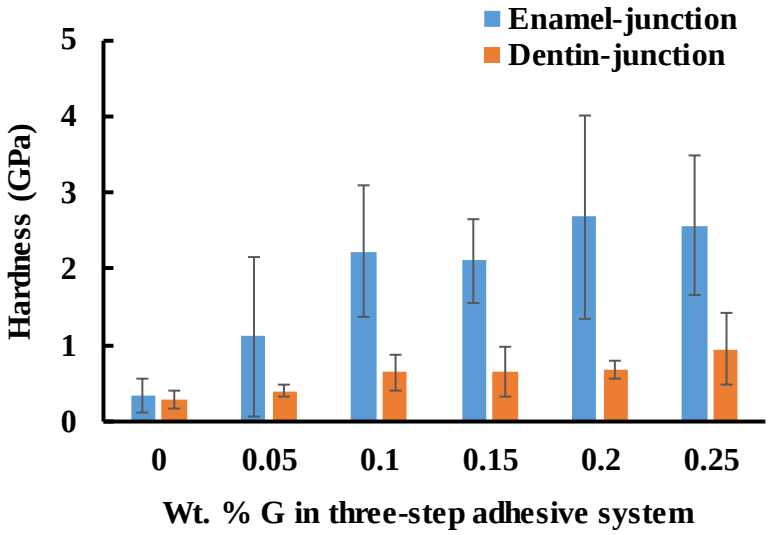

Figure 2.14. Hardness for three-step adhesive system with increasing concentration of G tested close to the enamel and dentin junctions, bars represent as a standard error

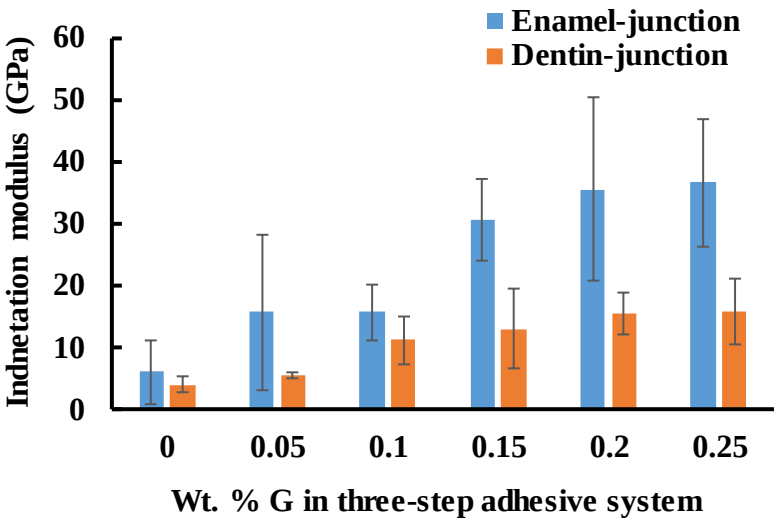

Figure 2.15. Indentation modulus for three-step adhesive system with increasing concentration of G tested close to the enamel and dentin junctions, bars represent as a standard error

2.6 Conclusion of the Preliminary Studies

Two types of commercial adhesives were applied to cow teeth and investigated in order to determine the current state-of-the-art. The two types of commercial adhesives were used, were self-etch and a three-step adhesive system. Two types of additives, HA and graphene, were added to the three-step adhesive to determine their effect. Microscopy results show that a gap forms between the cow tooth surface (dentin and enamel layers) and the adhesive for both the self-etch and three-step adhesive systems.

For the self-etch adhesive system, a larger gap forms at the dentin interface than at the enamel interface, which is attributed to the chemical composition and structural differences between the dentin and enamel. Furthermore, it is difficult to obtain a good bond between the self-etch adhesive with either the dentin or enamel cow tooth layers since a smear layer remains on the tooth surface. In the self-etch adhesive system, the etching, primer, and adhesive are all combined in one solution, so the smear layer stays on the tooth surface and becomes part of the bonding area. The smear layer smooths the tooth surface, rather than providing a rough surface with increased surface area, and the debris acts as a barrier to the adhesive system. As a result, a weak bond and big gap appears between the adhesive and the dental tissues, which explains the low mechanical properties in the composite-enamel and composite-dentin areas.

For the three-step adhesive system, a gap arises at the adhesive-dentin junction even before the restorative composite Z100 was applied. Thus, gap formation likely occurs due to a weak adhesive layer rather than due to polymerization shrinkage of the composite, as mentioned in previous studies.

Comparing the mechanical properties of the three-step adhesive with the self-etch adhesive system applied on cow teeth shows that the three-step adhesive system provides higher indentation modulus and hardness, and thus performs better, which means the separate etch step is very useful [57]. Additionally, indentation modulus and hardness were enhanced by the addition of HA and graphene to the three-step adhesives system, with graphene reinforcement providing higher hardness and indentation modulus than HA in both the enamel and dentin junction areas. These results may be related to the inherent mechanical properties of the additives themselves, since graphene can have higher mechanical properties than HA.

3 CHAPTER 3. EXPERIMENTAL METHODS

3.1 Materials

Diurethane dimethacrylate (UDMA) (≥ 97%, 470.56 g/mol Mw.), a high molecular weight monomer was used in this study with low molecular weight monomers as diluent (methyl methacrylate MMA, ≥ 98.5%, 100.12 g/mol Mw.). Camphorquinone, CQ (≥ 96.5%, 166.22 g/mol Mw.) was used as a photoinitiator and ethanol (≥ 99.5%, 46.07 g/mol Mw.) as a solvent. The chemical structures of functional monomers are illustrated in Figure 3.1.

The two additives investigated in this study were hydroxyapatite (HA) with an average particles size ≤ 200 nm (≥ 97% pure, 502.31 g/mol Mw.) and graphene (G) with an average dimension ≤ 150 µm. Graphite was purchased from Asbury Carbons (Asbury, NJ, USA) and converted to graphene by thermal expansion using a microwave treatment (1100w, 1 min), followed by ultrasonication for one hour, and drying at 80 ◦C overnight. The dry material was ball milled for 96 hours with a zirconia medium, then washed with a solution of 1:1 ratio deionized water: methanol, before drying again at 80°C for one night, and finally sieving with different meshes down to 320 mesh (63 micron). All chemicals except graphene were purchased from Sigma Aldrich, (St. Louis, MO USA) and used without any further purification.

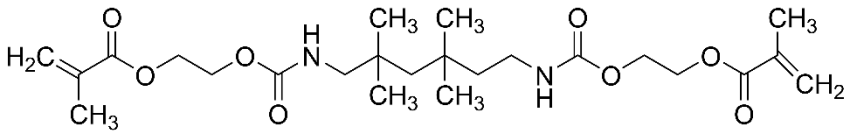

(a)

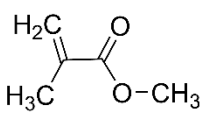

(b)

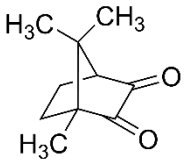

(c)

Figure 3.1. Chemical structure of: (a) UDMA; (b) MMA; and (c) CQ

3.2 Sample Preparation

Liquid blends were prepared using high molecular weight monomer (UDMA) and one low molecular weight monomer at the desired concentration ratio. The monomer blend was poured into silicone molds and photo-cured with a blue light source typical of those used in dentistry (wavelength 420-480 nm). This wavelength matches the optimum absorption wavelength to activate the CQ photoinitiater [58]. The light source tip position was controlled by mounting the light tip at a constant distance of 1 cm from the sample surface so that optimum light coverage was achieved (not overly disperse or too narrowly focused light on the sample surface). Nanoindentation, Raman, and FTIR samples were prepared using a silicone mold with each sample having a 5 mm diameter and 2 mm depth, while tensile samples were prepared using a silicone mold with dimensions 3.5 mm x 3.5 mm x 60 mm in the typical dog bone-shape used in tensile testing. Photo-curing times are dependent on the monomer ratios for the high viscosity and high molecular weight monomers used in this study. After light curing the cured specimens were stored for two weeks at room temperature in a dark room. This ensured that they were completely cured before further testing.

3.3 Characterization

3.3.1 Nanoindentation

A Hysitron TriboIndenter ^{TM} (USA) was used to measure the mechanical properties of the blends. A Berkovich diamond tip with a three-sided pyramidal shape and a nominal average tip radius of curvature of approximately 20 nm was used. The mechanical properties, including hardness, (H, GPa) and indentation modulus or reduced elastic

modulus, (Er, GPa) were found from the load-displacement curves for each nanoindent using the standard analysis. Fused quartz was used as a calibration material for the tip-area function, and a soft aluminum sample was used for the tip to optic translation calibration. The nanoindentation testing conditions for the samples and materials tested (and the chapter they are discussed) are detailed in Table 3.1. Three specimens were tested for each sample, except for UDMA/MMA for which five specimens were tested because it served as the baseline for the other tests. The statistical average and standard deviation (and standard error) for H and Er were calculated for each composition.

Table 3.1. Nanoindentation parameters for each chapter

Chapter	Sample	Indent Pattern	Nanoindentation Testing Parameters
4	UDMA/MMA	5x5 10 µm	displacement control (max. 800 nm) 40 sec load-unload/5 sec hold
5	G-UDMA/MMA HA-UDMA/MMA	6x6 10 µm	load control (max. 2,000 µN) 20 sec load-unload/5 sec hold
6	UDMA/MMA on cow teeth	5x5 10 µm	displacement control (max. 800 nm) 40 sec load-unload/5 sec hold

3.3.2 Tensile Test

Tensile properties were determined for the blends using a MTS Q Test/25 Elite Controller with a 5 kN load cell and extensometer (MTS model 632.26E-20) at a cross head speed of 1 mm/min, according to ASTM D 638 (Type V specimens). The width and thickness of each specimen were measured using a micrometer before each test to ensure the correct area was used in the analysis. Five specimens per composition were tested, and the statistical average and standard deviation were calculated.

3.3.3 Fourier Transform Infrared Spectroscopy (FTIR)

A Perkin Elmer FTIR was used to enable degree of conversion to be calculated for the photo-cured samples. This is a measure of the C=C double bonds convert to C-C single

bonds upon photopolymerization of the monomers to the final polymer. Liquid and solid samples were scanned over a wavenumber range 4000-400 cm^{-1} with a resolution 1 cm^{-1} and accumulation of 32 scans per sample. For liquid samples (n=3 for each composition), drops were placed directly on the sample holder plate. For solid samples (n=3 for each composition), circular specimens were prepared as previously mentioned. The degree of conversion (DC %) of carbon-carbon double bonds (C=C) to the carbon-carbon (C-C) single bonds was evaluated from the areas under the FTIR peaks [59] . The aliphatic C=C peak area ($A_{C=C}$ at ~ 1637 cm^{-1}) was compared to the areas under two internal standard peaks, which depends on the type of monomer used in the adhesive: C=O ($A_{C=O}$ at ~ 1710 cm^{-1}) and N-H (A_{N-H} at ~ 1528-1531 cm^{-1}). The areas for these peaks in both the liquid (uncured) and solid (cured) samples are used in the equation below [60-62]. For the N-H peak, $A_{C=O}$ is replaced with A_{N-H} in the equation. The areas under the peaks for the relevant bonds were determined from the FTIR scans using Origin Pro™ 2018b.

$$\mathrm{DC\%} = \left(1 - \frac{(\mathrm{A_{C=C}}/\mathrm{A_{C=O}})_{solid}}{(\mathrm{A_{C=C}}/\mathrm{A_{C=O}})_{liquid}}\right) \mathrm{x100}$$

Additional information is contained in the vibrational spectra for the local interactions of the carbonyl (C=O) group, specifically its hydrogen bonding to the N-H group. The arrangement of the vinyl (C=C) and neighboring groups (cis or trans) can also be seen in the FTIR and Raman data.

3.3.4 Micro-Raman Spectroscopy

Micro-Raman spectroscopy was performed on the liquid and solid blends using a Renishaw in Via™ confocal Raman microscope (West Dundee, IL 60118 USA) equipped with a laser wavelength of 785 nm and 5x magnification lens. The Raman spectra were obtained over a range of 3000-100 cm^{-1} at laser power (300 mW). A silicon sample was

used as a standard for calibration prior to testing. For liquid samples, drops of each blend were poured on silica plates and three specimens per composition were tested. For solid samples, three points spaced apart on the same sample were tested. The degree of conversion of the double bonds in going from liquid to solid phase was calculated using the areas under peaks via the same method as detailed for FTIR testing. The standard peak for N-H is not active in Raman so only the C=O peak was used as an internal standard peak.

3.3.5 Viscosity

A Malvern Kinexus Rotational Rheometer (Grovewood Road, Malvern, Worcestershire, UK, and WR14) was used to measure the viscosity of liquid blends. For monomer blends, a cone and plate geometry (4°/40 mm, # S90177 SS) was used with a gap of 0.15 mm and shear rates ($d\gamma/dt$) ranging from 1 s^{-1} to 10 s^{-1}. For monomer blends enhanced with additives HA or graphene, a 20 mm diameter parallel plate geometry was used with a gap of 0.5 mm and three shear rates ($d\gamma/dt$) of 2.155 s^{-1}, 4.624 s^{-1} and 10 s^{-1}. Three samples for each composition were tested at a temperature of 25 °C, and the average results, standard deviation, and standard error were calculated for each composition. The viscosity-shear rate graph is presented on a log-log base 10 scale for clarity.

3.3.6 Thermography

Thermography was performed during the light-curing process to monitor temperature changes as monomer converts to polymer. A Fluke RSE600 thermal camera with close-up lens (Macro Infrared Lens RSE, 0.5x) was used with sample area under observation of 10 x 10 mm^2. For all microscale thermography experiments, video of thermal event was recorded, and image frames were later separated at different time

intervals for data analysis. Our method measures temperature value at 640 x 480 pixels over a 100 mm^2 area in each frame, with each pixel representing one micro-sized point on the specimen (~20 µm size). Since the sample droplet under observation is ~4 mm in diameter, about 38,000 pixels or micro-sized point on the specimens are investigated for each sample type during the entire length of the test. Total duration of the test for each sample type is ~3 minutes and 20 seconds. During the test, each sample droplet was exposed to repeated light curing for 20 second followed by 20 seconds of break. The purpose of the break was to observe the real state of the sample curing, since during light exposure the thermal image is affected by radiation coming from the light itself. Fluke Smart view, MATLAB, Excel, and Origin software packages were utilized to perform data analysis.

3.3.7 Atomic Force Microscopy (AFM)

Morphology of the cured adhesive systems was examined using an NX-Hivac atomic force microscope (AFM) by Park (Santa Clara, CA 95054). The AFM images were taken over an area of 10 x10 µm at a resolution of 256 pixels for the entire area and processed with Gwyddion software (available under a GNU General Public License) to analyze the topographical information [63].

3.3.8 Optical Microscopy

A Nikon Eclipse LV150N Microscope with program NIS-Element D version 5.01.00 was used. 5X and 50X magnification images were focused on the junction area between the cow teeth and the UDMA-MMA photo-cured adhesive system.

3.3.9 Microindentation

A Vickers indenter (Leco LM248AT) was used to indent the junction area between the composite-enamel and composite-dentin. The Vickers indenter, applies a peak load (1 kg) with a 4-sided pyramid shaped diamond tip with an apex angle of 136^{o} [64].

3.3.10 Scanning Electron Microscopy (SEM)

A zeiss sigma field emission was used to view the morphology of the hybrid layer of 30 wt.% UDMA in MMA on cow teeth. The samples were prepared in the same way was presented in section 2.4.2.

3.4 Statistical Analysis

All the results and plots were expressed in terms of mean ± standard error of the mean. The results were analyzed with one-way ANOVA, followed by Tukey HSD (Honest Significance Difference) post-hoc test at the significance level of $p < 0.05$, where the p-value is the probability value. The bars in graphs represent standard error.

4 CHAPTER 4. MMA-UDMA ADHESIVE SYSTEM

4.1 Introduction

The chemical composition of the photo-cured adhesive system are important in determining the physical (mechanical) and chemical properties of the bonds between adhesive layer and dental tissues (enamel and dentin). The best composition of the photo-cured adhesive is determined by the application and the desired properties such as cure rate, viscosity of liquid and mechanical strength. For example, low viscosity adhesive systems that can penetrate rough surfaces to fill narrow, deep gaps are needed to obtain a strong mechanical bond in some applications, especially for filling cavities [65]. UDMA is the most commonly used monomer in dental applications. UDMA is a high molecular weight monomer with good flexibility, high strength, and higher viscosity, but this make it difficult to handle. Methyl methacrylate, MMA is commonly used in dental applications [66,67], due to its flexibility and high strength, helps reduce localized stress [68]. Additionally, MMA has a high cure speed, low toxicity, and is a good solvent for high molecular weight monomers [69]. The addition of UDMA to MMA aids in the photopolymerization process for dental application as it decreases shrinkage whereas just MMA tends to give greater shrinkage and can evaporate [70]. In some cases, blending low and high molecular weight monomers has been shown to increase the mechanical properties of photo-cured adhesive systems [71].

The objective of the research described in this chapter was to mix different compositions of UDMA and MMA monomers to determine the effect of composition on the mechanical properties, viscosity, and chemistry of the photo-cured adhesive system. Mechanical properties of the adhesive system were evaluated by nanoindentation to

measure hardness and indentation modulus, along with tensile testing to measure Young's modulus and tensile strength. Fourier transform infrared (FTIR) and micro-Raman spectroscopy were used to examine chemical changes and calculate degree of conversion of double bonds into single bonds during curing. This is important as mechanical properties are known to be dependent on degree of conversion. The viscosities of the UDMA-MMA blends in the liquid phase were measured by rheometry. Thermography was used to monitor temperature during the curing process and indicates curing rate and consequently changes in viscosity.

4.2 Adhesive Preparation

The adhesive system was prepared by mixing different weight percentage of UDMA in MMA with 1 wt. % CQ and 9 wt. % ethanol. Weight % ratios of UDMA: MMA were 30:60, 40:50, 50:40, 60:30, 70:20, and 100:0. In a dark room at room temperature, mixtures were blended in amber glass using a magnetic stirrer (Corning, USA) at a speed of 1000 rpm for 1 hour and placed on a shaking table to homogenize overnight [72].

Photo-curing times are dependent on the monomers used. High viscosity and high molecular weight monomers like UDMA require shorter curing times. Consequently, the curing time needed decreases with increasing UDMA percentage. The times used for 30, 40, 50, 60, 70, and 100 wt. % UDMA in MMA were 16, 13, 10, 6, 5, and 3 minutes, respectively; these were the times needed for the samples to solidify without signs of discoloration. For instance, 70 wt. % UDMA in MMA solidified after 5 minutes, but it showed discoloration with longer curing times. Other researchers have found that mechanical properties remain constant with increased curing time for methacrylates once the monomers have solidified. Examples including bis-DGEMA and TEGDMA resins [73]

where the degree of conversion as a function of light exposure time reaches a plateau that depends on chemical composition [74]. In this study, the curing times were optimized for each composition. After light exposure the specimens were stored for two weeks at room temperature in a dark room before further testing to ensure they were completely cured.

4.3 Results and Discussion

4.3.1 Nanoindentation

Nanoindentation results for the UDMA-MMA photo-cured adhesive system are shown in Figure 4.1. The hardness (H) ranged from 0.140±0.001 GPa to 0.176±0.001 GPa (Figure 4.1a), and indentation modulus, Er, ranged from 2.86±0.01GPa to 3.12±0.01 GPa (Figure 4.1b). These values are approaching those seen for PMMA when using low strain rate indentation tests [75]. For hardness, there is no significant effect of UDMA composition for 30, 40, 50, and 60 wt. % UDMA in MMA. However, the hardness for 70 wt. % UDMA and 100 wt. % UDMA were significantly higher than those of lower wt. % UDMA. Increasing UDMA concentration in MMA did not significantly affect the indentation modulus. The representative loading-unloading curves for each concentration are shown in Figure 4.1(c). The polymerization process is known to have an effect on the polymer's final mechanical properties [76], with important factors being photoinitiator, type of monomer(s), ratios of the monomers, light cure intensity, light position, light spot size, and light exposure time [77]. In this work, light cure intensity and light position were constant for each UDMA-MMA blend; however, light cure exposure time was varied as previously described to ensure both polymerization and solidification of the samples, as described earlier. The degree of polymerization depends on the free radicals generated in the first stage of polymerization, which then affects mechanical properties [78]. This

suggests that some of the variation in H and Er between compositions might be related to polymerization conditions. The role of hydrogen bonding is also important in polymer and it is evident in the spectroscopy data. It is possible that the stronger hydrogen bonds in the higher UDMA wt.% blends is contributing to their increase in hardness. The hydrogen bonding effects would not be expected to significantly alter elastic properties as evidenced by the data for indentation modulus.

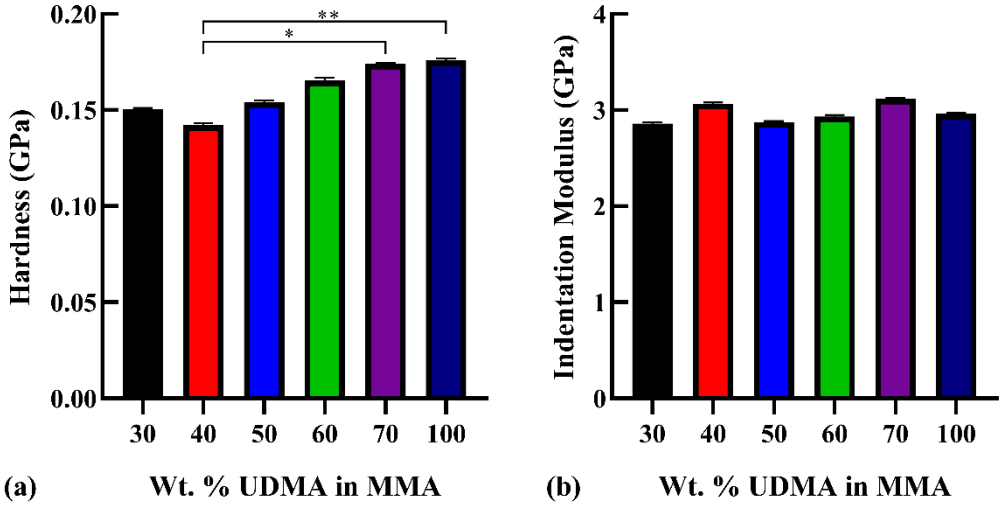

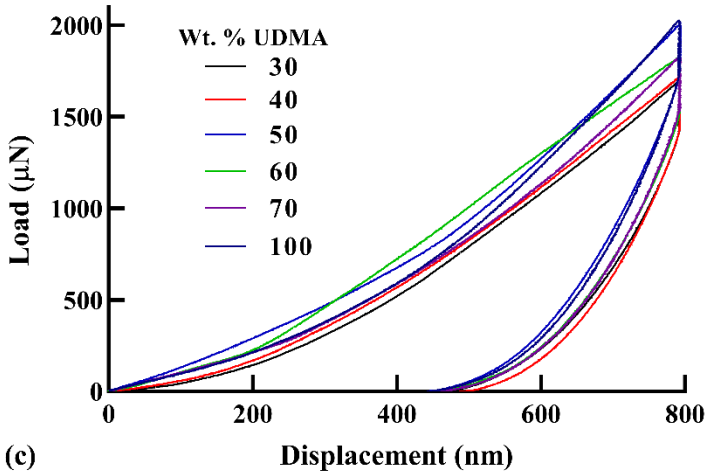

Figure 4.1. Nanoindentation results: (a) Hardness, H, as a function of UDMA-MMA composition; (b) Indentation Modulus, Er, as a function of UDMA-MMA composition; (c) representative load-displacement curves for each composition (* indicates a significant difference with $p < 0.05$ and ** indicating $p < 0.01$).

4.3.2 Tensile Test

Tensile results for 30, 40, 50, 60, 70, and 100 wt. % UDMA in MMA are shown in Figure 4.2. Tensile modulus values ranged from 0.92±0.05 GPa for 100 wt.% UDMA to around 1.60 GPa for the blends, as shown in Figure 4.2(a). Increasing UDMA concentration did not significantly affect tensile modulus based on statistical analysis ($p > 0.05$) with the exception of 100 wt. % UDMA, which was significantly lower than all of the other compositions. Tensile strength decreases with increasing UDMA concentration in MMA and is the lowest for 100 % UDMA, as shown in the stress-strain curves in Figure 4.2 (b). For 30 wt. % UDMA in MMA, tensile modulus is 109 % higher than UDMA alone, and tensile strength is 105 % higher than UDMA alone. Tensile modulus shows a slight decrease with increasing wt.% UDMA, though there is a noticeable decrease in ultimate tensile strength with increasing UDMA percentage. The optimum concentration, with regard to tensile properties, appears to be 30 wt. % UDMA in MMA.

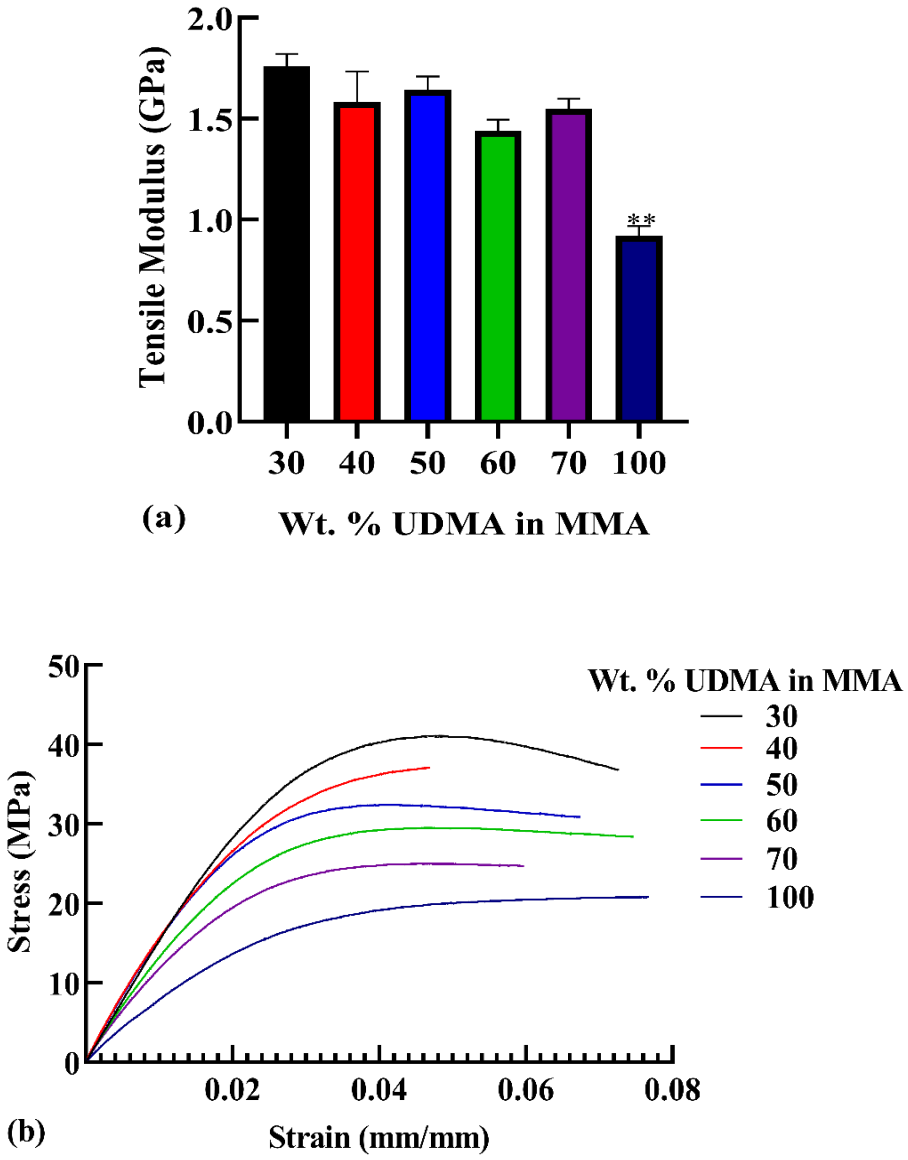

Figure 4.2 Tensile results for UDMA-MMA blends: (a) tensile modulus vs. wt. % UDMA in MMA, (** indicating $P < 0.01$); (b) tensile stress-strain curves (representative curve from each composition).

4.3.3 FTIR

The degree of conversion of C=C double bond to C-C single bonds in the UDMA-MMA blends and 100 wt. % UDMA is shown in Figure 4.3 (a and b). Increasing wt. %

UDMA, the high molecular weight monomer, causes a decrease in the degree of conversion. The degree of conversion using internal standard peak $A_{C=O}$ ranged from 28.38%±0.82 to 59.07%±0.90, while the degree of conversion using internal standard peak A_{N-H} ranged from 35.01%±0.84 to 62.66%±0.46. The results for degree of conversion show a dependence on the selected internal standard peak, that is C=O (Figure 4.3 a) or N-H (Figure 4.3 b), as well as the spectroscopic method (FTIR or Raman) used, as is consistent with the literature [79]. The polymerization process is impacted by the blend's composition and how this impacts the formation and mobility of free radicals. Changes in the peaks due to the impact on the spectra of hydrogen bonding involving the N-H group and any ambient water can give different values for the calculated degree of conversion. Given these limitations it is still possible to see the relative decrease in degree of conversion with increasing UDMA percentage. There is restricted mobility of free radicals and, hence, limited polymerization when there are large pendent groups present, as seen in the UDMA monomer [80].This becomes most noticeable at higher UDMA compositions. The differences in molecular weight and refractive index for UDMA and MMA can also affect the photo-polymerization process. UDMA and MMA have different refractive indices due to their different molecular weights with the refractive index of UDMA being higher than MMA. This causes light scattering during photoinitiation and a subsequent decrease in degree of conversion [81-83]. In general, attaining 100 % degree of conversion is not possible due to immobilization, gelation, and vitrification, and thus, about 25-45 % of double bonds always remain even in the polymerized solid [84]. Even though higher wt.% UDMA in MMA samples have lower degree of double bond conversion the rate of conversion is higher, as can be seen from the thermography results during curing Figure

4.7 (a and b). UDMA has more double bond sites for conversion along the polymer chain (Figure 3.1 a) leading to faster crosslinking of the polymer chains that are accessible to the photoinitiators.

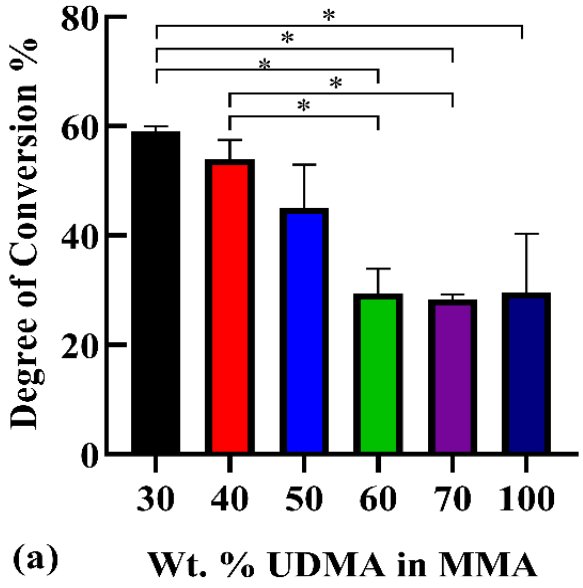

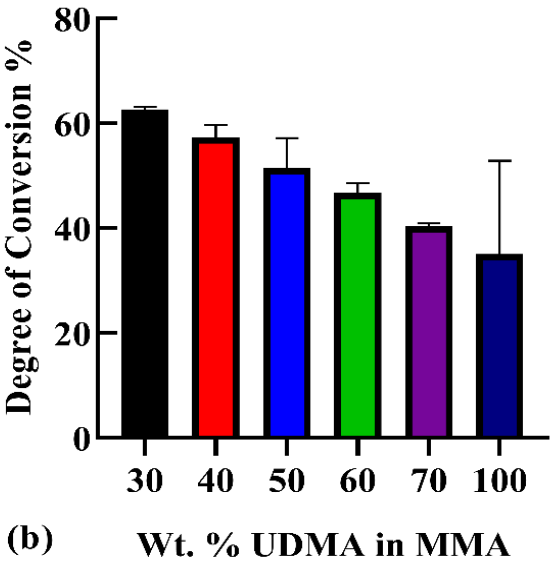

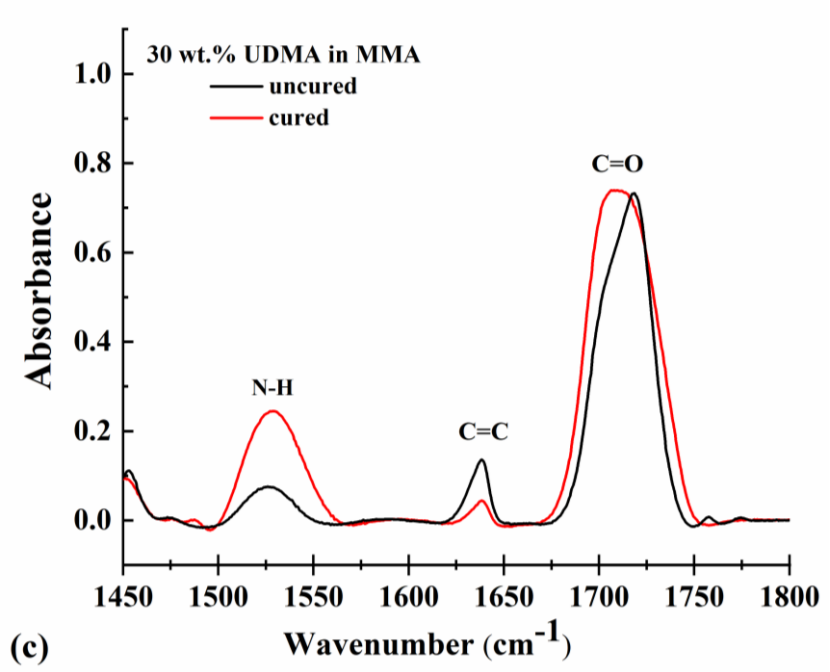

Figure 4.3. FTIR results for UDMA-MMA blends: (a) degree of conversion vs. wt. % UDMA using $A_{C=C}/A_{C=O}$ as an internal standard; (b) degree of conversion vs. wt. % UDMA using $A_{C=C}/A_{N-H}$ as an internal standard peak; (c) FTIR spectra for 30 wt. % UDMA in MMA cured and uncured (* indicating $p < 0.05$).

The values obtained for degree of conversion are a good relative measure for the different blends, but the composition and interactions in the polymer affect the position and width of peaks. This is seen especially in the carbonyl C=O peak, but also the vinyl C=C and amide N-H peaks can be affected. This impacts the absolute measurement of degree of conversion. Figure 4.3 (c) shows the C=O, C=C and N-H peaks in detail. Figure 4.4 (a) shows that increasing UDMA fraction lowers the frequency of the C=O peak this is due to the interactions with the N-H group (hydrogen bonding) which lowers the peak's frequency because of the stronger bonding to its neighbors [85,86]. The N-H peak is also affected by hydrogen bonding, but it is a smaller and less pronounced effect as shown by the uncured peaks and cured peaks of Figure 4.4 (b, c). The C=C peak can be affected by

the spatial configuration (cis or trans) of the attached groups [87], but there is no evidence of this in the FTIR data Figure 4.4 (d, e).

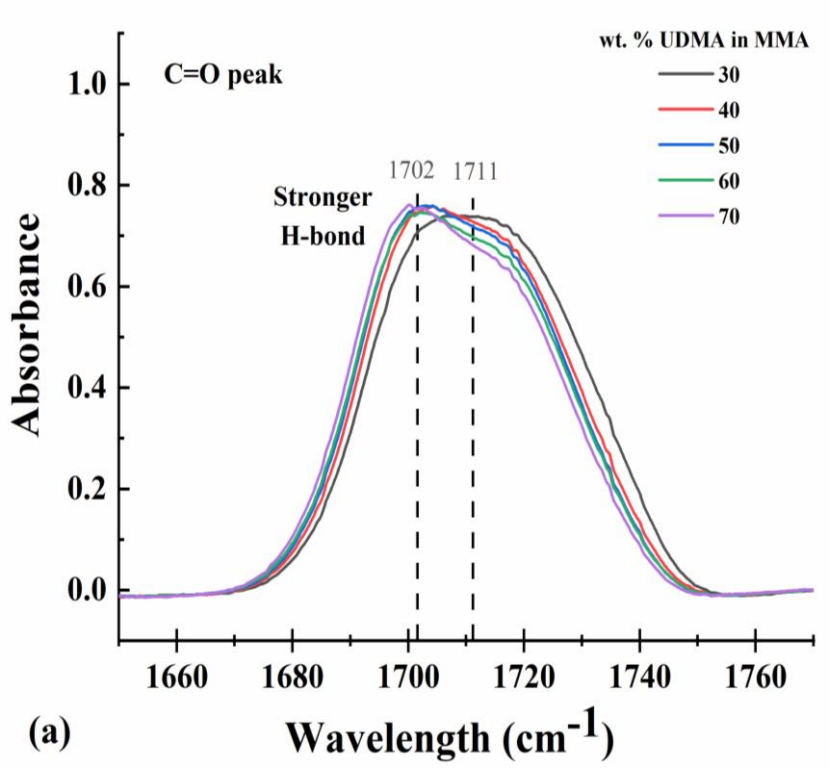

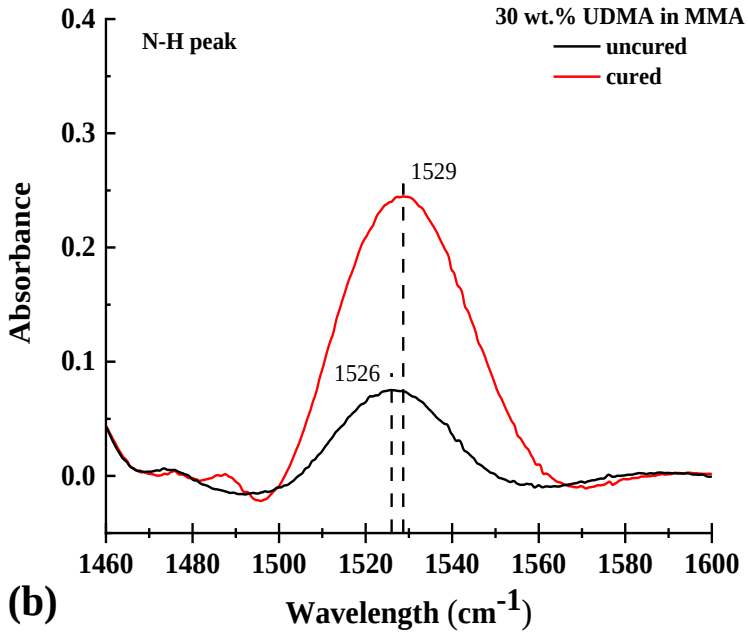

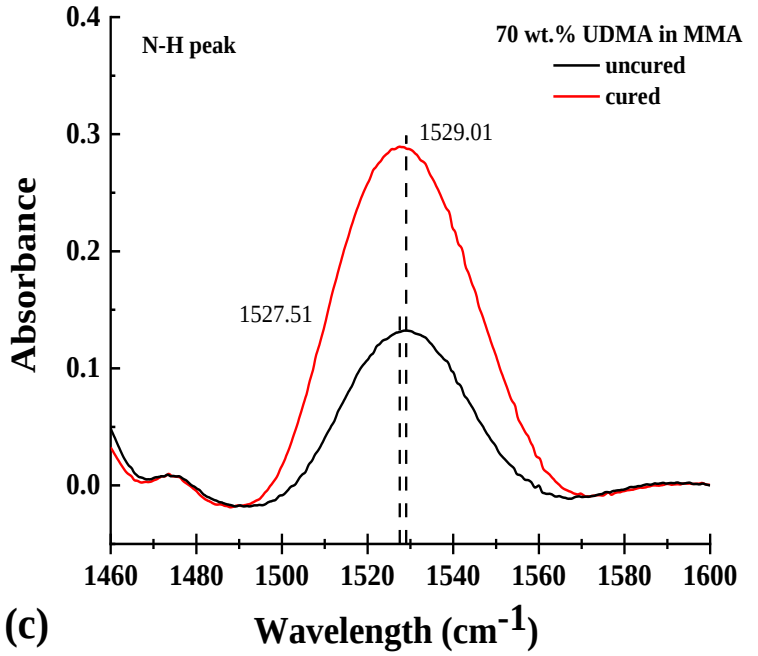
N-H peak
70 wt.% UDMA in MMA
uncured
cured
1529.01
1527.51
Absorbance
0.4
0.3
0.2
0.1
0.0
1460
1480
1500
1520
1540
1560
1580
1600
Wavelength (cm-1)

(c)

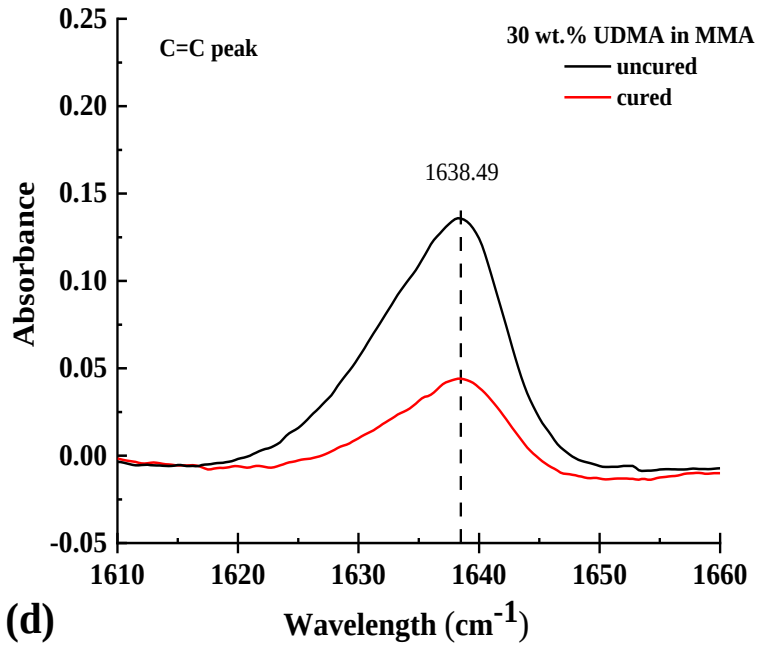
C=C peak
30 wt.% UDMA in MMA
uncured
cured
1638.49
Absorbance
0.25
0.20
0.15
0.10
0.05
0.00
-0.05
1610
1620
1630
1640
1650
1660
Wavelength (cm-1)

(d)

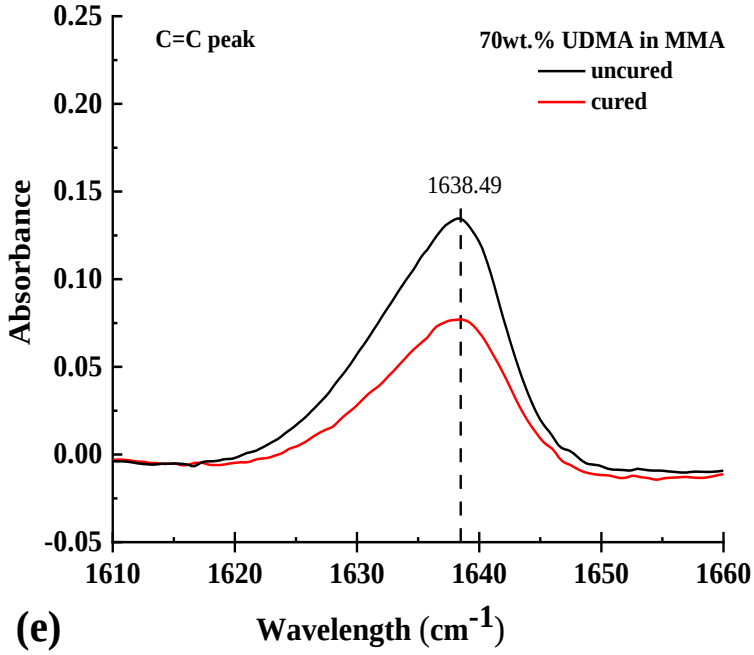

Figure 4.4. FTIR spectra areas of interest for (a) C=O bond for all concentrations of cured UDMA-MMA; (b, c) N-H bond showing cured and uncured samples for 30 and 70 wt. % UDMA in MMA; (d, e) C=C bond showing cured and uncured samples for 30 and 70 wt. % UDMA in MMA

4.3.4 Micro-Raman

Micro-Raman spectra of UDMA-MMA blends show peaks for C=C and C=O at approximately ~1630 cm^{-1}, and ~1715 cm^{-1}, respectively. The degree of conversion for UDMA-MMA blends and 100 wt. % UDMA using an internal standard peak $A_{C=O}$ ranged from 79.87%±0.59 to 95.37%±0.57, as shown in Figure 4.5 (a). Increasing wt. % UDMA, the high molecular weight monomer, causes a decrease in the degree of conversion, which matches FTIR results. After curing all UDMA-MMA concentrations, the intensity of C=C bond decreases, C-C bond increases, and C=O increases, as shown for 30 wt. % UDMA in MMA in Figure 4.5 (b). Looking at the area of interest around the C=C bond at ~ 1630.89 cm^{-1}, it is evident there is no shift in frequency for any of the concentrations, matching

previous studies reported in the literature [88], as shown in Figure 4.5 (c, d) for 30 and 70 wt. % UDMA in MMA, respectively. Looking at the area of interest around the C=O bond, Figure 4.5 (e) shows that increasing UDMA concentration causes a decreasing shift in the frequency, which may be due to the composition change [89] or the dominant C-C peak arising after curing. The intensity ratio of $A_{C=C}/A_{C-C}$ increases with increasing UDMA concentration, further confirming lower degree of C=C bond conversion to C-C bonds for higher UDMA concentrations, as shown in Figure 4.5 (f). The values for degree of conversion obtained with Raman are higher than the values for the degree of conversion obtained from FTIR. In the Raman method, the red laser (785 nm) used may affect the polymerization process by locally heating the samples during scanning. For example, scanning liquid samples multiple times leads to a progressive change in area under the peaks for C=O and C=C, decreasing by about 1.12 ±0.01 % between each test of the sample. A further difference between Raman and FTIR methods, is that geometry of the liquid drop can vary in the micro-Raman method, as the drop may spread across the plate and cause non-uniform thickness.

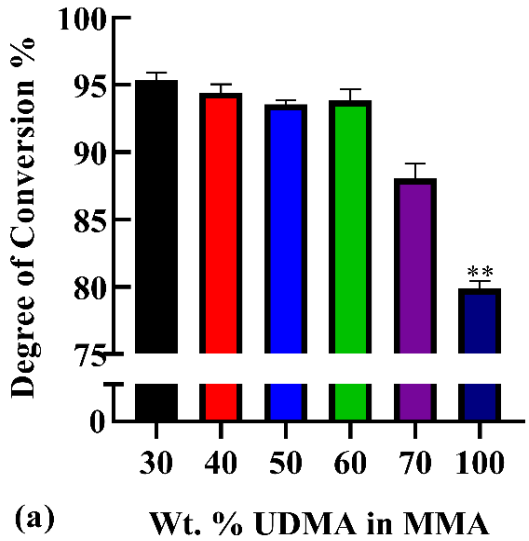

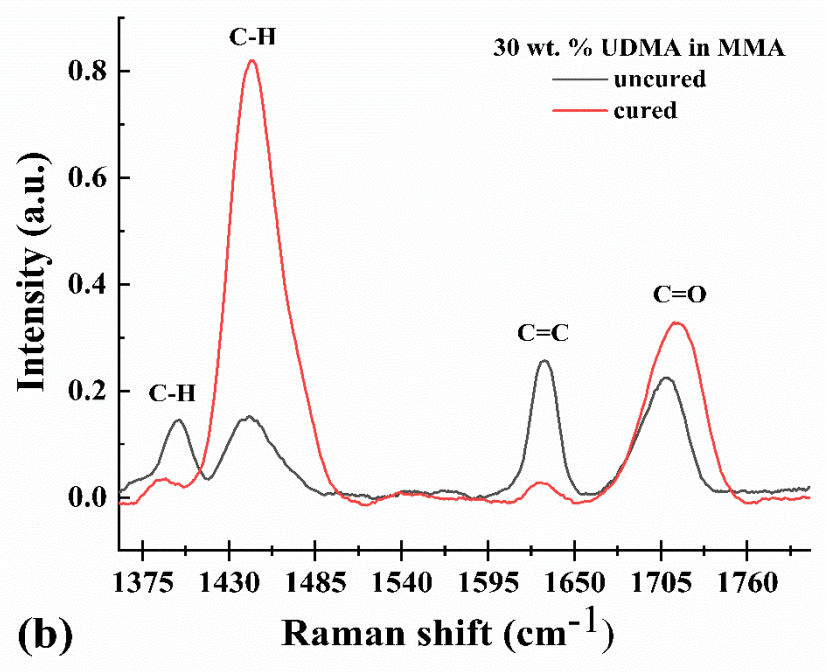
C-H
30 wt. % UDMA in MMA
uncured
cured
C=O
C=C
C-H
Intensity (a.u.)
0.0
0.2
0.4
0.6
0.8
1375
1430
1485
1540
1595
1650
1705
1760
(b)
Raman shift (cm-1)

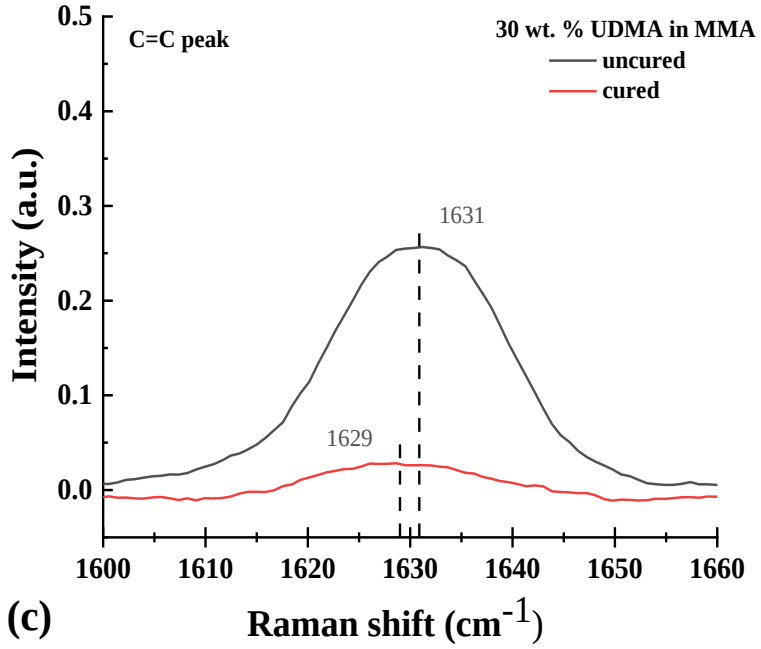
C=C peak
30 wt. % UDMA in MMA
uncured
cured
1631
1629
Intensity (a.u.)
0.0
0.1
0.2
0.3
0.4
0.5
1600
1610
1620
1630
1640
1650
1660
(c)
Raman shift (cm-1)

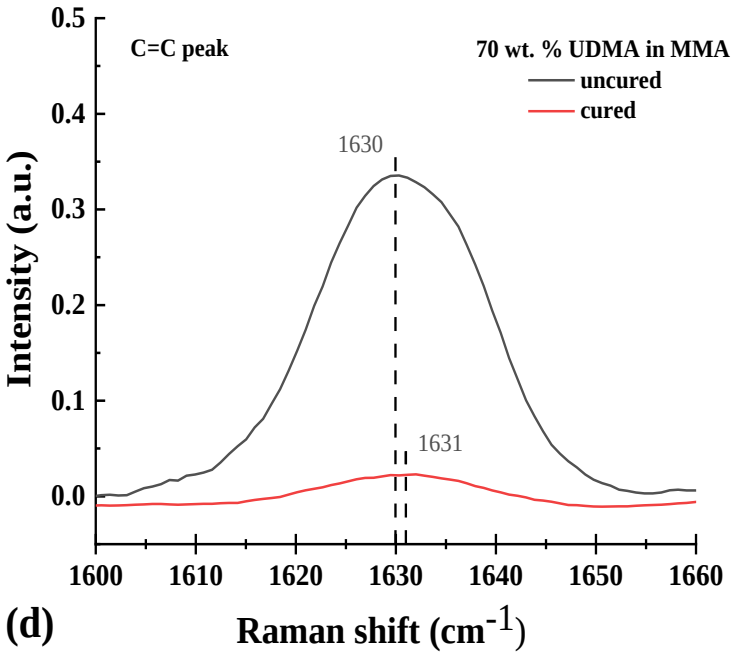
C=C peak
70 wt. % UDMA in MMA
uncured
cured
1630
1631
Intensity (a.u.)
0.0
0.1
0.2
0.3
0.4
0.5
1600
1610
1620
1630
1640
1650
1660
Raman shift (cm-1)

(d)

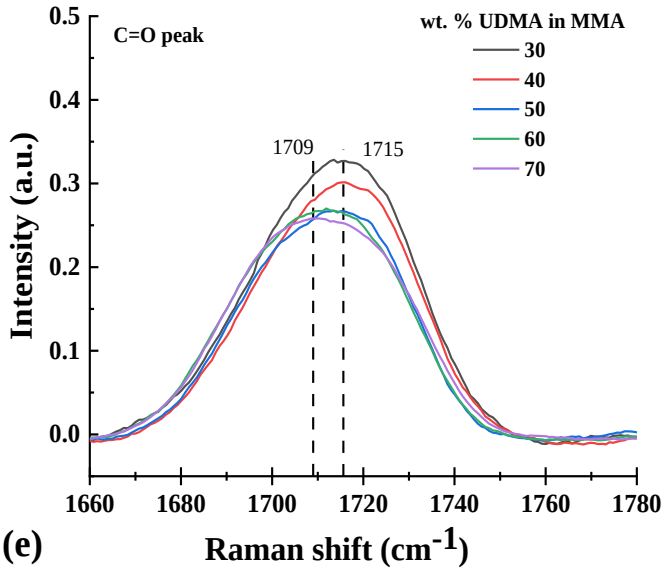
C=O peak
wt. % UDMA in MMA
30
40
50
60
70
1709
1715
Intensity (a.u.)
0.0
0.1
0.2
0.3
0.4
0.5
1660
1680
1700
1720
1740
1760
1780
Raman shift (cm-1)

(e)

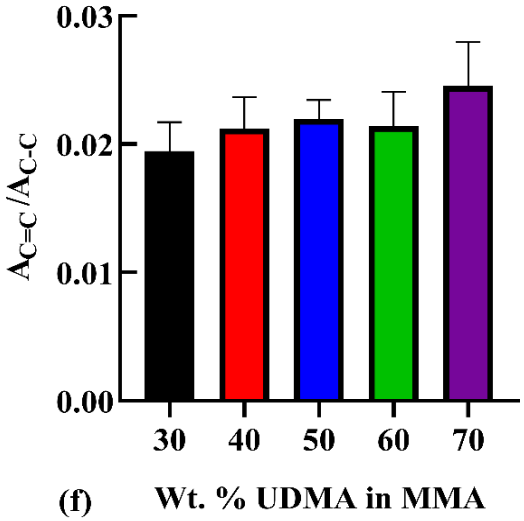

Figure 4.5. Micro-Raman results for UDMA-MMA blends: (a) degree of conversion vs. wt. % UDMA using $A_{C=C}/A_{C=O}$ as an internal standard peak; (b) Micro-Raman spectra of 30 wt. % UDMA in MMA uncured and cured samples; (c, d) Micro-Raman spectra for C=C bond showing cured and uncured samples for 30 and 70 wt. % UDMA in MMA; (e) Micro-Raman spectra of C=O bond for all concentration of UDMA-MMA; cured; (f) Ratio of area under curves C=C/C-C; (** indicating $p < 0.01$).

4.3.5 Viscosity

Rheology results for UDMA-MMA blends, MMA, and UDMA are shown in Figure 4.6. The viscosity of MMA and UDMA-MMA blends decreases with increasing shear rate, indicating thixotropic or non-Newtonian behavior [90,91], as shown in Figure 4.6 (a), while the viscosity of UDMA remains fairly constant and decreases only slightly. The viscosity of the UDMA-MMA blends increases with increasing UDMA concentration at all shear rates. For example, Figure 4.6 (b) shows that at a shear rate of 10/s the viscosity exhibits statistically significant increases with increasing UDMA percentages. Viscosity of the liquid samples showed a clear and strong trend of increasing viscosity with

increasing UDMA wt.% in MMA due to: (1) the urethane group (NH) in UDMA, which is able to form intermolecular hydrogen bonds with other functional groups [92]; (2) the large chain-length and chemical formula of the liquid monomer molecule, which determines the flow behavior of the solution [93]; and (3) the high molecular weight of the monomer [94], in this case UDMA. Higher viscosity for higher wt.% UDMA in MMA can also be visually observed in thermography results presented in Figure 4.7 (a) (more spherical the droplet, higher the viscosity).

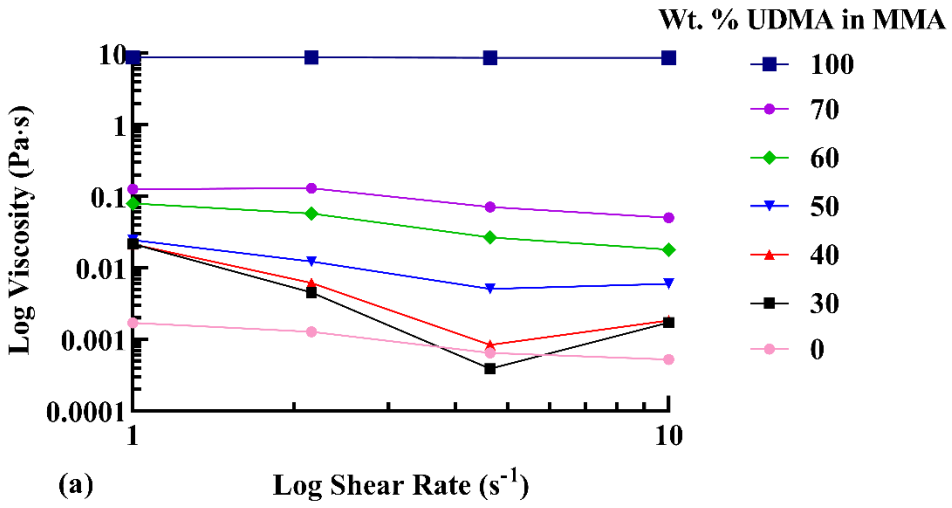

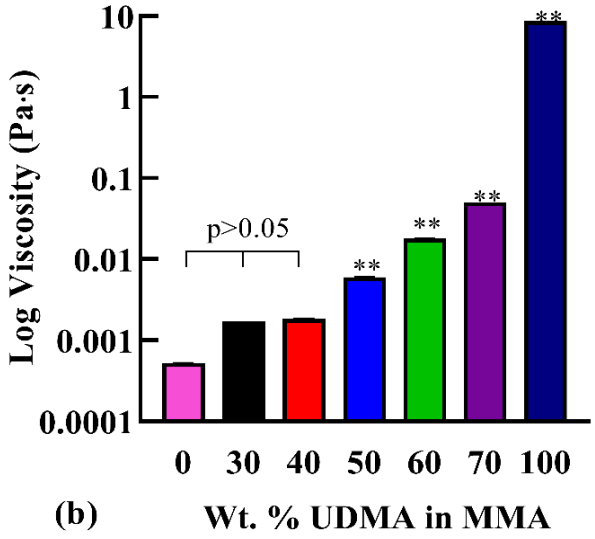

Figure 4.6. Viscosity results for UDMA-MMA blends at T =25 °C: (a) viscosity of UDMA-MMA blends as a function of shear rate; (b) viscosity vs. wt. % UDMA-MMA at shear rate 10/s. (** indicating $p < 0.01$)

4.3.6 Thermography

Thermography results for 30, 50, and 70 wt. % UDMA in MMA are shown in Figure 4.7. In thermography images, temperature changes during curing are indicated by color changes, and uniform color represents uniform temperature [95,96]. With increasing UDMA concentration, curing rate increases, as shown in Figure 4.7 (a). At 50 seconds of curing time, 70 wt.% UDMA shows a change in color to uniformly yellow, suggesting the sample is fully cured, whereas 50 wt. % UDMA still exhibits a variation in color, indicating the sample is partially cured. By comparison, 30 wt.% UDMA shows minimal color change and hence temperature change, indicating the sample is marginally cured. Additionally, the droplet shapes are indicative of the sample viscosity. The spherical shape for 70 wt. % UDMA indicates higher viscosity compared to 30 wt.% UDMA, for which the droplet is more spread out. The change in temperature of the 30, 50, and 70 wt. % UDMA in MMA during curing as monitored by thermography testing is shown in Figure 4.7 (b). The fast curing rate of 70 wt. % UDMA indicates that the energy supplied by the light cure and the exothermic polymerization process increase the temperature of the cured sample, whereas for 50 wt. % UDMA and 30 wt. % UDMA energy from the light curing is going towards converting C=C to C-C (or degree of conversion) with less heat generated by the polymerization process during the curing reaction so there is a less noticeable increase in temperature.

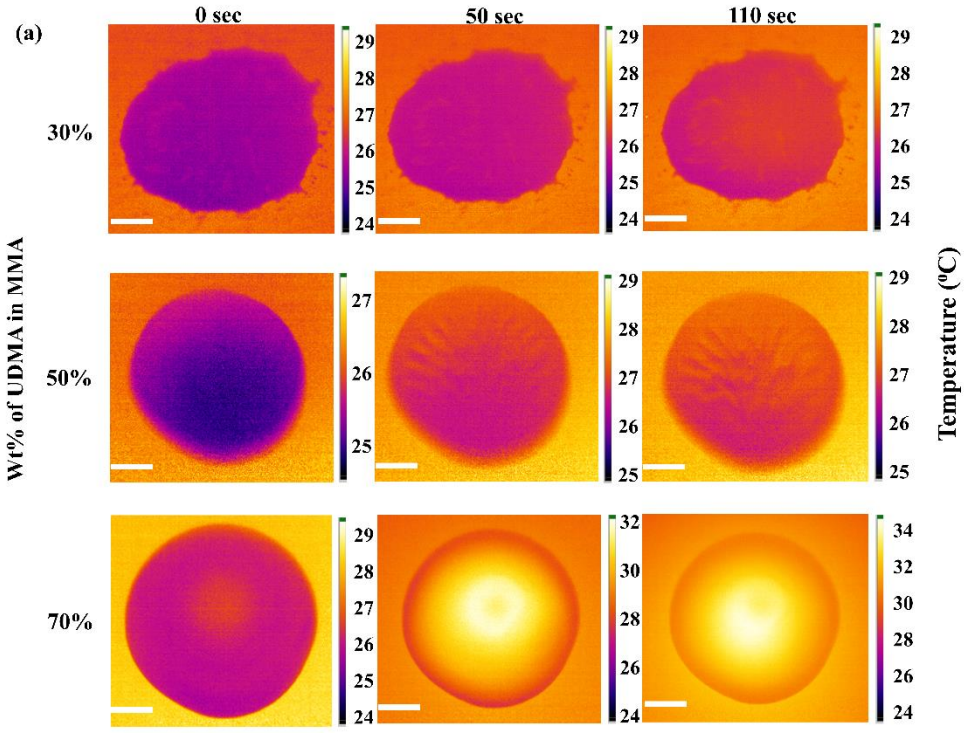
(a)
0 sec
50 sec
110 sec
30%
50%
70%
Wt% of UDMA in MMA
Temperature (°C)

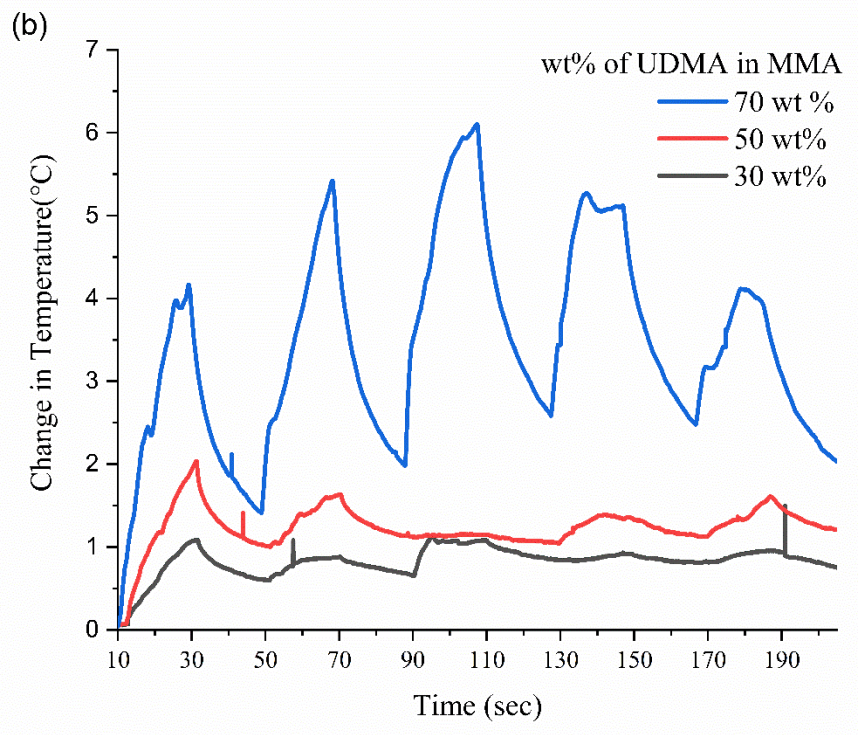
(b)
wt% of UDMA in MMA
70 wt %
50 wt%
30 wt%
Change in Temperature(°C)
Time (sec)

Figure 4.7. Thermography results for 30, 50, and 70 wt.% UDMA in MMA blends: (a) Thermal images at 0, 50, and 110 sec of light curing time showing temperature in °C. (Scale bar = 1 mm); (b) Change in temperature vs light curing time during polymerization.

4.4 Conclusion

The effect of UDMA-MMA composition on the properties of the photopolymerized blends was found to vary with some properties being more sensitive to composition than others. Increasing UDMA percentage had a small, but not significant effect on hardness, indentation modulus, and tensile modulus, however, tensile strength decreased and viscosity in the liquid phase increased. All of the UDMA-MMA blends tested had a higher tensile modulus and tensile strength than UDMA alone indicating that the blends are superior mechanically to UDMA. Increasing the high molecular weight monomer, UDMA, caused a decrease in the degree of conversion of double C=C bonds to single C-C bonds, as measured by FTIR and Raman. The degree of conversion obtained by micro-Raman was higher than by FTIR, which can be attributed to accelerated polymerization when exposed to laser light in the Raman system. Degree of conversion is reduced in the higher percentage UDMA blends due to a reduction in the mobility of free radicals and changes in the optical properties that impact photopolymerization. The dependency on composition of some of the different properties and the variations in photopolymerization rate indicate that blending UDMA with MMA allows tunability of some properties. Specifically, viscosity of the liquid phase can be varied independently of many mechanical properties and, hence, the composition can be selected to give the best viscosity and photo-curing conditions for a specific adhesive application. Of all the samples tested 30 wt. % UDMA in MMA gave what may be the best combination of good mechanical properties, including hardness and

high modulus, but the low viscosity that is needed for adhesive applications where penetration of deep and narrow gaps is important. Slightly higher percentages, like 40 wt. % and 50 wt. % UDMA, still have good mechanical properties and maybe preferable, if faster curing is important in the application.

5 CHAPTER 5. G AND HA ENHANCED MMA-UDMA ADHESIVE SYSTEM

5.1 Introduction

In recent years, reinforcement of adhesives with different types of additives to create a composite structure has become a popular way to improve the properties and functionality of the adhesives [97,98]. These additives have a direct influence on the mechanical properties and viscosity of the adhesive [99], with the effect being dependent on the size, morphology, and weight fraction of the additive [100]. In this chapter the research described is focused on the evaluation of graphene (G) and hydroxyapatite (HA) in photo-cured adhesive systems. The properties of both G and HA make them good candidate materials as additives to improve the performance of photo-cured adhesive systems in dental applications [101,102].

New photo-cured adhesive systems based on UDMA-MMA blends with small additional fractions (≤ 0.5 wt.%) of the two different additives, G and HA, were investigates. The differing geometries and size of G and HA are expected to give different mechanical properties in the adhesive systems. There is also the potential that the additives affect the photo-curing by changing the absorption and scattering of photons. To evaluate the mechanical properties of the adhesives, the photo-cured systems containing G and HA were tested using nanoindentation to measure hardness and indentation modulus. Mechanical properties are dependent on the curing process and the degree of conversion of the monomers, so Fourier transform infrared (FTIR) spectroscopy and Raman spectroscopy were used to examine chemical changes that occur during curing. The effect of the G and HA additives on the viscosity of the liquid phase adhesives were measured by rheometry.

5.2 Adhesive Preparation

The adhesive systems were prepared by mixing 40 wt. % MMA with 1 wt. % CQ and 9 wt. % ethanol. The remaining weight was a small amount of the additive (G or HA), with the balance being UDMA, according to Table 5.1. The weights of each component were measured using a Mettler Toledo weight scale with an accuracy of ±0.002g and an experimental accuracy of ±0.001 g. The HA enhanced photo-cured adhesive systems were prepared by mixing MMA, CQ, ethanol, and hydroxyapatite using a magnetic stirrer (Corning, USA) at a speed of 1000 rpm for 1 hour. UDMA was then added to the mixture before using a shaking table overnight to homogenize the mix. The G enhanced photo-cured adhesive was prepared by mixing MMA, CQ, ethanol, and graphene in a container surrounded by a water bath (to maintain temperature during mixing), inserting a mixing rod to stir it that was attached to a drill, hence, and shearing it for one minute, as shown in Figure 2.1 in chapter 2. This shearing technique is commonly used to obtain proper dispersion and exfoliation of G, and to decrease particle size, giving a good particle distribution while avoiding particle agglomeration [103-105]. UDMA was then added to the mixture and further stirred using a magnetic stirrer for one hour at 1000 rpm [106] . All the different compositions of the photo-cured adhesive systems were mixed in a dark room at room temperature in amber glass.

Table 5.1. Composition (wt. %) of enhanced photo-cured adhesive with graphene (G) or hydroxyapatite (HA).

Additives (G or HA)	UDMA	MMA	CQ	Ethanol
0	50	40	1	9
0.1	49.9	40	1	9
0.2	49.8	40	1	9
0.3	49.7	40	1	9
0.4	49.6	40	1	9
0.5	49.5	40	1	9

5.3 Results and Discussion

5.3.1 Nanoindentation

The data of Figure 5.1 shows the mechanical properties of the G or HA enhanced UDMA-MMA composites. A representative load-displacement curve was selected for each composition and shown in Figure 5.1 (e, f). The addition of even small amounts of G or HA caused substantial increases in hardness when compared to the unenhanced UDMA-MMA blend, as shown in Figure 5.1 (a, b). Both additives provide higher hardness values compared to that of each monomer alone [107]. The hardness value of UDMA-MMA alone was 0.154 ±0.001 GPa while hardness values of G-enhanced UDMA-MMA range from 0.181 ±0.001 GPa to 0.223 ±0.001 GPa, and hardness values of HA-enhanced UDMA-MMA range from 0.209 ±0.001 GPa to 0.226 ±0.001 GPa. Statistical analysis confirmed that the hardness of the UDMA-MMA without G or HA (0 wt.%) was significantly lower

than that with any of the different percentages of G or HA added to the UDMA-MMA system.

The indentation modulus of UDMA-MMA also showed substantial increases with the addition of each additive when compared to no additives (0 wt.%). The indentation modulus of UDMA-MMA was 2.873 ±0.011GPa while the indentation moduli for UDMA-MMA composites with G ranged from 3.585 ±0.008 GPa to 3.942 ±0.003 GPa and with HA ranged from 3.644 ±0.003GPa to 3.960 ±0.002 GPa, as shown in Figure 5.1 (c, d). In all cases for G-enhanced UDMA-MMA and HA-enhanced UDMA-MMA, the indentation modulus increased compared to unenhanced UDMA-MMA.

The addition of additives to the matrix increased the mechanical properties of the composite [108,109]. Previous research indicates that many factors may affect mechanical properties of composites measured with nanoindentation. Nanoindentation results can be affected by the size and shape of additives; for example, larger size can give higher indentation modulus compared to smaller size [110], and the distribution of additives within the matrix can affect the mechanical properties [111]. When the dimensions of the additive particles exceed that of the indenter tip, the indentation results may be dominated by the contact on the additive particle itself, or on the surrounding matrix, or the interface of these two. Furthermore, nanoindentation measurements require a smooth surface; otherwise, inconsistent values can be obtained from one position to the next [112]. AFM topography results indicate that surface roughness is more pronounced for G-enhanced UDMA-MMA specimens when compared with HA-enhanced UDMA-MMA specimens. The higher surface roughness of G-enhanced UDMA-MMA specimens may have caused lower hardness values to be measured when compared with HA-enhanced UDMA-MMA

specimens that did not have the same roughness issues during nanoindentation experiments.

When adding HA, the hardness increases by an average of 41% and the indentation modulus increased by an average of 32%. For comparison a rule-of-mixtures approach can be used to estimate the expected mechanical properties of the composite when it contains HA. Based on a polymer density of 1.16 g/cm^3, HA density of 3.16 g/cm^3, HA hardness of 10 GPa and HA indentation modulus of 150 GPa, a much lower increase in hardness (≤12%) and indentation modulus (≤10%) would be expected even for the highest weight fraction of HA used. For G applying a rule-of-mixtures estimate is problematic because the hardness and indentation modulus are meaningless for a 2-dimensional material. None-the-less the composites when compared to the UDMA-MMA blend on its own exhibit a remarkable increase in hardness, averaging 31%, and indentation modulus, averaging 30%.

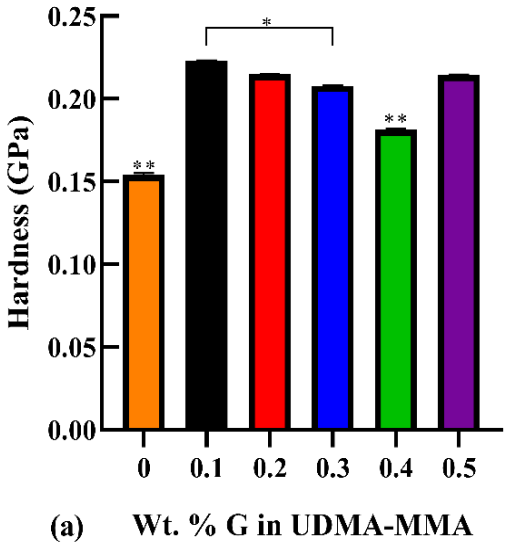

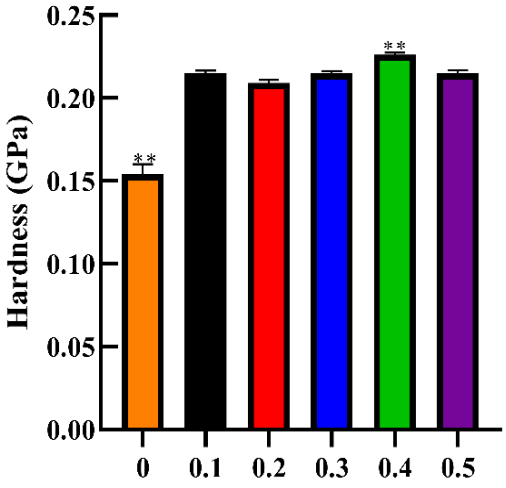

(b) Wt. % HA in UDMA-MMA

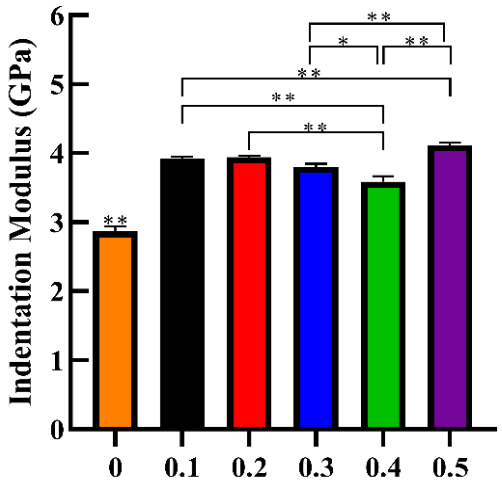

(c) Wt. % G in UDMA-MMA

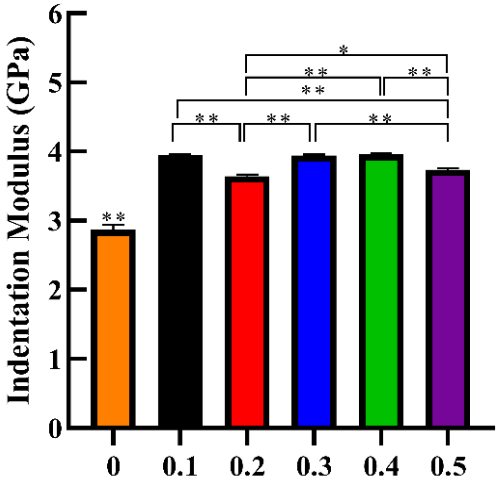
Indentation Modulus (GPa)
0
1
2
3
4
5
6
*
**
**
**
**
**
**
**
0
0.1
0.2
0.3
0.4
0.5
Wt. % HA in UDMA-MMA

(d)

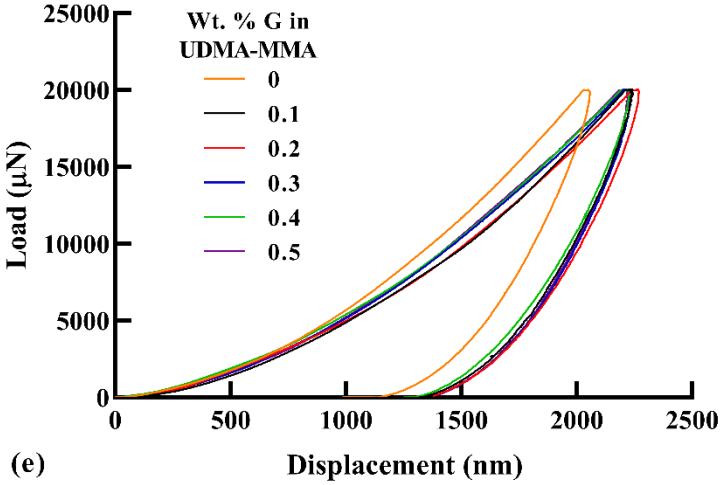
Wt. % G in
UDMA-MMA
0
0.1
0.2
0.3
0.4
0.5
Load (µN)
0
5000
10000
15000
20000
25000
0
500
1000
1500
2000
2500
Displacement (nm)

(e)

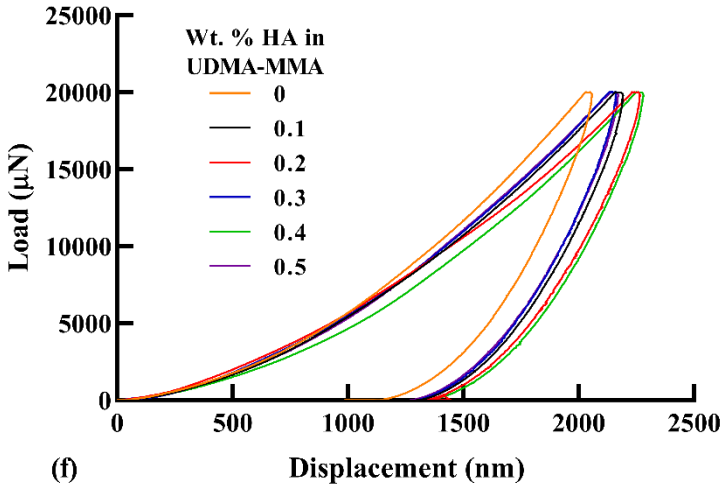

Figure 5.1. Nanoindentation results for wt. % G and HA additives in UDMA-MMA blends: (a, b) Hardness, H, (c, d) Indentation Modulus, Er, and (e, f) load-displacement curves for each composition. The statistical significances are: * indicating $p < 0.05$; ** indicating $p < 0.01$.

5.3.2 FTIR

The degree of conversion and FTIR spectra for G-enhanced UDMA-MMA and HA-enhanced UDMA-MMA composites are shown in Figure 5.2. Degree of conversion for G-enhanced UDMA-MMA is less than that of HA-enhanced UDMA-MMA, ranging from 7.2±5.8% to 20.6±2.0% and 15.8±6.8% to 43.9±3.8% for G and HA, respectively, as shown in Figure 5.2 (a, b). Degree of conversion decreased with the addition of both G and HA to the UDMA-MMA system, as compared with 0 wt. % additive in UDMA-MMA (Figure 5.2 a, b). In general, degree of conversion decreases with increasing additive concentration in UDMA-MMA, which may be due to the reduced concentration of carbon-carbon double bonds available in the monomers [113]. Several factors influence the degree of conversion, such as curing light, which depends on light density, wavelength, and light tip size, as well as additive properties like concentration [114], size, shape, and composition

[115]. It is also important to note that graphene oxide in particular, and to a lesser extent graphite and graphene, have strong absorption peaks in the wavenumber range examined [116] this may have a direct impact on the ability to measure degree of conversion. Others have observed a decrease in the mobility of the free radicals during the photo-curing process with the addition of additives to the monomer, this in turn may affect the polymerization process [117]. When G is included in the composite the FTIR spectra shows some effects due to the many vibrational modes seen in carbon based materials. In particular, there is evidence of different hybridized carbon states as well as oxygen in the spectra in the low wavenumber range 1000-1200 cm^{-1}. The double peaks at 1440/1450 cm^{-1} are present in the polymer spectra, but these do change shape and shift with the addition of G which is expected for graphene and related materials like graphene oxide. The polymers have a peak at around 1635 cm^{-1}, which does not change when the G is added, this would have been expected if there was a significant amount of graphite present. Peaks are expected at 1130 cm^{-1} and 1344 cm^{-1} for diamond [118,119], but these are not present.

The FTIR spectra of HA has a number of peaks associated with stretching and bending vibrational modes of the phosphate group, PO_4. These are seen in the detailed spectra, which show the ν_1 and ν_3 stretch modes, and the ν_4 bending mode [120,121]. However, the main peaks associated with the polymer are mostly unchanged with the exception of very small shifts in the N-H peak ~ 1528 cm^{-1} and the C=O double overlapping peaks ~ 1701 and ~ 1710 cm^{-1}. These are both affected by hydrogen bonding [85,86,122], which is slightly modified by the hydroxyl group of the HA.

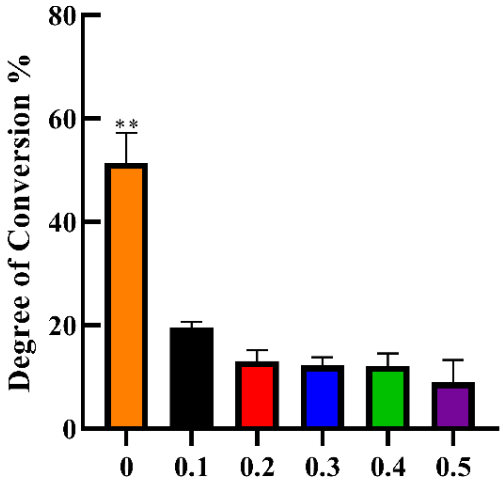

(a) Wt. % G in UDMA-MMA

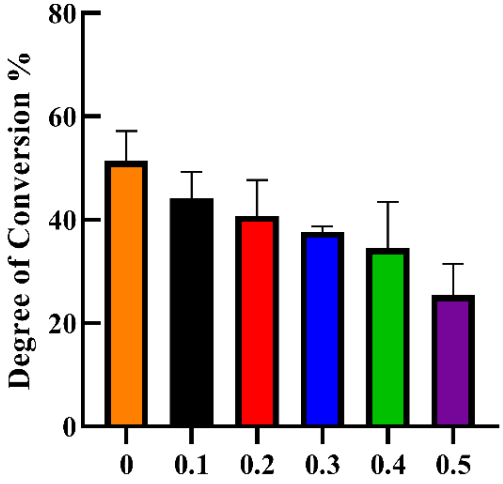

(b) Wt. % HA in UDMA-MMA

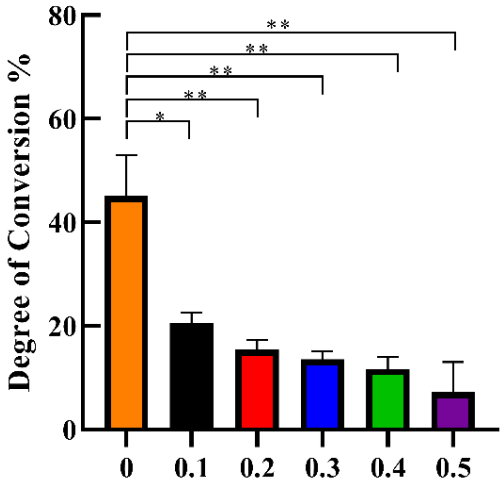

(c) Wt. % G in UDMA-MMA

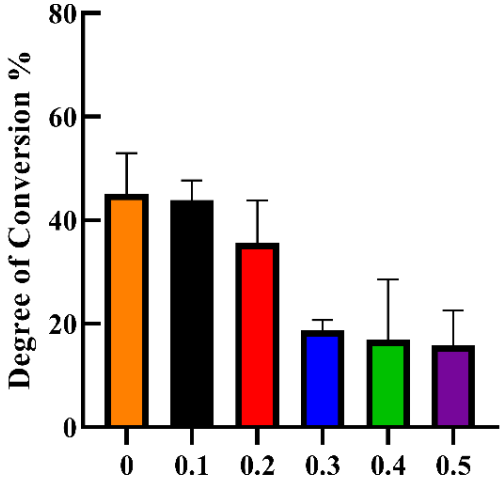

(d) Wt. % HA in UDMA-MMA

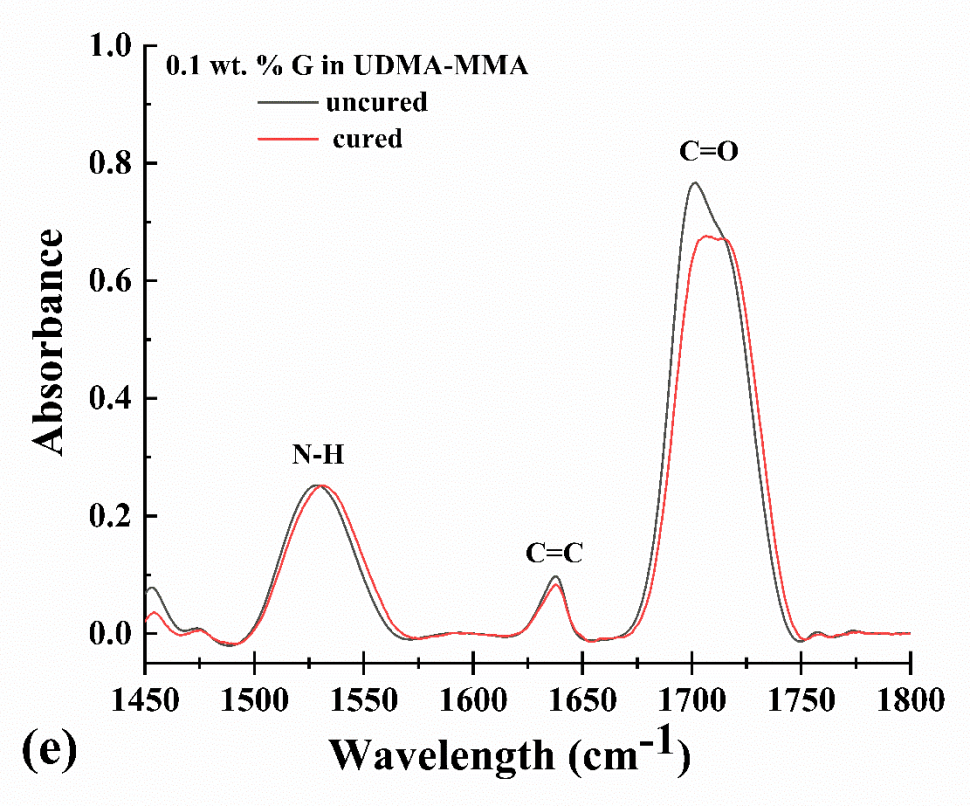
0.1 wt. % G in UDMA-MMA
uncured
cured
C=O
N-H
C=C
Absorbance
1.0
0.8
0.6
0.4
0.2
0.0
1450
1500
1550
1600
1650
1700
1750
1800
Wavelength (cm-1)
(e)

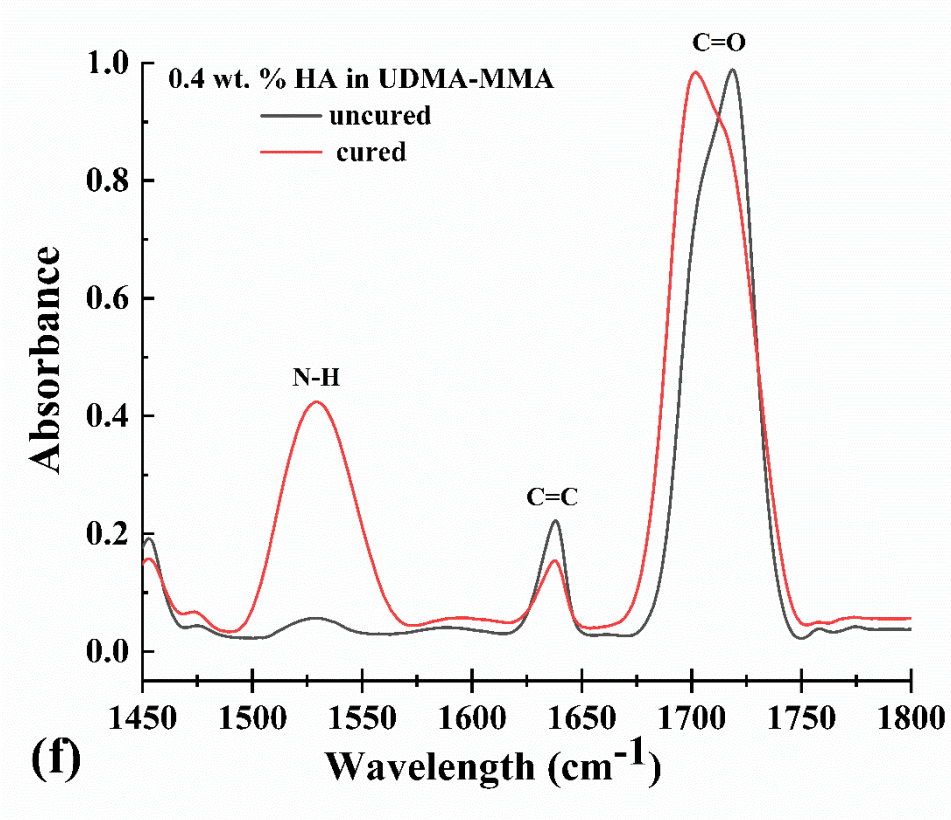
0.4 wt. % HA in UDMA-MMA
uncured
cured
C=O
N-H
C=C
Absorbance
1.0
0.8
0.6
0.4
0.2
0.0
1450
1500
1550
1600
1650
1700
1750
1800
Wavelength (cm-1)
(f)

Figure 5.2. FTIR results for enhanced UDMA-MMA blends:(a, b) the degree of conversion vs. wt. % G and HA with internal standard peak A_{N-H}; (c, d) the degree of conversion vs. wt. % G and HA with internal standard peak $A_{C=O}$; (e, f) spectra of uncured and cured samples of 0.1 wt. % G in UDMA-MMA and 0.4 wt. % HA in UDMA-MMA; Statistical significance of differences is given by * indicating $p < 0.05$ and ** indicating $p < 0.01$

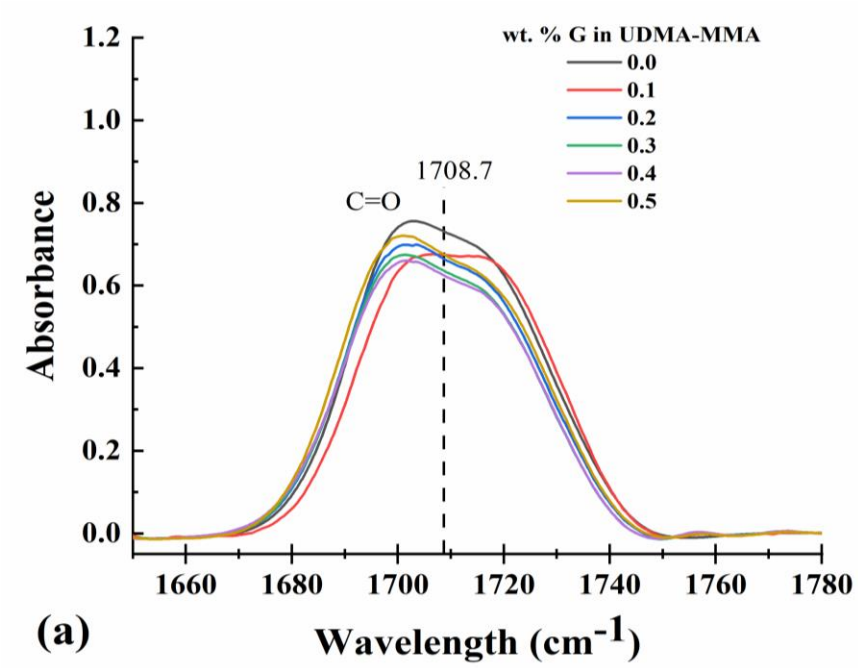

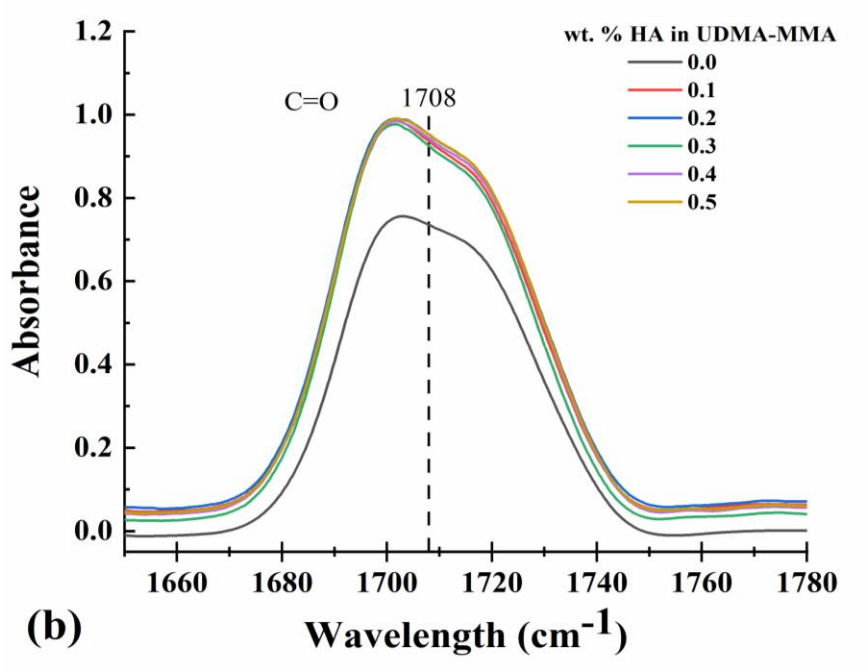
wt. % HA in UDMA-MMA
0.0
0.1
0.2
0.3
0.4
0.5
C=O
1708
Absorbance
Wavelength (cm-1)
(b)

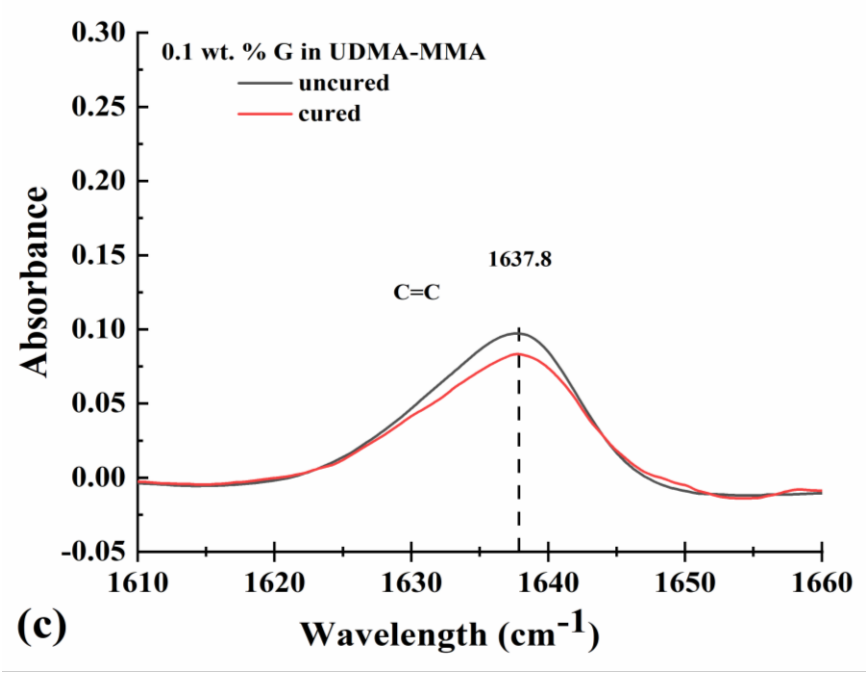
0.1 wt. % G in UDMA-MMA
uncured
cured
1637.8
C=C
Absorbance
Wavelength (cm-1)
(c)

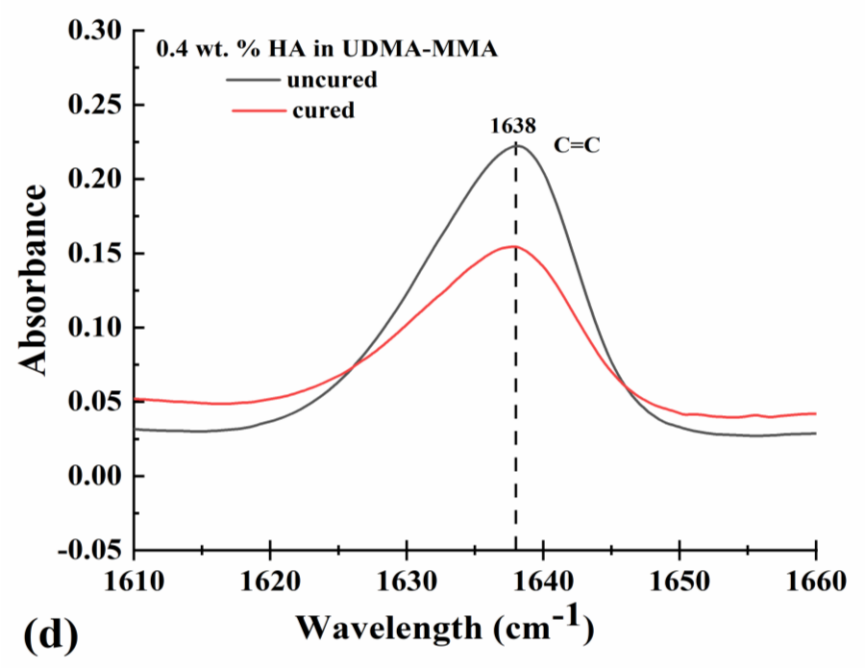
0.4 wt. % HA in UDMA-MMA
uncured
cured
1638
C=C
Absorbance
0.30
0.25
0.20
0.15
0.10
0.05
0.00
-0.05
1610
1620
1630
1640
1650
1660
Wavelength (cm-1)
(d)

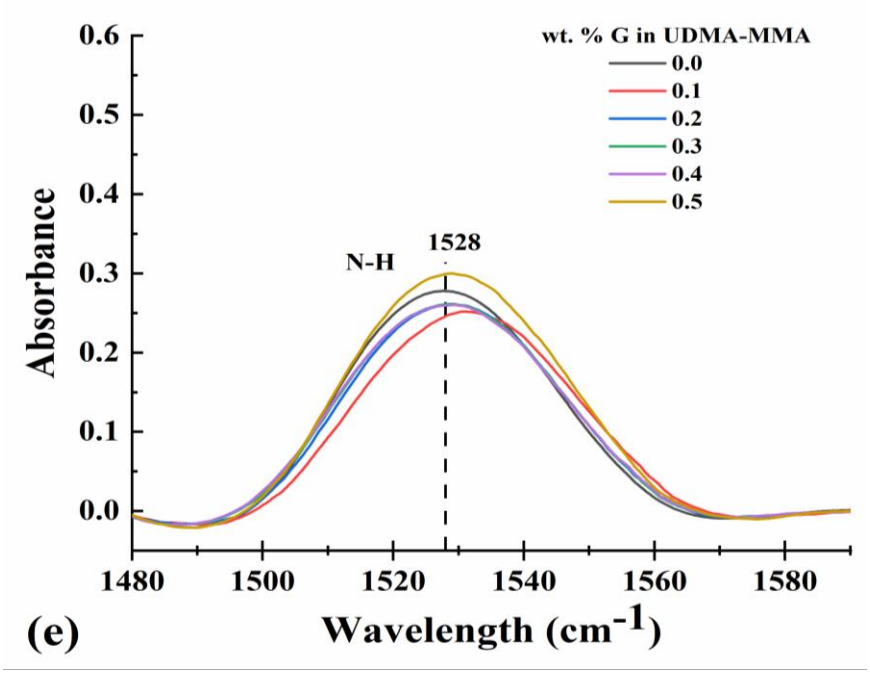
wt. % G in UDMA-MMA
0.0
0.1
0.2
0.3
0.4
0.5
N-H
1528
Absorbance
0.6
0.5
0.4
0.3
0.2
0.1
0.0
1480
1500
1520
1540
1560
1580
Wavelength (cm-1)
(e)

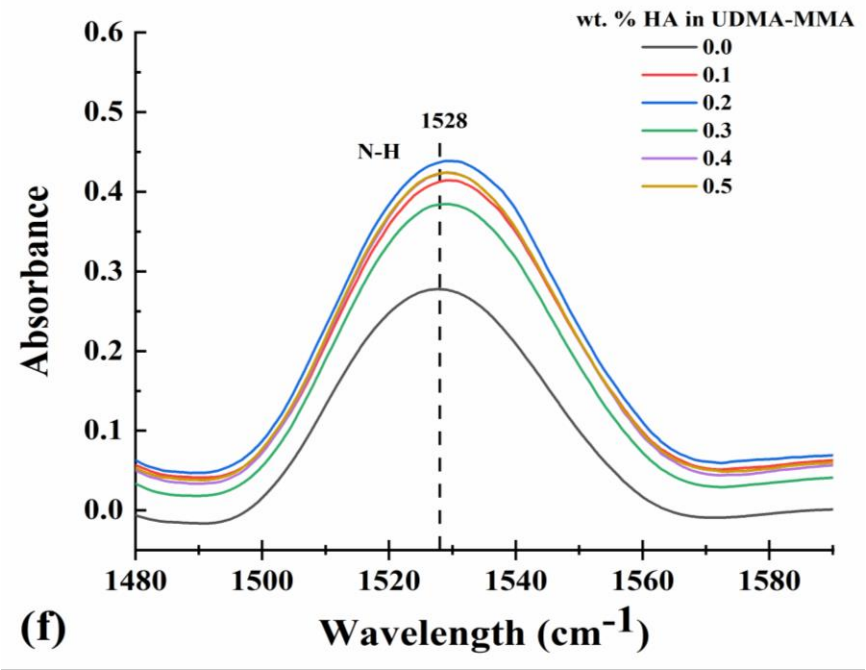

Figure 5.3. FTIR results for UDMA-MMA blends: (a, b) FTIR spectra of C=O bond for all concentration of UDMA-MMA with 0.1 wt. % G and 0.4 wt. % HA cured; (c, d) FTIR spectra for C=C bond showing cured and uncured samples for 0.1 wt. % G and 0.4 wt. % HA in UDMA in MMA; (e, f) FTIR spectra of N-H bond for all concentration of UDMA-MMA 0.1 wt. % G and 0.4 wt. % HA cured;

5.3.3 Micro-Raman Spectroscopy

Much like FTIR, micro-Raman is another vibrational spectroscopy method that may be used to examine the degree of conversion of double C=C bonds to single C-C bonds. Degree of conversion and the micro-Raman spectra for G-enhanced UDMA-MMA and HA-enhanced UDMA-MMA composites are shown in Figure 5.4 (a, b). Intriguingly, for G-enhanced UDMA-MMA, results indicate no statistical significant difference between any of the concentrations, which is a different result, to that obtained using FTIR spectra. For HA-enhanced UDMA-MMA, the degree of conversion was lower, when compared to the 0 wt. % HA in the UDMA-MMA system, and only the lowest concentration of 0.1 wt.

% HA did not have a significant impact on the measured degree of conversion. Not only do FTIR and micro-Raman spectra provide information on the degree of conversion of C=C double bonds to C-C single bonds, there is additional information contained in the peaks that can help explain how G and HA affect the UDMA-MMA adhesive system. In this work, FTIR spectra indicate higher degree of conversion for HA-enhanced UDMA-MMA than G-enhanced UDMA-MAA. However, the micro-Raman spectra indicate a lower degree of conversion for G-enhanced UDMA-MAA than HA-enhanced UDMA-MMA. In general, degree of conversion is less for G-enhanced UDMA-MAA and HA-enhanced UDMA-MMA composites when compared with UDMA-MMA alone. Similar results have been obtained previously for additives to the Bis-GMA/TEGDMA matrix [123].

It is important to note that the degree of conversion analysis assumes that the only changes in the vibrational spectra due to the additives result from changes in the conversion of bonds. The data is more consistent with the additives impacting not just conversion of bonds, but also the absorption and scattering of the blue light used during the cure process. Differences in refractive index of the additives and monomers will affect the degree of conversion, since light transmission during the photopolymerization process is dependent upon refractive index of the medium, especially at the interface between the additives and matrix. The additives themselves will also have vibrational spectra, which can modify the observed peaks [124]. Beyond the blue-light curing, it is possible that when using the micro-Raman laser (red color) there may cause be local heating that also affects the conversion of bonds.

The micro-Raman spectra for the composites are particularly significant since there are strong Raman peaks associated with the phosphate group, PO_4, in HA and carbon polytypes are commonly characterized and identified using Raman [125]. When G is added there are three regions of interest: the characteristic G-peak ~1570 cm^{-1} that is expected for graphene [126], plus a number of features associated with defective graphene and edges of graphite sheets that give rise to a D′-peak ~1630 cm^{-1} and D-peaks ~1270-1400 cm^{-1} [120,121,127]. With HA the micro-Raman spectra the presence of all the expected PO_4 vibrational modes, ν_1, ν_2, ν_3 and ν_4 [128].

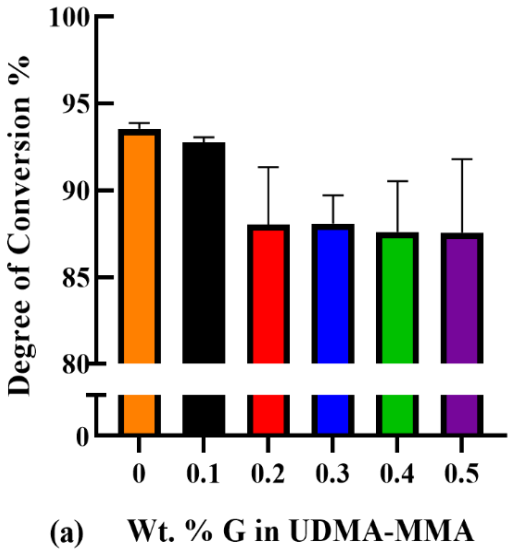

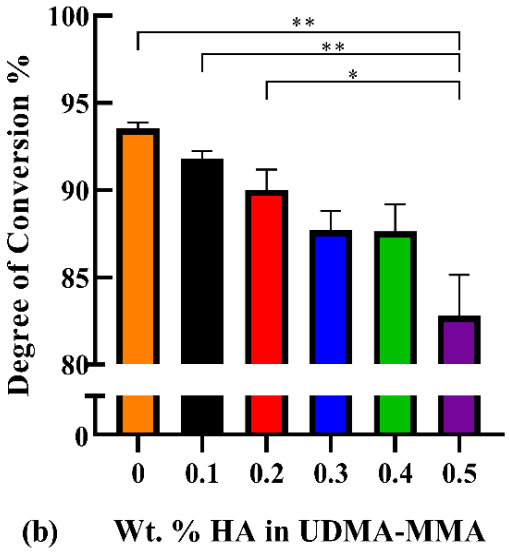
100
95
90
85
80
0
Degree of Conversion %
**
**
*
0
0.1
0.2
0.3
0.4
0.5
(b) Wt. % HA in UDMA-MMA

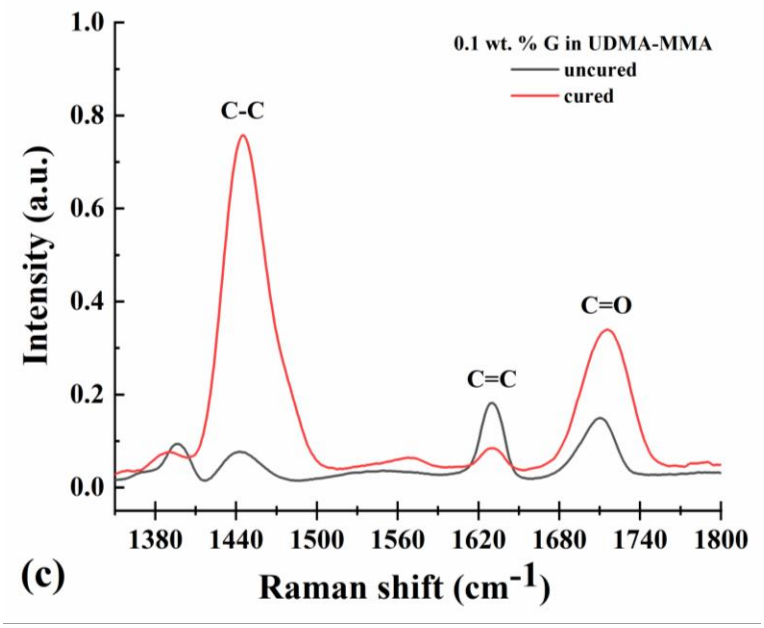
0.1 wt. % G in UDMA-MMA
uncured
cured
C-C
C=C
C=O
Intensity (a.u.)
1.0
0.8
0.6
0.4
0.2
0.0
1380
1440
1500
1560
1620
1680
1740
1800
(c)
Raman shift (cm-1)

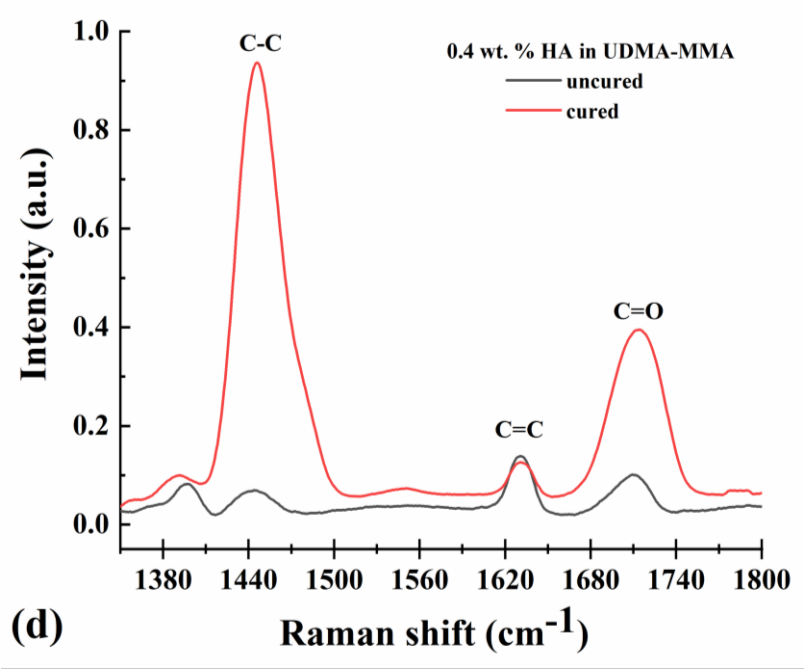

Figure 5.4. Micro-Raman results for enhanced UDMA- MMA blends: (a, b) the degree of conversion vs. wt. % G and HA with internal standard peak $A_{C=O}$; (c, d) Micro-Raman spectra of uncured and cured samples for 0.1 wt. % G and 0.4 wt. % HA in UDMA-MMA. Statistically significant differences are given by * indicating $p < 0.05$ and ** indicating $p < 0.01$

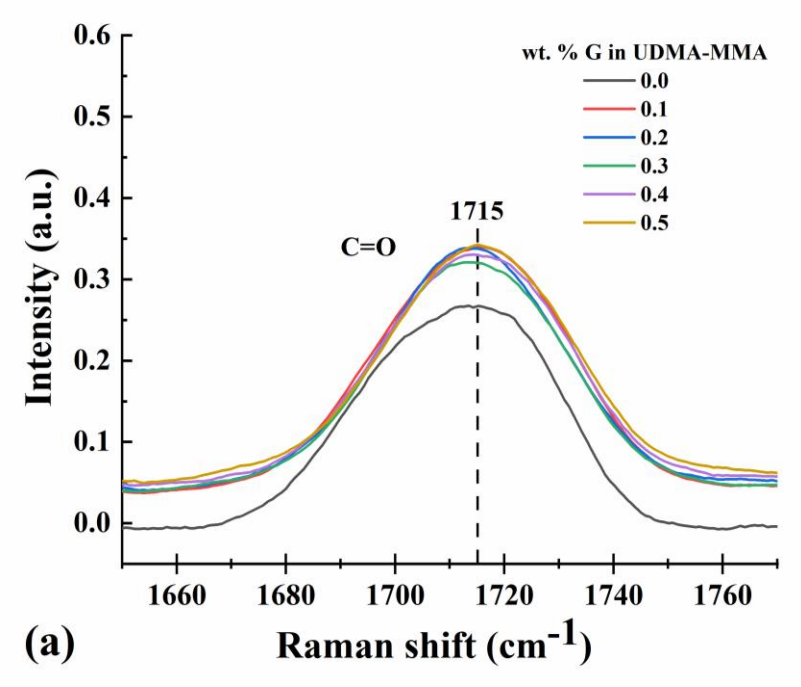
wt. % G in UDMA-MMA
0.0
0.1
0.2
0.3
0.4
0.5
1715
C=O
Intensity (a.u.)
0.0
0.1
0.2
0.3
0.4
0.5
0.6
1660
1680
1700
1720
1740
1760
(a)
Raman shift (cm-1)

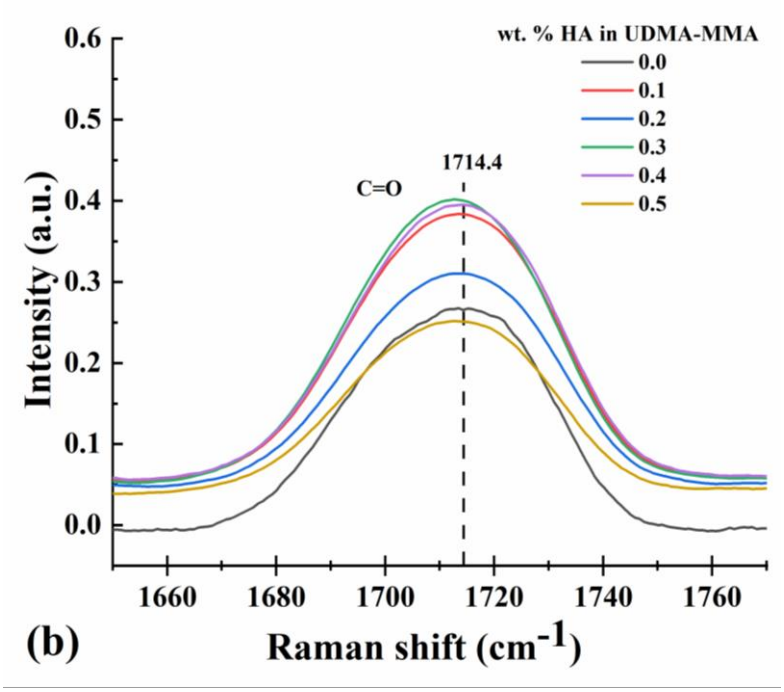
wt. % HA in UDMA-MMA
0.0
0.1
0.2
0.3
0.4
0.5
1714.4
C=O
Intensity (a.u.)
0.0
0.1
0.2
0.3
0.4
0.5
0.6
1660
1680
1700
1720
1740
1760
(b)
Raman shift (cm-1)

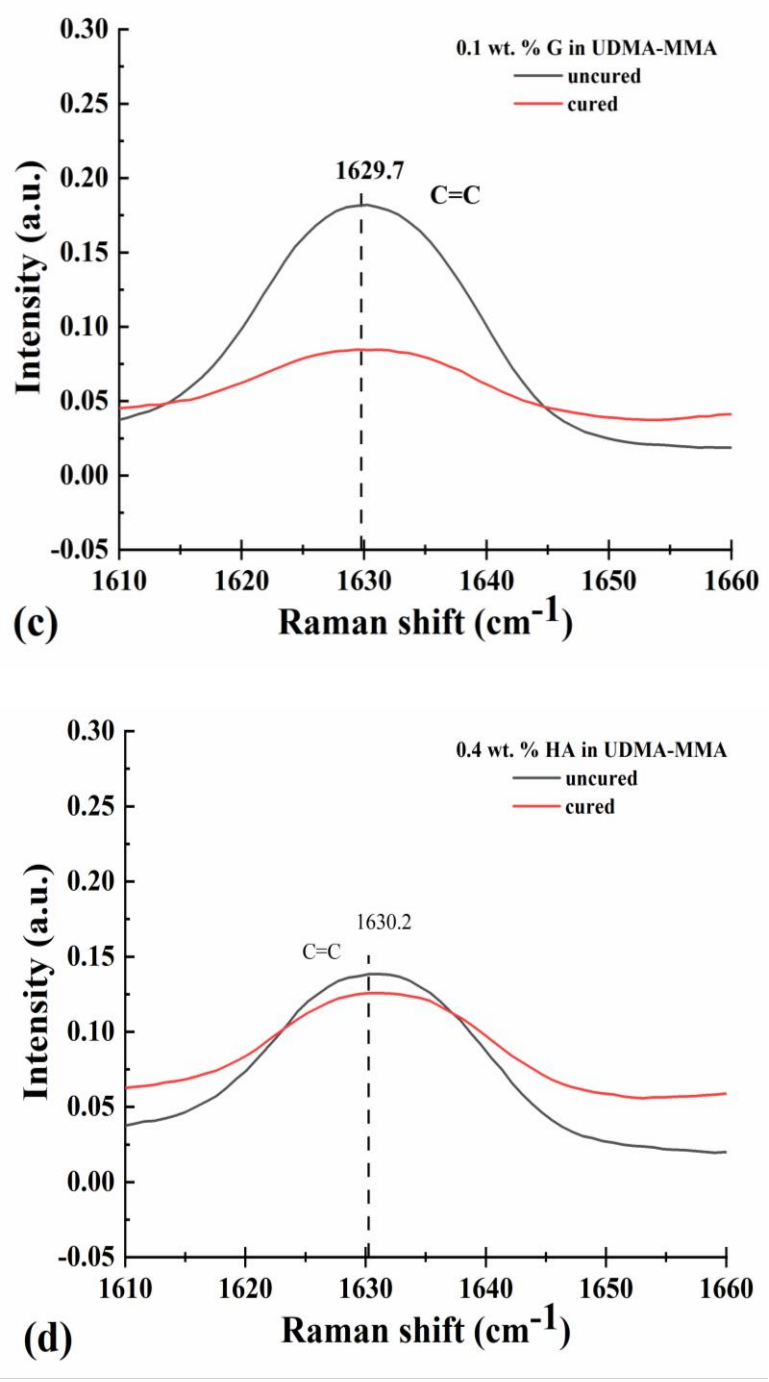

Figure 5.5. Micro-Raman results for enhanced UDMA- MMA blends: (a, b) Micro-Raman spectra of C=O bond for all concentration of UDMA-MMA with G and HA cured; (c, d) Micro-Raman spectra of C=C bond for 0.1 wt. % G and 0.4 wt. % HA in UDMA-MMA

5.3.4 Viscosity

Viscosity results for G-enhanced UDMA-MMA and HA-enhanced UDMA-MMA composites are shown in Figure 5.6 (a, b). Viscosity decreases with increasing shear rate for all UDMA-MMA composites when enhanced with either G or HA, indicating thixotropic or non-Newtonian behavior [129], as shown in Figure 5.6 (a, b). Viscosity increases with increasing G or HA concentration in UDMA-MMA composites, as shown in Figure 5.6 (c, d), which is typical what would be expected when increasing additive concentration in polymers [130,131]. The viscosity of G-enhanced UDMA-MMA ranges from 0.024±0.001 Pa·s to 0.043±0.001 Pa·s, while the viscosity of HA-enhanced UDMA-MMA ranges from 0.024±0.001 Pa·s to 0.074±0.001 Pa·s. Interestingly, for the same concentration of additive in UDMA-MMA, the viscosity is higher for HA than G for graphite and graphene can be sheared easily, which could lower viscosity. They may be acting as solid lubricants in UDMA-MMA. Statistical analysis confirms the significance of the viscosity increases in UDMA-MMA when enhanced with G or HA compared to UDMA-MMA without any additives.

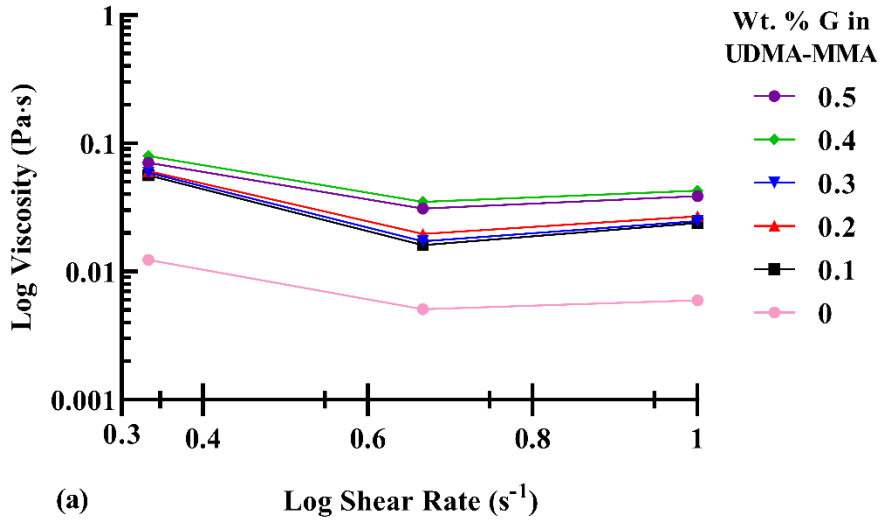
Log Viscosity (Pa·s)
1
0.1
0.01
0.001
0.3
0.4
0.6
0.8
1
Log Shear Rate (s-1)
Wt. % G in UDMA-MMA
0.5
0.4
0.3
0.2
0.1
0

(a)

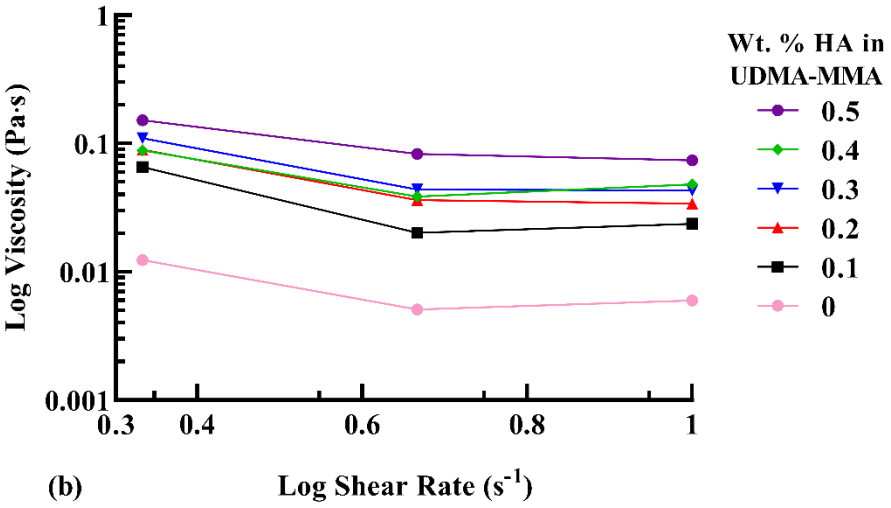
Log Viscosity (Pa·s)
1
0.1
0.01
0.001
0.3
0.4
0.6
0.8
1
Log Shear Rate (s-1)
Wt. % HA in UDMA-MMA
0.5
0.4
0.3
0.2
0.1
0

(b)

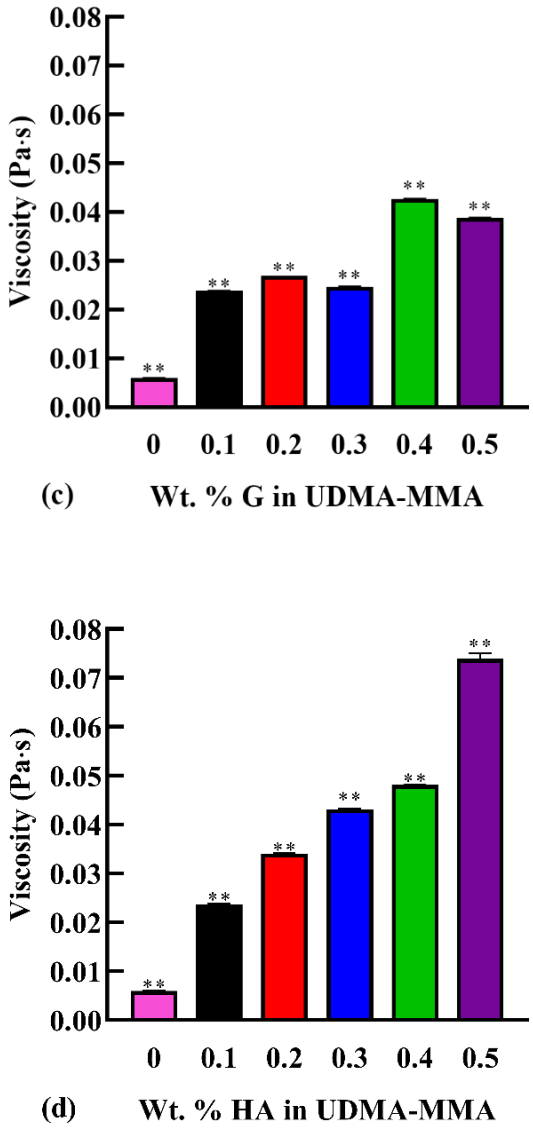

Figure 5.6. Viscosity results for UDMA-MMA blends with different concentrations of G and HA at T = 25 °C: (a, b) viscosity of UDMA-MMA blends as a function of shear rate; (c, d) viscosity vs. wt. % of G and HA at shear rate of 10/s. Statistically significant differences are shown with ** indicating $p < 0.01$.

5.3.5 AFM

AFM images of G-enhanced UDMA-MMA and HA-enhanced UDMA-MMA are shown in Figure 5.7. The 3D morphology shows some differences with the G additive

giving more “plateau” like features compared to the HA additive (Figure 5.7 a, b). Statistical measurement of roughness gives values for 0.1 wt. % G that are higher than those of 0.1 wt. % HA (Figure 5.7 c, d) and are presented in Table 5.2.

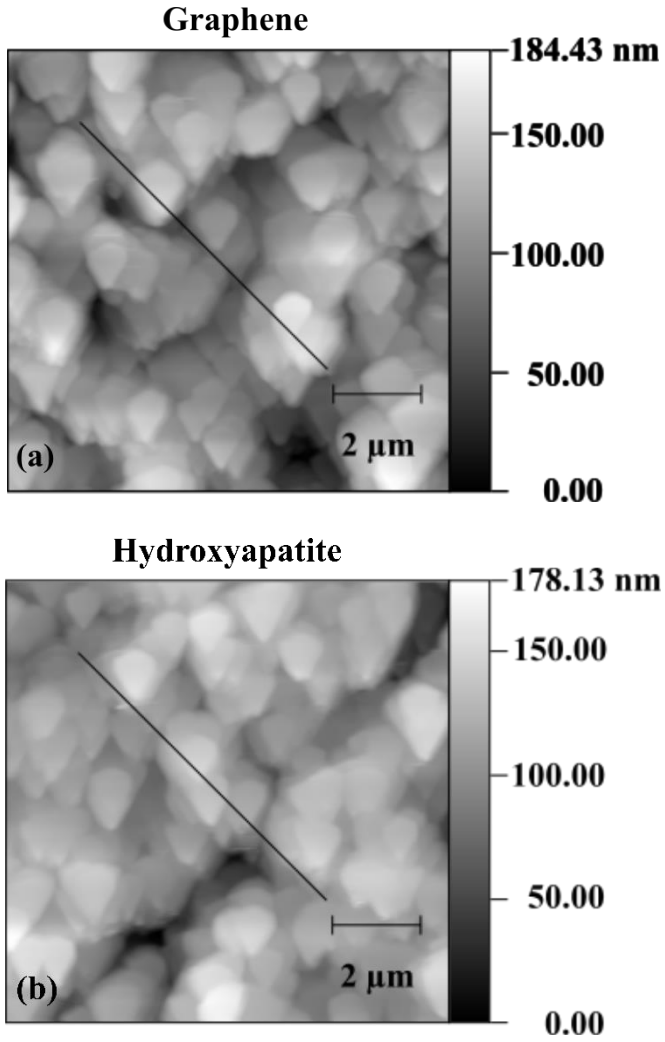

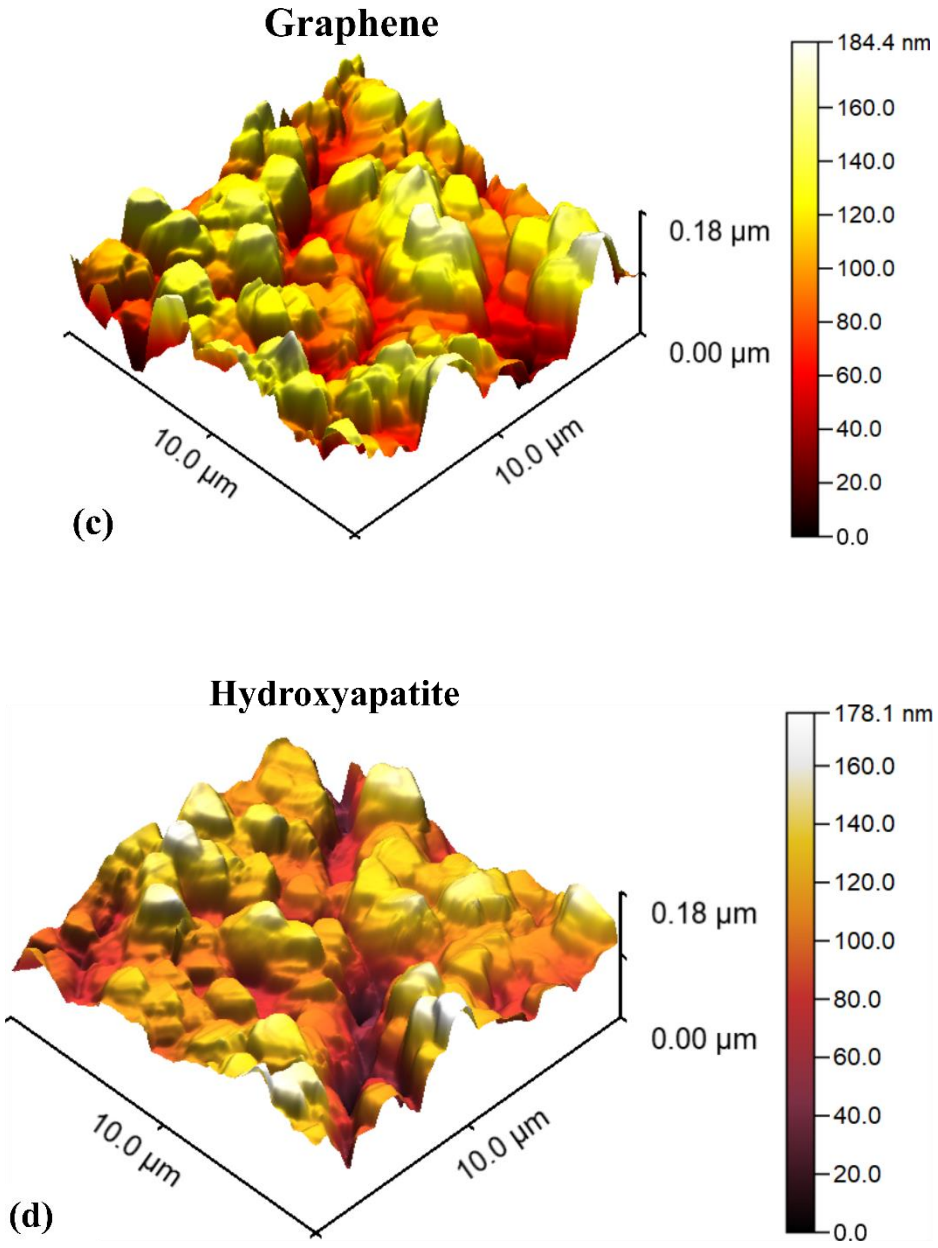

Figure 5.7. AFM results for 0.1 wt. % G-enhanced UDMA-MMA (a, c) and 0.1 wt. % HA-enhanced UMDA-MMA (b, d) surface morphology and showing 3D topography, respectively

Table 5.2. The roughness properties of UDMA-MMA blends with 0.1 wt. % G and 0.1 wt.% HA.

Roughness Properties	Graphene	Hydroxyapatite
Average	5.8 nm	3.5 nm
Root mean square	7.9 nm	4.3 nm
Maximum height	48.9 nm	20.6 nm

5.3.6 Thermography

Thermographic images of the UDMA-MMA blends without or with 0.1 wt.% G and 0.1 wt. % HA additives are shown in Figure 5.8 (a, b and c). The thermographic images show temperature as color, which change during the curing process. For example, Figure 5.8 a shows curing of the UDMA-MMA specimen without any additive; the colors indicate that the curing is faster and more uniform than the other. Figure 5.8 (b, c) show the thermographic images of the UDMA-MMA blends with G and HA additives, which take a longer time to cure. The ranges and distributions of temperature in these samples are likely related to the light scattering and absorption properties of the matrix and additives during the curing process. Comparing the G-enhanced UDMA-MMA to the HA enhanced system shows a much more uniform temperature distribution at the same time of curing, which may be related to the thermal conductivity of graphene being higher than hydroxyapatite. For example, at 40 sec cure the G-enhanced UDMA-MMA is almost cured whereas HA enhanced UDMA-MMA is still not fully cured. This is a clear sign that the curing process is impacted by the additives and that this may be more important in determining properties that the effect of simply creating a simple composite by adding G and HA to the blends.

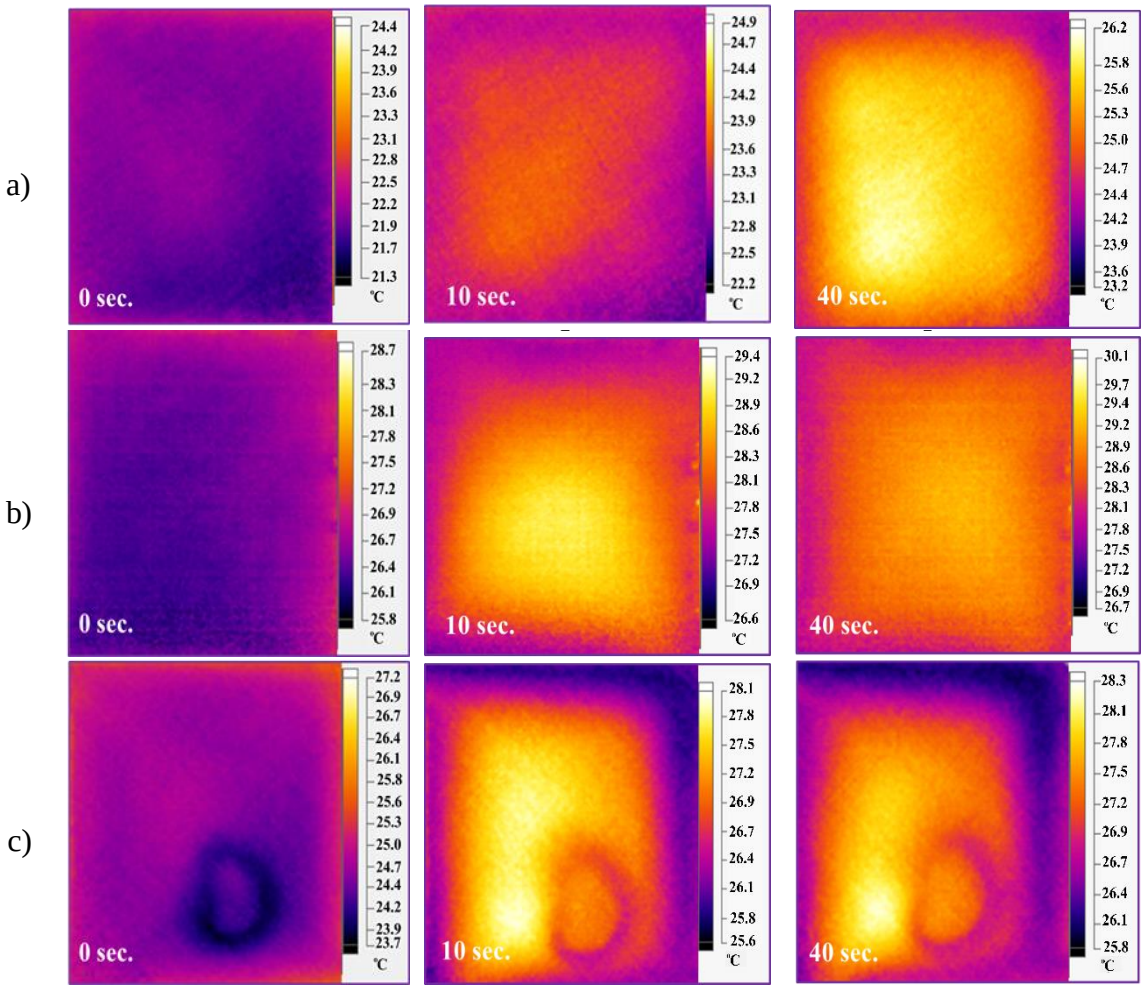

Figure 5.8. Thermographic images for: (a) 50wt.% UDMA-MMA blend, (b) 0.1 wt.% G-enhanced UDMA-MMA, (c) 0.1 wt. % HA-enhanced UDMA-MMA

5.4 Conclusion

The effect of graphene and hydroxyapatite in UDMA-MMA on the mechanical properties of the photopolymerized blends was found to be significant even at very low wt.% when compared with UDMA-MMA alone. Concentration of the additives (G or HA) had a noticeable effect on the measured degree of conversion of double C=C bonds to single C-C bonds. Specifically, FTIR data indicated a decrease in the degree of conversion as did micro-Raman, though to a lesser extent. These values should be viewed as a

qualitative measure because the additives likely had many effects on the observed spectra including modifying the heights, widths and positions of peaks. The refractive index, scattering and absorption of photons by the additives impacts the vibrational spectra obtained with FTIR and micro-Raman, as well as the photo-curing process itself.

The net effect of the addition of either graphene or hydroxyapatite to the UDMA-MMA was to increase the hardness and indentation modulus beyond what would be expected for a simple composite structure. This is indicative that the curing and, hence, the properties of the blends is changed by the additives. It is possible that the curing may be affected by the catalytic properties of the additives, see for instance the review by Nia and Binder[132]. Collectively, the vibrational spectra, mechanical properties and imaging suggest the additives change the mechanical properties by modifying the curing and bonding in the composites. This combination of modified curing rates and additional bonding between the matrix and additives is likely the source of the increased mechanical properties seen in the cured state. In the uncured state the liquid's viscosity is affected by the additives, but the impact is less. This suggests the use of these additives could be a way to improve the mechanical properties of the adhesive system while still retaining low viscosity in the uncured state. There is the additional benefit that both G and HA have functional properties that may beneficial in specific applications, for instance HA in biomedical hard tissue applications where it's biocompatibility may encourage biomineralization.

6 CHAPTER 6. UDMA-MMA ADHESIVE SYSTEM APPLIED TO COW TEETH

6.1 Introduction

Dental adhesives are essential materials used to bind composite restorative with dental tissues (enamel and dentin) using a process called hybridization (this involves micromechanical bonding). The hybridization process occurs when the dental adhesive is applied to the tooth and penetrates to the underlying tooth tissues that in the dentin surround the collagen I fibers forming the hybrid layer [133]. The integrity of the hybrid layer depends on many factors such as: (1) roughness of the tooth's surface, which is related to the preceding etching process time and type of etchant, as well as their pH [134,135]; (2) The thickness of the adhesive layer, and the composition of the adhesive layer [136,137]. An insufficient penetration of the adhesive into the dental tissues, that does not contain collagen I fiber increases the probability of failure of the composite resin [138].

In this chapter an assessment of the efficacy of the UDMA-MMA adhesive system as prepared in chapter 4 for adhesion to teeth is described. The photo-cured adhesive system with different weight percentage compositions of the UDMA-MMA adhesive system were applied to cow teeth and these were then characterized. The UDMA as previously discussed was used as a high molecular weight monomer combined with various weight percentages of MMA, which is a lower molecular weight and lower viscosity monomer, in order to improve the infiltration of the adhesive system [139]. It is hypothesized that the improved infiltration combined with good mechanical properties will give a better bond between the adhesive/composite and the teeth. Nanoindentation was used to calculate the mechanical properties of the hybrid layer formed between the adhesive and the teeth. Microhardness (Vickers indentation) was used to determine delamination in

the junction area between the hybrid layer and the dental tissues (both enamel and dentin). Scanning Electron microscopy and optical microscopy were used to image the hybrid layer as a way of assessing the contiguity of the bonding.

6.2 Materials and Methods

6.2.1 Materials

The photo-cured adhesive system used in this chapter is the same adhesive as described in chapter 4, which included five different compositions of UDMA-MMA. Cow teeth were used (instead of human teeth) and prepared as mentioned in chapter two section 2.3.2.

6.2.2 Sample Preparation

Cow teeth were used as the substrate with the UDMA-MMA photo-cured adhesive systems being applied to the surface. Each concentration of UDMA-MMA was applied to three specimens of cow teeth. The cow teeth were prepared as mentioned in section 3.2.1, which included extracting the teeth from the skull, removing all the soft tissues (skin) and blood from the teeth. The teeth were cut to suitable specimen sizes, the surface of the teeth were then polished to obtain flat and smooth surfaces. Etching of the surface was performed using 37 % phosphoric acid for 10 sec and then washing it with water. The UDMA-MMA adhesive system was then applied to the surface, cured with blue light for different length of time dependent on the viscosity, and lastly, applying and curing the commercial composite resin Z100 on the adhesive layer.

For nanoindentation testing the coated cow teeth samples were mounted using cyanoacrylic and stored in Hank's buffer solution until testing. Hank's buffer solution is a balanced salt solution that has been shown to be best for storage of the teeth prior to

mechanical testing [140]. For SEM testing a representative composition of 30 wt. % UDMA in MMA was gold coated with a thickness of ~10 nm and stored in a vacuum for one week prior to viewing on the SEM. For microhardness testing, the same representative composition of 30 wt. % UDMA in MMA was used.

6.3 Results and Discussion

6.3.1 Nanoindentation

The results of nanoindentation on the junction area between the adhesive-enamel and between the adhesive-dentin are shown in Figure 6.1 and Figure 6.2. The hardness values for the adhesive-enamel junction ranged from 1.148±0.03GPa to 1.547±0.006 GPa, while the hardness values for the adhesive-dentin junction ranged from 0.248±0.001 GPa to 0.315±0.03 GPa. The indentation modulus values for the adhesive-enamel junction ranged from 29.440±0.062 GPa to 88.838±0.109 GPa, while the indentation modulus for the adhesive-dentin junction area ranged from 6.382±0.059 GPa to 8.238±0.056 GPa. For the narrow hybrid layer that forms at the interface of the adhesive and the teeth, the hardness value is 0.278±0.001 GPa, and the indentation modulus value is 4.613±0.010 GPa. Figure 6.3 (a) shows nanoindentation test regions between adhesive-enamel junction and adhesive-dentin junction areas. The hardness and indentation modulus for the adhesive-enamel junction area is higher than for the adhesive-dentin junction area, which is attributed to: (1) the mechanical properties of enamel are higher than dentin; (2) the different chemical composition of enamel and dentin, since dentin contains higher percentage of organic materials; (3) dentin is more porous than enamel and so the morphology is different.

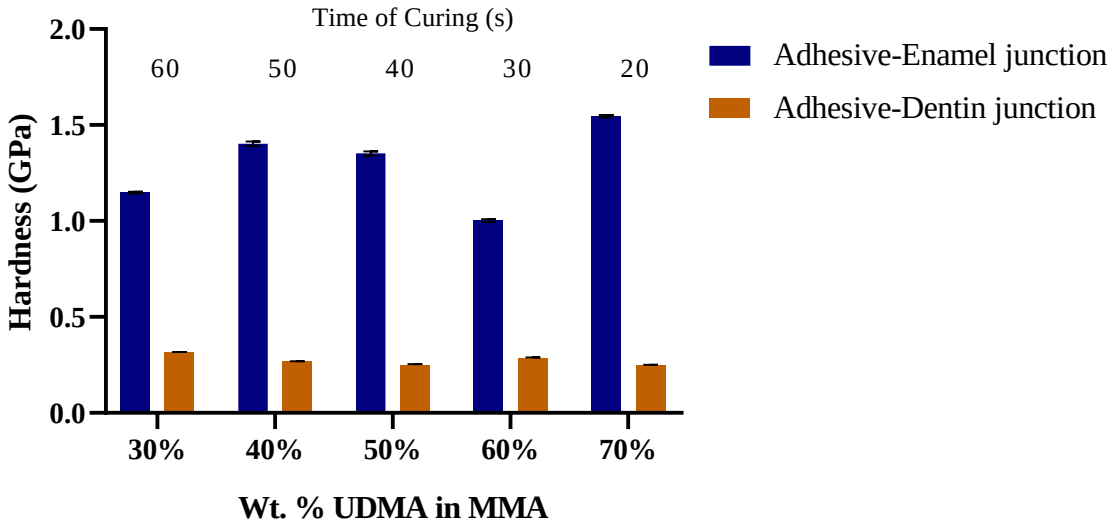

Figure 6.1. The hardness vs. wt.% UDMA in MMA in junction area with cow tooth layers

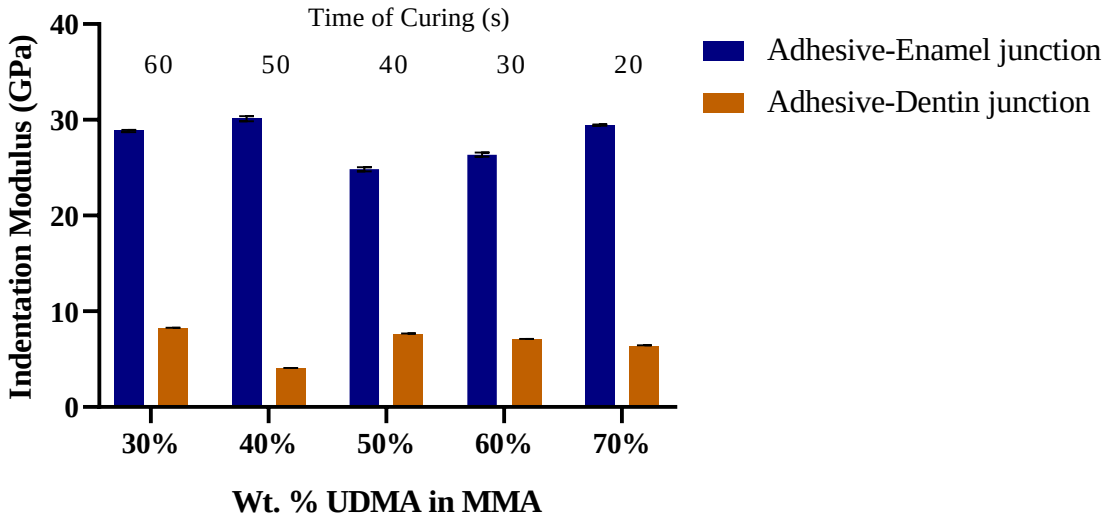

Figure 6.2. The Indentation modulus vs. wt.% UDMA in MMA in junction area with cow tooth layers

6.3.2 Microscopy

Figure 6.3 shows the microscopy image of the junction area of the cow tooth specimen coated with 30 wt. % UDMA-MMA adhesive. Figure 6.3 (a) show there is a good bond between the adhesive layer and composite with no noticeable gaps, and a good

bond between the adhesive and cow tooth, enamel and dentin. Figure 6.3 (b), which is a higher magnification shows the hybrid layer resulting from application of 30 wt.% UDMA in MMA as the adhesive layer on the cow tooth.

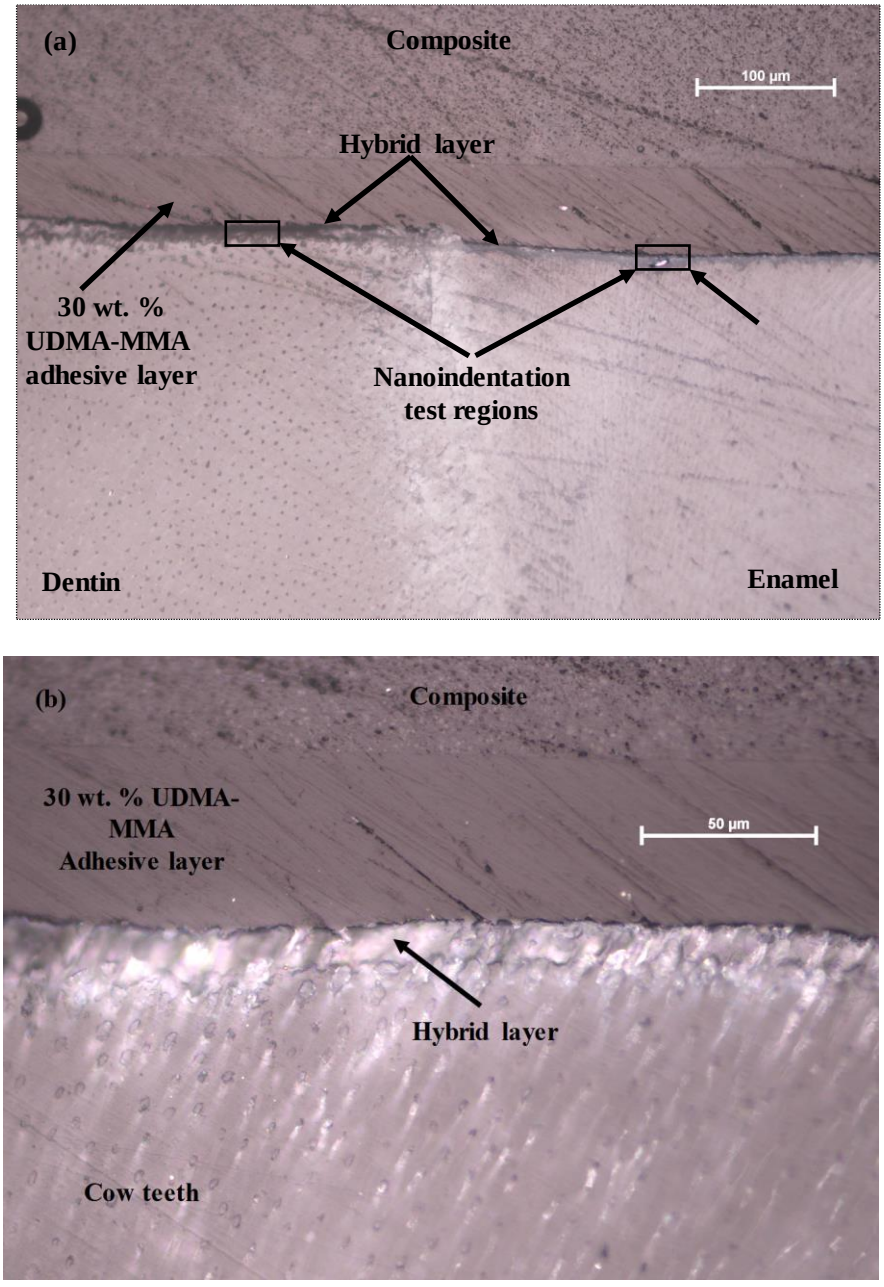

Figure 6.3. Microscopy image: (a) 5X magnification image of cow teeth with 30 wt. % UDMA in MMA; (b) 50X magnification image of the hybrid layer

6.3.3 Microindentation

An indentation created on the surface of the 30 wt. % UDMA in MMA coated cow tooth specimen is shown in Figure 6.4. The indent can be seen in the junction areas of the (a) adhesive-enamel and (b) adhesive-dentin areas. The microindentation was made in the specimen using a Vickers shaped indenter tip loaded with a maximum force of 1 kg. The images show that no delamination occurred in the junction area between the adhesive-enamel and the adhesive-dentin area, indicating that 30 wt. % UDMA in MMA provides a strong bond with both enamel and dentin of the tooth.

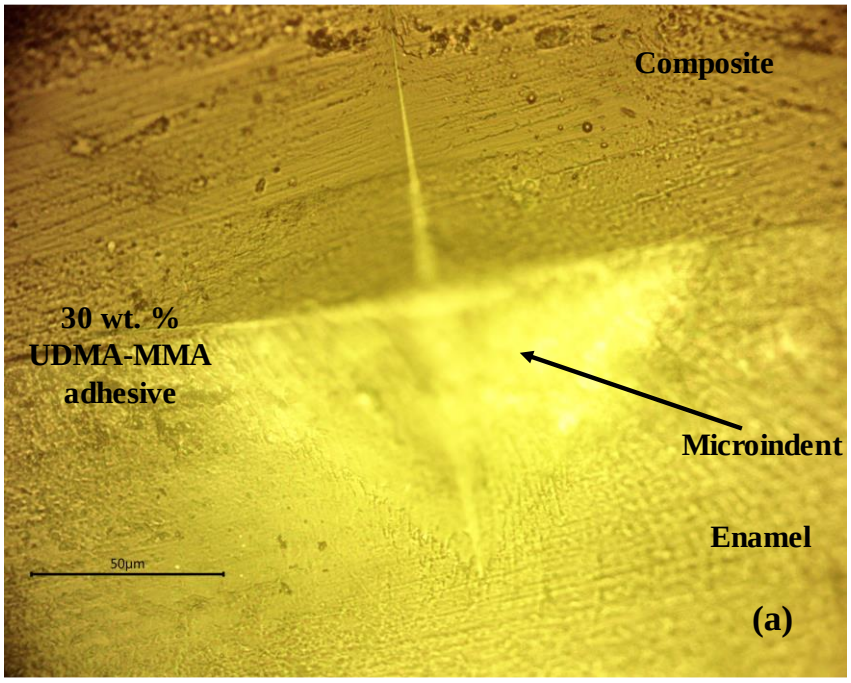

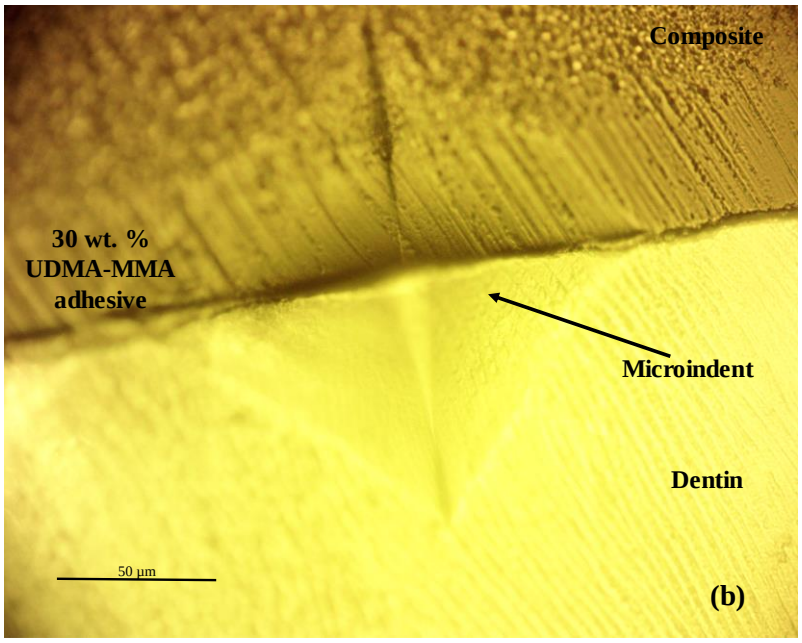

Figure 6.4. Microindentor test images of 30 wt. % UDMA in MMA on cow tooth with load 1Kg: (a) Adhesive-enamel junction; (b) Adhesive -dentin junction

6.3.4 SEM

Figure 6.5 (a and b) shows the hybrid layer is formed after applied 30 wt.% UDMA in MAA on cow teeth tissues. The 30 wt.% UDMA in MMA is the lowest viscosity was presented in chapter 4, therefore, there is no gap between the adhesive system and cow tooth tissues. This results obtained because penetrate the low viscosity adhesive system into the tooth layers and formed chemical and mechanical bonds in this area. This chemical and mechanical bonds occurs between the monomers and the ionic, which is already exist in the tooth layers. As well as a good hybrid layer and strong bond obtain better mechanical properties, which is also important to not form gap after curing the composite resin to fill the cavity.

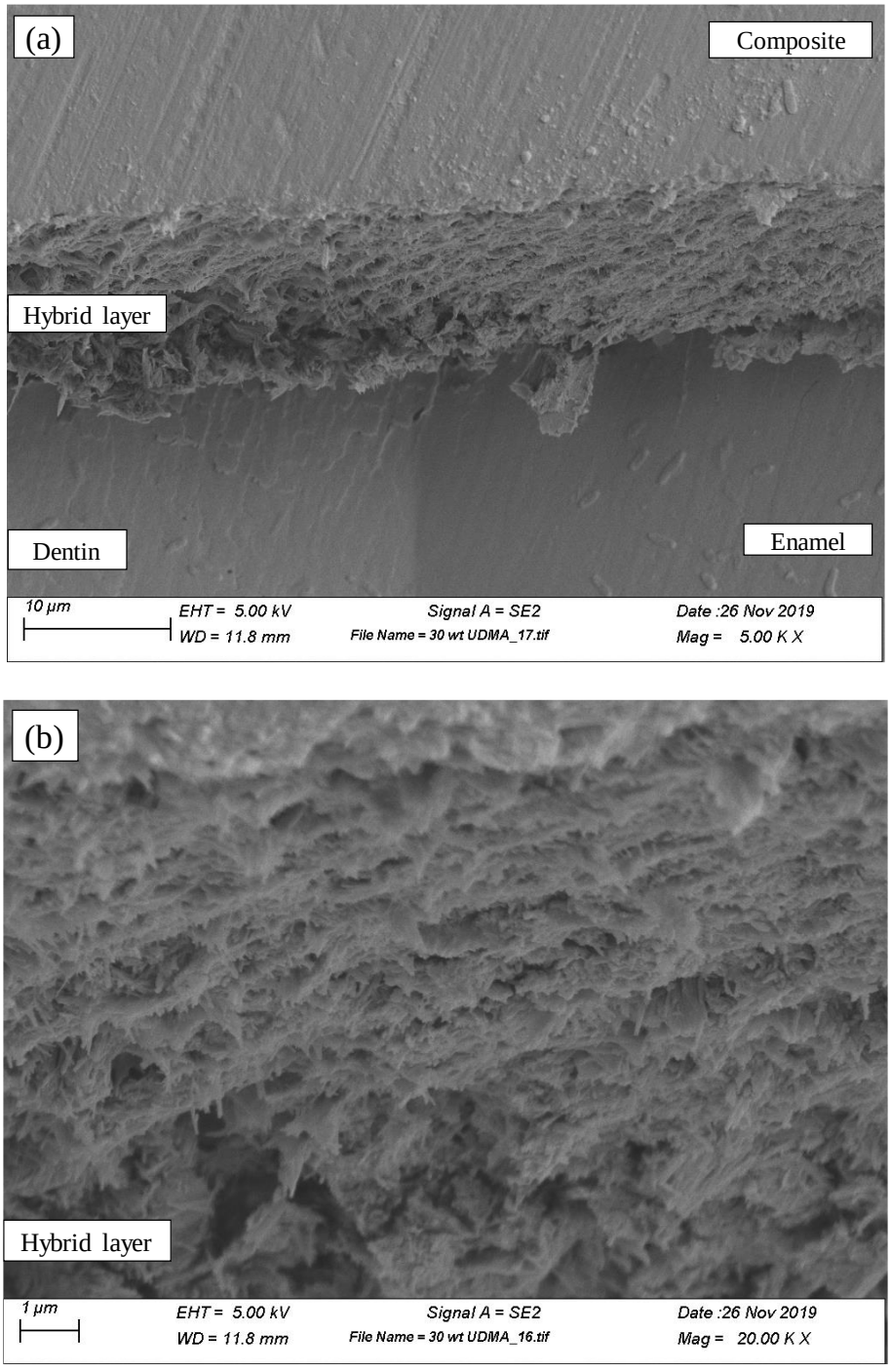

Figure 6.5. SEM image: (a) hybrid layer with enamel and dentin; (b) high magnification of the hybrid layer

6.4 Conclusion

A strong bond between adhesive system and tooth layers are the goal of this chapter. Different compositions of UDMA in MMA as presented in chapter 4 were applied on cow teeth. The 30 wt.% UDMA in MMA is the lowest viscosity of the adhesive system was used in this project. The nanoindentation test shows that the 30 wt.% UDMA in MMA gives a good mechanical properties values (hardness and indentation modulus) with both enamel and dentin layers compare with other concentration. These results are related to formation a strong bond in the junction areas between adhesive-enamel and adhesive-dentin. Therefore, there is no delamination occurs after microindentation test with maximum load. As well as, the hybrid layer was show in SEM images proved there is no gap occur after cured the adhesive layer. This related to improved infiltration of lower viscosity adhesive system into the tooth layers, Therefore, no secondary cavity will appear.

7 CHAPTER 7. CONCLUSIONS AND FUTURE WORK

This dissertation is focused on resolving the problem of gap formation between dental composite resins and cow teeth tissues. Dental composite restorations (fillings) can fail due to the formation of secondary caries at the base of the restorations. This is often the result of a gap forming at the composite-tooth junction which is an ideal location for the proliferation of acidogenic bacteria that cause caries. Hence, avoiding the formation of gaps between the restoration and the tooth is vital to the long-term performance of restorations. Before a composite restoration is used to fill a cavity an adhesive layer is used that bonds the composite to the tooth. The performance of this adhesive layer is the focus of the work in this thesis.

The gap occurs due to the weak bond between the adhesive and tooth layers. This in turn is related to the properties of the adhesive system, like viscosity, mechanical properties and chemical bonding, as well as contraction as the polymer cures. The work presented in the thesis is largely focused on the viscosity and mechanical properties, with a particular emphasis on their dependency on the composition of the adhesive system. In this study, the basic approach was to make an adhesive system that combines two monomers with different basic properties. Thus, the system investigated was chosen so that it contained a high molecular weight monomer, like UDMA, and MMA, as a low molecular weight monomer. MMA was chosen as the diluent in this study due to its widespread usage in dental applications. Using different weight percentages of MMA enabled the optimization of the viscosity and mechanical properties of the adhesive system.

The results show that low wt. % UDMA in MMA provides good mechanical properties (hardness and modulus) when cured that are essential for a strong bond. It also

has the low viscosity in the uncured state that is desirable for penetrating narrow tubules in dentin and surface pores in etched enamel. Optical microscopy and SEM imaging have shown that there is no gap with low weight percentage of UDMA. Microhardness testing and images of the indentations show there is no delamination in the junction area, which is indicative of a strong bond between the adhesive and cow tooth layers.

The two main considerations in developing the adhesive are viscosity of the uncured phase and the mechanical strength of the cured phase. It was found that good viscosity could be obtained for a range of different monomer ratios which suggests obtaining good mechanical properties in the cured state is the most important factor. To improve the mechanics composites containing small amounts of relative high strength additives were examined.

Two additives were considered, graphene and hydroxyapatite, which were added at a range of different low concentrations to examine their impact on the mechanical properties of the adhesive system. Even the very low concentrations of these additive used in these studies had a noticeable effect on the mechanical properties. This is likely due to changes in bonding resulting from the presence of the additive. This is supported by the observed changes in the vibrational spectra peaks. The results suggest that the performance of the adhesive layer in dental applications can be further improved by the addition of small amounts of either graphene or hydroxyapatite. Furthermore, enhancement with graphene provided higher mechanical properties than with the hydroxyapatite additive, presumably due to the interactions between the hybridized carbon and the polymer. Overall, the results indicate that the properties of the adhesive system are tunable via changes in monomer

ratio and the addition of the selected additives. There is the potential that these methods could be used to optimize the adhesive's properties for particular applications.

There are a number of things that could be tried in terms of future work for improving the adhesive layer. Examples include using other low molecular weight monomers in combination with different high molecular weight monomers. This will allow the investigation of the effect of different monomer chemistries on properties. For example, the low molecular weight monomer,3-(Trimethoxysilyl) propyl methacrylate (3-TMSPMA) could be used instead of MMA. 3-TMSPMA is a large organic compound that contains silicon atoms in the silyl group. This type of chemical structure makes it attractive as an "active" monomer for bonding dissimilar organic-inorganic compounds (i.e. dual reactive). The silicon atom in the chemical structure has the potential to bind with HA in the cow's teeth tissues to provide a very strong bond between the adhesive and the cow tooth.

As in the work already described further enhancements may be provided with the addition of graphene and hydroxyapatite to the 3-TMSPMA in a mixture with the high molecular weight UDMA. Other high molecular weight monomers such as Bis-phenol A glycerolate dimethacrylate (Bis-GMA), could also be used instead of UDMA. Bis-GMA has good mechanical properties but very high viscosity, therefore another diluent maybe added to help decrease viscosity of the adhesive system. Bis-GMA, as the high molecular weight monomer, could be mixed with MMA and/or 3-TMSPMA, as the low molecular weight monomer. These in turn could be enhanced by adding graphene and hydroxyapatite to the mixtures to further tune properties. To aid the curing process, cointiators can be used with CQ, like an amino coinitiator, which may increase the degree of conversion of the

carbon double bonds to single bonds and in a very short time. The time of curing is very important for dental adhesive applications, since the time to fill a cavity and the mechanical properties of the cured adhesive depend on the curing time

Lastly, different additives could be used to give different properties and bonding. For example, using silica with T-3MSPMA may optimize the bond between the additives and the matrix. The effects of particle size for the additives (hydroxyapatite, graphene and silica) could be varied to determine their effect on the light scattering during the polymerization process. This then raises the possibility of identifying the optimal particle size to improve degree of conversion as well as mechanical properties.

REFERENCES

[1] 3M ESPE. Low shrinkage posterior restorative. 2008.

[2] H. O. Heymann, E. J. S. Jr, and A. V. Ritter. Sturdevant's Art and Science of Operative Dentistry, 5th ed. 2007;31(1).

[3] M. Hoffman and M D. The Teeth (Human Anatomy): Diagram, Names, Number, and Condition. 2015.

[4] Marshall GW, Balooch M, Gallagher RR, Gansky SA, Marshall SJ. Mechanical properties of the dentinoenamel junction: AFM studies of nanohardness, elastic modulus, and fracture. Journal of Biomedical Materials Research 2001;54(1):87-95.

[5] Imbeni V, Marshall GW, Marshall SJ, Ritchie RO, Kruzic JJ. The dentin-enamel junction and the fracture of human teeth. Nature Materials 2005;4(3):229-232.

[6] R.H. Selwitz, A. I. Ismail, and N. B. Pitts. Dental caries. 2007;369 (9555):51-59.

[7] D. K. Sanghi1, Rakesh Tiwle. Comprehensive Review on Dental Caries . Journal of Innovations in Pharmaceuticals and Biological Sciences 2015;2 (4):369-377.

[8] Khushbu Yadav SP. Dental Caries. Asian Journal of Biomedical and Pharmaceutical Sciences 2016;6 (53):1-7.

[9] Collier. Tooth Loss and Root Canal Infection. 2019.

[10] Chan KH, Mai Y, Kim H, Tong KC, Ng D, Hsiao JC. Review: Resin Composite Filling. Materials 2010;3(2):1228-1243.

[11] Dönmez N, Mağrur Kazak2. Use of Adhesive Systems in Dentistry. 2018:119-140.

[12] Lee S, González-Cabezas C, Kim K, Kim K, Kuroda K. Catechol-Functionalized Synthetic Polymer as a Dental Adhesive to Contaminated Dentin Surface for a Composite Restoration. Biomacromolecules 2015;16(8):2265-2275.

[13] Sofan E, Sofan A, Palaia G, Tenore G, Romeo U, Migliau G. Classification review of dental adhesive systems: from the IV generation to the universal type. Annali di stomatologia 2017;8(1):1-17.

[14] Giannini M, Makishi P, Ayres APA, Vermelho PM, Fronza BM, Nikaido T, Tagami J. Self-Etch Adhesive Systems: A Literature Review. Brazilian Dental Journal 2015; 26(1):3-10.

[15] Swift J, Edward J. Dentin/enamel adhesives: review of the literature. Pediatric dentistry 2002;24(5):456-461.

[16] Peutzfeldt A. Resin composites in dentistry: the monomer systems. European Journal of Oral Sciences 1997;105(2):97-116.

[17] Kuzhir P, Paddubskaya A, Plyushch A, Volynets N, Maksimenko S, Macutkevic J, Kranauskaite I, Banys J, Ivanov E, Kotsilkova R, Celzard A, Fierro V, Zicans J, Ivanova T, Merijs Meri R, Bochkov I, Cataldo A, Micciulla F, Bellucci S, Lambin P. Epoxy composites filled with high surface area-carbon fillers: Optimization of electromagnetic shielding, electrical, mechanical, and thermal properties. Journal of Applied Physics 2013;114(16):164304.

[18] Kaisarly D, Gezawi ME. Polymerization shrinkage assessment of dental resin composites: a literature review. Odontology 2016;104(3):257-270.

[19] Kim Y, Kim CK, Cho BH, Son HH, Um CM, Kim OY. A new resin matrix for dental composite having low volumetric shrinkage. Journal of Biomedical Materials Research Part B: Applied Biomaterials 2004;70 B(1):82-90.

[20] Gonçalves F, Azevedo CLN, Ferracane JL, Braga RR. BisGMA/TEGDMA ratio and filler content effects on shrinkage stress. Dental Materials 2011;27(6):520-526.

[21] Jian Y, He Y, Zhao L, Kowalczyk A, Yang W, Nie J. Effect of Monomer Structure on Real-Time UV-Curing Shrinkage Studied by a Laser Scanning Approach. Advances in Polymer Technology 2013;32(1):1-9.

[22] Świderska J, Czech Z, Świderski W, Kowalczyk A. Reducing of on Polymerization Shrinkage by Application of UV Curable Dental Restorative Composites. Polish Journal of Chemical Technology 2014;16(3):51-55.

[23] Podgórski M. Structure–property relationship in new photo-cured dimethacrylate-based dental resins. Dental Materials 2011;28(4):398-409.

[24] He J, Liu F, Vallittu PK, Lassila LVJ. Synthesis and characterization of new dimethacrylate monomer and its application in dental resin. Journal of Biomaterials Science, Polymer Edition 2013;24(4):417-430.

[25] Baroudi K, Mahmoud S. Improving Composite Resin Performance Through Decreasing its Viscosity by Different Methods. The open dentistry journal 2015;9(1):235-242.

[26] Yin M, Guo S, Liu F, He J. Synthesis of fluorinated dimethacrylate monomer and its application in preparing Bis-GMA free dental resin. Journal of the Mechanical Behavior of Biomedical Materials 2015;51:337-344.

[27] Luo S, Zhu W, Liu F, He J. Preparation of a Bis-GMA-Free Dental Resin System with Synthesized Fluorinated Dimethacrylate Monomers. International Journal of Molecular Sciences 2016;17(12):1-11.

[28] Endo T, Sudo A. Development and application of novel ring-opening polymerizations to functional networked polymers. Journal of Polymer Science Part A: Polymer Chemistry 2009;47(19):4847-4858.

[29] Ricardo Acosta Ortiz, Amy G. Savage Gomez, Maria L. Berlanga Duarte, and Aida E. Garcia Valdez. The effect of a dithiol spiroorthocarbonate on mechanical properties and shrinkage of a dental resin. Designed Monomers and Polymers 2014;18(1):73-78.

[30] Sun X, Li Y, Xiong J, Hu X, Chen J. Shrinkage properties of a modified dental resin composites containing a novel spiroorthocarbonate expanding monomer. Materials Letters 2011;65(23):3586-3589.

[31] Fu J, Liu W, Hao Z, Wu X, Yin J, Panjiyar A, Liu X, Shen J, Wang H. Characterization of a Low Shrinkage Dental Composite Containing Bismethylene Spiroorthocarbonate Expanding Monomer. International journal of molecular sciences 2014;15(2):2400-2412.

[32] Acosta Ortiz R, Savage Gomez AG, García Valdez AE, Aguirre Flores R, Sangermano M. Development of Low-Shrinkage Polymers by Using Expanding Monomers. Macromolecular Symposia 2017;374(1):1-6.

[33] Tai Y, Hsu S, Chen R, Su W, Chen M. Liquid crystalline epoxy nanocomposite material for dental application. Journal of the Formosan Medical Association 2014;114(1):46-51.

[34] Kundie F, Azhari CH, Muchtar A, Ahmad ZA. Effects of Filler Size on the Mechanical Properties of Polymer-filled Dental Composites: A Review of Recent Developments. Journal of Physical Science 2018;29(1):141-165.

[35] Ilie N, Hickel R. Resin composite restorative materials. Australian Dental Journal 2011;56:59-66.

[36] Satterthwaite JD, Vogel K, Watts DC. Effect of resin-composite filler particle size and shape on shrinkage–strain. Dental Materials 2009;25(12):1612-1615.

[37] Habib E, Wang R, Wang Y, Zhu M, Zhu XX. Inorganic Fillers for Dental Resin Composites: Present and Future. ACS Biomaterials Science and Engineering 2016;2(1):1-11.

[38] Tsujimoto A, Barkmeier WW, Takamizawa T, Latta MA, Miyazaki M. Mechanical properties, volumetric shrinkage and depth of cure of short fiber-reinforced resin composite. Dental Materials Journal 2016;35(3):418-424.

[39] de Oliveira, Dayane Carvalho Ramos Salles, de Menezes LR, Gatti A, Correr Sobrinho L, Ferracane JL, Sinhoreti MAC. Effect of Nanofiller Loading on Cure Efficiency and Potential Color Change of Model Composites. Journal of Esthetic and Restorative Dentistry 2016;28(3):171-177.

[40] Arikawa H, Kanie T, Fujii K, Takahashi H, Ban S. Effect of Filler Properties in Composite Resins on Light Transmittance Characteristics and Color. Dental Materials Journal 2007;26(1):38-44.

[41] Alvim HH, Campos NM, Vasconcellos WA, Silva VA, Moreira AN, Gatti A. Influence of Different Photoinitiators on Polymerization Kinetics and Marginal Microleakage in Restorations using Photopolymerizable Dental Composites. Brazilian Research in Pediatric Dentistry and Integrated Clinic 2017;17(1):1-9.

[42] Leprince JG, Palin WM, Hadis MA, Devaux J, Leloup G. Progress in dimethacrylate-based dental composite technology and curing efficiency. Dental Materials 2012;29(2):139-156.

[43] Swathi A, Jayaprakash T, Chandrasekhar V. Effect of single and multiple consecutive applications of all-in-one adhesive on tensile bond strength to dentin. Journal of Interdisciplinary Dentistry 2014;4(2):81-84.

[44] H Mirmohammadi, K Khosravi, K Kashani, CJ Kleverlaan, and AJ Feilzer. Influence of filler existence on microleakage of a self-etch adhesive system. Journal of Conservation Dentistry 2014;17(2):175-178.

[45] Yoshihara K, Yoshida Y, Nagaoka N, Hayakawa S, Okihara T, De Munck J, Maruo Y, Nishigawa G, Minagi S, Osaka A, Van Meerbeek B. Adhesive interfacial interaction affected by different carbon-chain monomers. Dental Materials 2013;29(8):888-897.

[46] Feitosa VP, Sauro S, Ogliari FA, Stansbury JW, Carpenter GH, Watson TF, Sinhoreti MA, Correr AB. The role of spacer carbon chain in acidic functional monomers on the physicochemical properties of self-etch dental adhesives. Journal of Dentistry 2014;42(5):565-574.

[47] Krejci I, Stavridakis M. New perspectives on dentin adhesion differing methods of bonding. Practical Periodontics and Aesthetic Dentistry 2000;12(8):727-732.

[48] Yassen GH, Platt JA, Hara AT. Bovine teeth as substitute for human teeth in dental research: a review of literature. Journal of Oral Science 2011;53(3):273-282.

[49] B Galindo, S Gil Alcolea, J Gómez. Graphene-polymer composites. Materials Science and Engineering 2018;40:1-6.

[50] Pepla E, Besharat LK, Palaia G, Tenore G, Migliau G. Nano-hydroxyapatite and its applications in preventive, restorative and regenerative dentistry: a review of literature. Annali di Stomatologia 2014;5(3):108-114.

[51] Al-Sanabani JS, Madfa AA, Al-Sanabani FA. Application of Calcium Phosphate Materials in Dentistry. International Journal of Biomaterials 2013;2013:876132-12.

[52] W. C. Oliver. An improved technique for determining hardness and elastic modulus using load and displacement sensing indentation experiments. Journal Materials Research 1992;7(6):1564-1583.

[53] D. C. Joy. Helium Ion Microscopy: Principles and Applications. 2013.

[54] Y. R. Zhang, W. Du, X. D. Zhou, and H. Y. Yu. Review of research on the mechanical properties of the human tooth. International journal of oral science 2014;6(2):61-69.

[55] Swathi A, Jayaprakash T, Chandrasekhar V. Effect of single and multiple consecutive applications of all-in-one adhesive on tensile bond strength to dentin. Journal of Interdisciplinary Dentistry 2014;4(2):81.

[56] Carneiro KK, Meier MM, Santos CCD, Maciel AP, Carvalho CN, Bauer J. Adhesives Doped with Bioactive Niobophosphate Micro-Filler: Degree of Conversion and Microtensile Bond Strength. Brazilian dental journal 2016;27(6):705.

[57] Bedran-Russo A, Leme-Kraus AA, Vidal CMP, Teixeira EC. An Overview of Dental Adhesive Systems and the Dynamic Tooth–Adhesive Interface. Dental Clinics of North America 2017;61(4):713-731.

[58] Tonetto MR, Pinto SCS, Rastelli, Alessandra de Nara Souza, Borges AH, Saad JRC, Pedro FLM, de Andrade MF, Bandéca MC. Degree of Conversion of Polymer-matrix Composite assessed by FTIR Analysis. The journal of contemporary dental practice 2013;14(1):76-79.

[59] Moharam LM, Botros SA, El-Askary FS, Özcan M. Effect of polymerization protocol on the degree of conversion of photo- and dual-polymerized self-etch adhesives. Journal of Adhesion Science and Technology 2016;30(3):262-274.

[60] He J, Garoushi S, Vallittu PK, Lassila L. Effect of low-shrinkage monomers on the physicochemical properties of experimental composite resin. Acta Biomaterialia Odontologica Scandinavica 2018;4(1):30-37.

[61] Lempel E, Czibulya Z, Kunsági-Máté S, Szalma J, Sümegi B, Böddi K. Quantification of Conversion Degree and Monomer Elution from Dental Composite Using HPLC and Micro-Raman Spectroscopy. Chromatographia 2014;77(17):1137-1144.

[62] Borges BCD, Sousa-Lima RXd, Moreno GBP, Moreira DGL, Oliveira, Dayane Carvalho Ramos Salles, Souza-Junior EJC, Sinhoreti MAC. Polymerization and adhesion behavior of experimental dental bonding materials with different initiator systems. Journal of Adhesion Science and Technology 2018;32(3):239-246.

[63] Skienhe H, Habchi R, Ounsi H, Ferrari M, Salameh Z. Evaluation of the Effect of Different Types of Abrasive Surface Treatment before and after Zirconia Sintering on Its Structural Composition and Bond Strength with Resin Cement. BioMed research international 2018;2018:1803425-12.

[64] Palacios T, Abad C, Pradíes G, Pastor JY. Evaluation of resin composites for dental restorations. Procedia Manufacturing 2019;41:914-921.

[65] Cheng E, Sun X. Effects of wood-surface roughness, adhesive viscosity and processing pressure on adhesion strength of protein adhesive. Journal of Adhesion Science and Technology 2006;20(9):997-1017.

[66] Yu X, Pfaendtner J, Broadbelt LJ. Ab Initio Study of Acrylate Polymerization Reactions: Methyl Methacrylate and Methyl Acrylate Propagation. The journal of physical chemistry. A 2008;112(29):6772-6782.

[67] Pedraza EP, Cano CI, VanDalen J, Pipes RB, Youngblood JP. Reduction in fixture time of a two-component structural acrylic adhesive. International Journal of Adhesion and Adhesives 2008;28(6):283-290.

[68] Bula A, Kozłowski M, Hulimka J, Chmielnicki B. Analysis of methyl methacrylate adhesive (MMA) relaxation with non-linear stress–strain dependence. International Journal of Adhesion and Adhesives 2019;94:40-46.

[69] Khromiak U, Levytskyi V, Stepova K, Tarnawsky A. Synthesis and Properties of Adhesive Polymer-Methylmethacrylate Materials. International Journal of Polymer Science 2018;2018:1-9.

[70] Takei T, Araki K, Terazono K, Ozuno Y, Hayase G, Kanamori K, Nakanishi K, Yoshida M. Highly Efficient Encapsulation of Ingredients in Poly(methyl methacrylate) Capsules Using a Superoleophobic Material. Polymers and Polymer Composites 2017;25(2):129-134.

[71] Nicolae LC, Shelton RM, Cooper PR, Martin RA, Palin WM. The Effect of UDMA/TEGDMA Mixtures and Bioglass Incorporation on the Mechanical and Physical Properties of Resin and Resin-Based Composite Materials. Conference Papers in Science Mar 12, 2014;2014:1-5.

[72] Park J, Ye Q, Singh V, Kieweg SL, Misra A, Spencer P. Synthesis and evaluation of novel dental monomer with branched aromatic carboxylic acid group. Journal of Biomedical Materials Research Part B: Applied Biomaterials 2012;100B(2):569-576.

[73] Dolez P, Marek M, Love BJ. Photopolymerizable acrylic resin: Effect of curing time and temperature. Journal of Applied Polymer Science 2001;82(3):546-554.

[74] Kitano H, Ramachandran K, Bowden NB, Scranton AB. Unexpected visible-light-induced free radical photopolymerization at low light intensity and high viscosity using a titanocene photoinitiator. Journal of Applied Polymer Science 2013;128(1):611-618.

[75] Briscoe BJ, Fiori L, Pelillo E. Nano-indentation of polymeric surfaces. Journal of Physics D: Applied Physics 1998;31(19):2395-2405.

[76] Leprince JG, Palin WM, Hadis MA, Devaux J, Leloup G. Progress in dimethacrylate-based dental composite technology and curing efficiency. Dental Materials 2012; 29(2):139-156.

[77] Atai M, Watts DC, Atai Z. Shrinkage strain-rates of dental resin-monomer and composite systems. Biomaterials 2005;26(24):5015-5020.

[78] Besegato JF, Jussiani EI, Andrello AC, Fernandes RV, Salomão FM, Vicentin BLS, Dezan-Garbelini CC, Hoeppner MG. Effect of light-curing protocols on the mechanical behavior of bulk-fill resin composites. Journal of the mechanical behavior of biomedical materials 2019;90:381-387.

[79] Collares FM, Portella FF, Leitune VCB, Samuel SMW. Discrepancies in degree of conversion measurements by FTIR. Brazilian Oral Research 2014;28(1):9-454.

[80] Moraes LGP, Rocha RSF, Menegazzo LM, de Araújo EB, Yukimito K, Moraes JCS. Infrared spectroscopy: a tool for determination of the degree of conversion in dental composites. Journal of applied oral science : revista FOB 2008;16(2):145-149.

[81] Miletic V, Jakovljevic N, Manojlovic D, Marjanovic J, Rosic AA, Dramićanin MD. Refractive indices of unfilled resin mixtures and cured composites related to color and translucency of conventional and low-shrinkage composites. Journal of biomedical materials research. Part B, Applied biomaterials 2017;105(1):7-13.

[82] Shortall AC, Palin WM, Burtscher P. Refractive Index Mismatch and Monomer Reactivity Influence Composite Curing Depth. Journal of Dental Research 2008;87(1):84-88.

[83] Oliveira, Dayane Carvalho Ramos Salles de, Silva CBd, Muniz BV, Volpato MC, Costa AR, Sinhoreti MAC. Effect of 4-(N,N-dimethylamino)phenethyl Alcohol on Degree of Conversion and Cytotoxicity of Photo-Polymerized CQ-Based Resin Composites. Brazilian Dental Journal 2014;25(6):538-542.

[84] Podgórski M. Structure–property relationship in new photo-cured dimethacrylate-based dental resins. Dental Materials 2011;28(4):398-409.

[85] Léonard C, Halary JL, Monnerie L. Hydrogen bonding in PMMA-fluorinated polymer blends: FTi.r. investigations using ester model molecules. Polymer 1985;26(10):1507-1513.

[86] Ryu IS, Liu X, Jin Y, Sun J, Lee YJ. Stoichiometric analysis of competing intermolecular hydrogen bonds using infrared spectroscopy. RSC advances 2018; 8(42):23481-23488.

[87] Gauthier MA, Stangel I, Ellis TH, Zhu XX. A new method for quantifying the intensity of the C=C band of dimethacrylate dental monomers in their FTIR and Raman spectra. Biomaterials 2005;26(33):6440-6448.

[88] Shin WS, Li XF, Schwartz B, Wunder SL, Baran GR. Determination of the degree of cure of dental resins using Raman and FT-Raman spectroscopy. Dental Materials 1993;9(5):317-324.

[89] Yang Y, Urbas A, Gonzalez-Bonet A, Sheridan RJ, Seppala JE, Beers KL, Sun J. A composition-controlled cross-linking resin network through rapid visible-light photo-copolymerization.e. Polymer Chemistry 2016;7(31):5023-5030.

[90] Kim D, Lee DG, Kim JC, Lim CS, Kong NS, Kim JH, Jung HW, Noh SM, Park YI. Effect of molecular weight of polyurethane toughening agent on adhesive strength and rheological characteristics of automotive structural adhesives. International Journal of Adhesion and Adhesives 2017;74:21-27.

[91] Madrid M, González-Gutiérrez L, Martínez MA, Garriga A. Modeling the rheology of anaerobic adhesive formulations. Journal of Adhesion Science and Technology 2006;20(7):677-691.

[92] Amirouche-Korichi A, Mouzali M, Watts DC. Effects of monomer ratios and highly radiopaque fillers on degree of conversion and shrinkage-strain of dental resin composites. Dental Materials 2009;25(11):1411-1418.

[93] Stansbury JW. Dimethacrylate network formation and polymer property evolution as determined by the selection of monomers and curing conditions. Dental Materials 2011;28(1):13-22.

[94] Poh BT, Yee KW, Lim HB. Viscosity and shear strength of natural-rubber-based adhesives in the presence of gum rosin and petroresin. Journal of Applied Polymer Science 2008;110(6):4079-4083.

[95] Ashraf A, Jani N, Farmer F, Lynch-Branzoi JK. Non-Destructive Investigation of Dispersion, Bonding, and Thermal Properties of Emerging Polymer Nanocomposites Using Close-Up Lens Assisted Infrared Thermography. MRS Advances 2020:1-8.

[96] Robertson ID, Yourdkhani M, Centellas PJ, Aw JE, Ivanoff DG, Goli E, Lloyd EM, Dean LM, Sottos NR, Geubelle PH, Moore JS, White SR. Rapid energy-efficient manufacturing of polymers and composites via frontal polymerization. Nature 2018; 557(7704):223-227.

[97] Roberto Vega Baudrit J. Basis and Applications of Silicon Reinforced Adhesives. Organic & Medicinal Chemistry International Journal 2018;5(1):1-11.

[98] Abou Neel EA, Kiani A, Valappil SP, Mordan NM, Baek S, Zakir Hossain KM, Felfel RM, Ahmed I, Divakarl K, Chrzanowski W, Knowles JC. Glass microparticle- versus microsphere-filled experimental dental adhesives. Journal of Applied Polymer Science 2019;136(32):47832-n/a.

[99] Cocco AR, Lima GS, Leal FB, Munchow EA, Ogliari FA, Piva E. Addition of nanoparticles for development of radiopaque dental adhesives. International Journal of Adhesion and Adhesives 2018;80:122-127.

[100] Bansal SA, Singh AP, Kumar A, Kumar S, Kumar N, Goswamy JK. Improved mechanical performance of bisphenol-A graphene-oxide nano-composites. Journal of Composite Materials 2018;52(16):2179-2188.

[101] Lezaja M, Jokic BM, Veljovic DN, Miletic V. Shear bond strength to dentine of dental adhesives containing hydroxyapatite nano-fillers. Journal of Adhesion Science and Technology 2016;30(24):2678-2689.

[102] Leitune VCB, Collares FM, Trommer RM, Andrioli DG, Bergmann CP, Samuel SMW. The addition of nanostructured hydroxyapatite to an experimental adhesive resin. Journal of Dentistry 2013;41(4):321-327.

[103] Bensadoun F, Kchit N, Billotte C, Trochu F, Ruiz E. A Comparative Study of Dispersion Techniques for Nanocomposite Made with Nanoclays and an Unsaturated Polyester Resin. Journal of Nanomaterials 2011;2011:1-12.

[104] Masuda K, Araki K, Hidema R, Suzuki H, Komoda Y. Dispersion and Re-aggregation of Particles in a Suspension Flowing in an Abrupt Contraction Channel. Journal of Society of Rheology, Japan 2016;44(3):153-158.

[105] Pullicino E, Pullicino E, Zou W, Zou W, Gresil M, Gresil M, Soutis C, Soutis C. The Effect of Shear Mixing Speed and Time on the Mechanical Properties of GNP/Epoxy Composites. Appl Compos Mater 2017;24(2):301-311.

[106] Xiong J, Sun X, Chen J, Tang L. Influence of filler content on physicomechanical and bonding properties of an experimental dental resin cement. Journal of Applied Polymer Science 2013;127(4):2427-2434.

[107] Chadda H, Satapathy BK, Patnaik A, Ray AR. Mechanistic interpretations of fracture toughness and correlations to wear behavior of hydroxyapatite and silica/hydroxyapatite filled bis-GMA/TEGDMA micro/hybrid dental restorative composites. Composites Part B 2017;130:132-146.

[108] Li J, Gunister E, Barsoum I. Effect of graphene oxide as a filler material on the mechanical properties of LLDPE nanocomposites. Journal of Composite Materials 2019;53(19):2761-2773.

[109] Vemulapalli AK, Penmetsa RMR, Nallu R, Siriyala R. HAp/TiO2 nanocomposites: Influence of TiO2 on microstructure and mechanical properties. Journal of Composite Materials 2020;54(6):765-772.

[110] Masouras K, Akhtar R, Watts D, Silikas N. Effect of filler size and shape on local nanoindentation modulus of resin-composites. J Mater Sci: Mater Med 2008;19(12):3561-3566.

[111] Kiran MD, Govindaraju HK, Jayaraju T, Kumar N. Review-Effect of Fillers on Mechanical Properties of Polymer Matrix Composites. Materials Today: Proceedings 2018;5(10):22421-22424.

[112] El-Safty S, Akhtar R, Silikas N, Watts DC. Nanomechanical properties of dental resin-composites. Dental Materials 2012;28(12):1292-1300.

[113] Gonçalves F, Azevedo CLN, Ferracane JL, Braga RR. BisGMA/TEGDMA ratio and filler content effects on shrinkage stress. Dental Materials 2011;27(6):520-526.

[114] Galvão MR, Caldas, Sergei Godeiro Fernandes Rabelo, Bagnato VS, de Souza Rastelli, Alessandra Nara, de Andrade MF. Evaluation of degree of conversion and hardness of dental composites photo-activated with different light guide tips. European journal of dentistry 2013;7(1):86-93.

[115] Wang J, Yu Q, Yang Z. Effect of loading chemically and mechanically pre-treated fumed silica as filler on an etch & rinse model dental adhesive. Journal of Adhesion Science and Technology 2018;32(5):527-541.

[116] Kartick B, Srivastava SK, Srivastava I. Green Synthesis of Graphene. Journal of nanoscience and nanotechnology 2013;13(6):4320-4324.

[117] D′Alpino PHP, Araújo RP, González AHM, di Hipólito V, Valduga CJ, dos Santos DI, Graeff CF. Inorganic characterizations and filler particles morphology of self-adhesive cements. International Journal of Adhesion and Adhesives 2016;68:62-69.

[118] Stuart BH. Infrared Spectroscopy Fundamentals and Applications. 2004.

[119] Ţucureanu V, Matei A, Avram AM. FTIR Spectroscopy for Carbon Family Study. Critical reviews in analytical chemistry 2016;46(6):502-520.

[120] Rehman Iu, Movasaghi Z, Rehman S. Vibrational Spectroscopy for Tissue Analysis. 2012;25.

[121] Antonakos A, Liarokapis E, Leventouri T. Micro-Raman and FTIR studies of synthetic and natural apatites. Biomaterials 2007;28(19):3043-3054.

[122] Alabdali Z. N, Reiter MP, Lynch-Branzoi, J. K., Mann, A. B. Compositional Effects on Mechanical Properties and Viscosity in UDMA-MMA Blends. J. Adhes. Sci. Technol 2020.

[123] Zeng W, Zeng W, Liu F, Liu F, He J, He J. Physicochemical Properties of Bis-GMA/TEGDMA Dental Resin Reinforced with Silanized Multi-Walled Carbon Nanotubes. Silicon 2019;11(3):1345-1353.

[124] Stammeier JA, Purgstaller B, Hippler D, Mavromatis V, Dietzel M. In-situ Raman spectroscopy of amorphous calcium phosphate to crystalline hydroxyapatite transformation. MethodsX 2018; 5:1241-1250.

[125] L.M. Malarda, M.A. Pimentaa, G. Dresselhaus b, M.S. Dresselhaus. Raman spectroscopy in graphene. Physics reports 2009; 473:51-87.

[126] Dresselhaus MS, Jorio A, Hofmann M, Dresselhaus G, Saito R. Perspectives on Carbon Nanotubes and Graphene Raman Spectroscopy. Nano Letters 2010;10(3):751-758.

[127] Martins Ferreira EH, Moutinho MVO, Stavale F, Lucchese MM, Capaz RB, Achete CA, Jorio A. Evolution of the Raman spectra from single-, few-, and many-layer graphene with increasing disorder. Physical review. B, Condensed matter and materials physics 2010;82(12).

[128] Khan AF, Awais M, Khan AS, Tabassum S, Chaudhry AA, Rehman IU. Raman Spectroscopy of Natural Bone and Synthetic Apatites. Applied spectroscopy reviews 2013;48(4):329-355.

[129] Costa, M. R. M. M, Pereira E, Pileggi RG, Cincotto MA. Study of the influential factors on the rheological behavior of adhesive mortar available in the market. Revista Ibracon de Estruturas e Materiais 2013;6(3):399-413.

[130] Rameshbabu AP, Mohanty S, Bankoti K, Ghosh P, Dhara S. Effect of alumina, silk and ceria short fibers in reinforcement of Bis-GMA/TEGDMA dental resin. Composites Part B 2015;70:238-246.

[131] Carvalho CN, Francci CE, Costa JF, Bauer J. Effect of filler and application mode on micro-shear bond strength of etch-and-rinse adhesive systems. Revista Portuguesa de Estomatologia, Medicina Dentária e Cirurgia Maxilofacial 2015;56(2):89-94.

[132] Shaygan Nia A, Binder WH. Graphene as initiator/catalyst in polymerization chemistry. Progress in polymer science 2017;67:48-76.

[133] Münchow EA, Bossardi M, Priebe TC, Valente LL, Zanchi CH, Ogliari FA, Piva E. Microtensile versus microshear bond strength between dental adhesives and the dentin substrate. International Journal of Adhesion and Adhesives 2013;46:95-99.

[134] Naumova EA, Ernst S, Schaper K, Arnold WH, Piwowarczyk A. Adhesion of different resin cements to enamel and dentin. Dental Materials Journal 2016;35(3):345-352.

[135] Gateva N, Gusyiska A, Stanimirov P, Kabaktchieva R, Raichev I. Effect of Etching Time and Acid Concentration on Micromorphological Changes in Dentin of Both Dentitions. Journal of IMAB - Annual Proceeding (Scientific Papers) 2016;22(2):1099-1110.

[136] Dalia A. Abuelenain, Ensanya A. Abuo Neel, and Tariq Abu-Haimed. Effect of dentin modifiers on surface and mechanical properties of acid etched dentin . International journal of adhesion and adhesives 2018;81:43-47.

[137] Matos AB, Trevelin LT, Silva, Beatriz Togoro Ferreira da, Francisconi-Dos-Rios LF, Siriani LK, Cardoso MV. Bonding efficiency and durability: current possibilities. Brazilian oral research 2017;31(1):1-22.

[138] Starling J, de Fátima Â, Dantas MSS, Oréfice RL. Interactions between a collagen-binding adhesive and dental substrate. Journal of Adhesion Science and Technology 2014;28(24):2393-2401.

[139] Betancourt DE, Baldion PA, Castellanos JE. Resin-Dentin Bonding Interface: Mechanisms of Degradation and Strategies for Stabilization of the Hybrid Layer. International Journal of Biomaterials 2019;2019:1-11.

[140] Habelitz S, Marshall GW, Balooch M, Marshall SJ. Nanoindentation and storage of teeth. Journal of Biomechanics 2002;35(7):995-998.